

Faculdade de Engenharia da Universidade do Porto



**New numerical methodology to simulate tumour
cell proliferation**

Catarina Isabel Ribeiro Assunção Maia dos Santos


June 2017


A Dissertação intitulada

“New Numerical Methodology to Simulate Tumour Cell Proliferation”

foi aprovada em provas realizadas em 28-06-2017

o júri


Presidente **Prof. Doutor João Manuel Ribeiro da Silva Tavares**
Professor Associado c/ Agregação do Departamento de Engenharia Mecânica da FEUP - U.Porto


Doutora Ana Xavier de Carvalho
Investigadora Principal do Instituto de Biologia Molecular e Celular da U. Porto


Doutor Jorge Américo Oliveira Pinto Belinha
Investigador Pós-Doutoramento do Departamento de Engenharia Mecânica da FEUP - U. Porto

O autor declara que a presente dissertação (ou relatório de projeto) é da sua exclusiva autoria e foi escrita sem qualquer apoio externo não explicitamente autorizado. Os resultados, ideias, parágrafos, ou outros extratos tomados de ou inspirados em trabalhos de outros autores, e demais referências bibliográficas usadas, são corretamente citados.


Autor - Catarina Isabel Ribeiro Assunção Maia dos Santos

Faculdade de Engenharia da Universidade do Porto

Resumo

Ao longo de décadas que a biologia da célula é estudada com o objectivo de compreender-se como esta se desenvolve, reproduz e morre. Quanto maior o nível de compreensão mais facilmente se consegue interferir no crescimento celular, divisão celular e na alteração de ADN, tendo tal conhecimento implicações no tratamento e cura de doenças. O cancro é uma anomalia celular que mata cerca de 9 milhões de pessoas todos os anos. É uma doença em constante investigação e crescimento pois a sua cura ainda não foi encontrada. Assim, o objetivo deste trabalho é mostrar a vantagem de usar modelos matemáticos adaptados à biologia animal como o intuito de complementar a investigação experimental.

Este trabalho utiliza um software de crescimento e divisão celular baseado em métodos sem malha. O software utiliza um modelo matemático para o crescimento e proliferação tumoral combinado com o “Radial Point Interpolation Method” (RPIM). Este é um método sem malha que permite discretizar livremente o domínio do problema com apenas um conjunto de pontos.

Este trabalho apresenta uma revisão bibliográfica sobre a incidência do cancro, a qual mostra: a necessidade de criação de novas metodologias de combate ao mesmo; como se desenvolve o cancro; tipos de cancro; os nutrientes essenciais ao seu crescimento; tipo de linha celular; crescimento celular e mecanismos essenciais para a compreensão do modelo.

Neste trabalho são apresentados brevemente os três conceitos usuais dos modelos matemáticos: modelos contínuos, discretos e híbridos. O modelo utilizado no âmbito da tese faz parte dos modelos discretos porque a análise discretiza uma célula e não uma população.

O modelo de difusão e do método numérico são também apresentados. Aqui é explicado como o oxigénio e os nutrientes (glicose) entram na célula por diferença de concentrações; como é formulado o modelo baseado no RPIM e a criação de leis de crescimento essenciais à divisão celular.

Na validação do modelo conclui-se quais os parâmetros melhores a serem inseridos no programa do RPIM de forma a torna-lo mais eficiente.

Os resultados são apresentados mostram o crescimento da célula durante a interfase, a mudança de forma na mitose até à divisão em duas células filhas. Além disso, é apresentado o consumo de oxigénio e glucose durante um ciclo celular. Este trabalho é um bom exemplo da aplicação dos modelos matemáticos à medicina/biologia, mostrando ser executável, realista e útil.

Abstract

During decades cell biology has been studied trying to understand how cells grow, reproduce and die. Increasing the level of knowledge allows to easily interfere with cell growth, division and DNA alteration to cure and treat diseases. Cancer is a cellular anomaly that kills annually almost 9 million people worldwide. Since it is a disease without a definitive cure, cancer is in constant research and development.

So, the objective of this work is to show the advantage of mathematical models in the simulation of animal biology in order to complement experimental investigation.

This work uses a meshless software to predict the cell growth and division. The software uses a mathematical model for tumour growth and proliferation combined with the Radial Point Interpolation Method (RPIM). This is a meshless method that allows to freely discretize the problem domain using only a set of nodes.

This work presents a literature review about the incidence of cancer, exhibiting the importance of new methodologies to combat cancer, how cancer is developed, types of cancer, essential nutrients for cancer growth, type of cell line and the indispensable mechanisms for model understanding.

In this work, the three usual classes of mathematical models are briefly presented: continuous, discrete and hybrid models. The model used in the scope of this thesis is a discrete model because the analysis discretizes a single cell and not a population.

The diffusion model and the numerical method are also presented. Here it is explained how oxygen and nutrients (glucose) enter the cell by difference in concentrations, how the RPIM-based model is built and how the cellular growth laws (essential to cell division) are obtained.

In model validation it is concluded which are the best parameters to use in RPIM programme, trying to make it more efficient and cost effective.

The results show cellular growth during interphase, the shape change in mitosis and the formation of two daughter cells. Besides that, it is presented the oxygen and glucose consumption during one cellular cycle. This work is a good example of the application of mathematical models to medicine / biology, showing to be executable, realistic and useful.

Acknowledgments

Mestrado completo com os maiores desafios e objetivos cumpridos. Foram dois anos repletos de aventuras e novos conhecimentos que teriam sido impossíveis de ultrapassar sem a ajuda do meu orientador, Professor Jorge Belinha. Quero agradecer-lhe por toda a dedicação e persistência para fazer o projeto funcionar. Desde o início acreditou que seria possível a sua realização, o que me deu sempre força e vontade de continuar. Agradeço também ao meu co-orientador, Professor Renato Natal pela confiança e acompanhamento.

Da mesma forma fundamentais, aos meus pais e ao meu irmão deixo um forte agradecimento por me acompanharem nesta etapa com carinhos, sorrisos e palavras sábias. Ao meu namorado e fiel amigo que sempre esteve presente e me soube guiar pelas melhores decisões. Também à minha amiga Paula que me orientou com os seus conhecimentos e saberes. Por fim aos meus amigos que se encontram comigo desde a escola que provam o significado da amizade e que são fundamentais ao meu bem-estar.

Institutional Acknowledgments and Funding

The author truly acknowledges the work conditions provided by the Applied Mechanics Division (SMAp) of the department of mechanical engineering (DEMec) of FEUP and by the project NORTE-01-0145-FEDER-000022 - SciTech - Science and Technology for Competitive and Sustainable Industries, co-financed by Programa Operacional Regional do Norte (NORTE2020), through Fundo Europeu de Desenvolvimento Regional (FEDER).

The author truly acknowledge the funding provided by Ministério da Educação e Ciência - Fundação para a Ciência e a Tecnologia (Portugal), by project funding UID/EMS/50022/2013 - “BoneSys - Bone biochemical and biomechanic integrated modeling: addressing remodeling, disease and therapy dynamics” (funding provided by the inter-institutional projects from LAETA and INEGI).

Index

Resumo.....	iii
Abstract.....	v
Acknowledgments	vii
Institutional Acknowledgments and Funding	ix
Index.....	xi
List of figures	xiii
List of tables	xvii
Abbreviations and symbols	xix
Chapter 1	21
Introduction.....	21
Numerical Methods.....	22
1.2 - Mechanical models applied to cancer cells proliferation.....	23
1.3 - Objectives.....	24
1.4 - Thesis structure	24
Chapter 2.....	27
Cell biology	27
2.1 - Cell History	27
2.2 - The nucleus	29
2.3 - The Composition of Cells	30
2.4 - Cell Cycle.....	32
2.5 - Aerobic Respiration.....	34
2.6 - Growth law.....	35
2.7 - Cell Senescence	37
2.8 - Cell Death and Cell Renewal: Apoptosis and Necrosis	38
Chapter 3.....	41
Cancer	41
3.1 - Socioeconomic.....	42
3.2 - Types of Cancer	46
3.3 - The development of Cancer	47
3.4 - Tumours Growth	49
3.5 - Causes of Cancer	50
3.6 - Selection of Cell Line	50

Chapter 4	53
Mathematical models	53
4.1 - Discrete Model.....	54
4.2 - Continuum Model	54
4.3 - Hybrid Model.....	55
Chapter 5	57
Methods.....	57
5.1 - Meshless Method: RPIM	57
5.2 - Reaction-diffusion model.....	64
5.3 - Algorithm scheme.....	68
5.4 - Discrete Equation System	71
5.5 - Developed growth law	73
Chapter 6	79
Model Validation	79
6.1 - Time scale.....	79
6.2 - Convergence study	82
6.3 - Influence domain study	85
6.4 - Integration scheme	88
6.5 - Gradient mesh.....	89
Chapter 7	93
Results and Discussion	93
Chapter 8	101
Conclusions and Future Works	101
References	103

List of figures

Figure 2.4 - Representation of a prokaryotic cell.	27
Figure 2.5 - Cells evolution. The current cells evolved from a prokaryotic ancestor [52].	28
Figure 2.6 - Animal cell structure. Animal cell are surrounded by a plasma membrane and within there are a nucleus, a cytoskeleton and many cytoplasmic organelles [52].	29
Figure 2.7 - Schematic of the nucleus structure [52].	30
Figure 2.8 - a) Cell duplication (Mitosis) in five steps. It occurs to healthy and cancer cells, but in cancer cell it happen more times than in healthy cells[2]. b) Representation of four phases: G1, S, G2 and M [2].	33
Figure 2.9 - Embryo cell cycle[52].	33
Figure 2.10 - (a) Cell reenter in G1 phase due to the addition of growth factors. (b) Place of checkpoints on the cell cycle.	34
Figure 2.11 - Aerobic respiration steps inside and outside the mitochondria.	35
Figure 2.12 - (a) Measurements were done in cells from hour 0 to 24 to obtain the size distribution along 2.5 cycles [61]. (b) Measures of cells growth during cell cycle progression using ERA [59]. (c) Dry mass quantity during cell cycle.	37
Figure 2.13 - Chromosomes lose their telomeres with each cell division until they stop to divide.	38
Figure 2.14 - Main differences between apoptosis and necrosis.	39
Figure 3.1 - In culture, normal cells proliferate until they reach a finite cell density at which point cells stop to divide and enter in G0 (quiescent). However, tumour cells continue to proliferate independent of the number of cells [52].	42
Figure 2.1 - Cancer mortality rates by deprivation quintile[42].	43
Figure 2.2 - Answer for the question if cancer (physical condition and treatment) lead to financial problems [44].	44
Figure 2.3 - Incidence of breast cancer by race 2006-2010 [1].	45
Figure 3.2 - Evolution and progression of a tumour [52].	48
Figure 3.3 - VEGF is secreted by cells deprived of nutrients, leading to the formation of new capillaries, improving blood supply.	49

Figure 3.4 - Division of a spheroid according to its healthy state due to availability of oxygen and nutrients. From the periphery to the centre, the concentration of oxygen and nutrients available decreases and consequently cell's ability to proliferate decreases also. ...	52
Figure 5.1 - (a) Problem domain with the essential and natural boundaries applied. (b) Regular nodal discretization. (c) Irregular nodal discretization.....	57
Figure 5.2 - (a) Fixed size circular influence-domain. (b) Variable size circular influence-domain.....	58
Figure 5.3 - a. Quadrilateral integration cell background mesh with 1 integration point. b. Triangular integration cell background mesh with 1 integration point. c. Quadrilateral grid background mesh with 2x2 integration points.....	59
Figure 5.4 - (a) Transformation of the initial quadrilateral integration cell into an isoparametric square shape and application of the 2x2 quadrature point rule followed by the return to the initial quadrilateral shape. (b) Transformation of the initial triangle integration cell into an isoparametric triangle shape and application of the 3-point quadrature point rule followed by the return to the initial triangle.	59
Figure 5.5 - (a) The cell (circle) in yellow represents low concentration and the medium in blue represents high concentration. (b) Due to diffusion, the concentration will be the same in circle and surround medium.....	65
Figure 5.6 - The arrows show the directions that molecules can take and the initial concentration in both sites.	65
Figure 5.7 - Preferential movement of the molecules in the boundary between the cell and the medium. There are more molecules pass from the medium to the cell than the other way around.	65
Figure 5.8 - General representation of the algorithm used by the RPIM software tested in this work.....	68
Figure 5.9 - General representation of the algorithm for the simulation of the cell division. This algorithm is contained into the block "Cell division" of the general algorithm presented in figure 6.8.....	69
Figure 5.10 - Scheme of the cell and medium domain and the periodic boundary condition. Molecules of oxygen and glucose can movement from one boundary $\tau_u^{(+)}$ to $\tau_u^{(-)}$ and vice versa.	70
Figure 5.11 - Comparison between data from literature and new ones formed with growth laws created in this work.....	77
Figure 6.1 - Computational costs between each time scale chosen in logarithmic scale.	81
Figure 6.2 - Time scale of 100 seconds comparing with 200, 600, 1000, 2000 and 6000 seconds. (a) ΔO_2 and (b) ΔGL	82
Figure 6.3 - Nodal discretization of a regular mesh. (a) 16x16 - 289 nodes, (b) 32x32 - 1089 nodes and (c) 64x64 - 4225 nodes.	83
Figure 6.4 - Convergence study to decide the best number of nodes to use. The values were obtained in the end of 5, 10, 15, 20 and 25 hours. (a) $\Delta Cs.O_2$ and (b) $\Delta Cs.GL$. Both axis are in logarithmic scale.	85
Figure 6.5 - Comparison between the number of nodes in the influence domain in the middle of the program, relatively to oxygen in (a) and to glucose in (b).	86

Figure 6.6 - Comparison between the number of nodes of the influence domain in the last iteration, relatively to oxygen in (a) and to glucose in (b).	87
Figure 6.7 - Comparison between integration scheme of 4x4 and 1x1, 2x2 and 3x3. (a) $\Delta I_s.O_2$ and (b) $\Delta I_s.GL$	89
Figure 6.8 - Gradient mesh increasing the number of divisions in the centre and consequently the number of nodes.	90
Figure 6.9 - Comparison between different meshes: (a) only between different regular meshes; (b) between the best divisions using regular mesh with gradient mesh.	91
Figure 6.10 - Computational costs between the number of nodes in logarithmic scale.	92
Figure 7.1 - Variation of oxygen during interphase of cell cycle, corresponding to (a) 33 minutes, (b) 5 hours, (c) 9 hours and (d) 14 hours of cell cycle.	94
Figure 7.2 - Variation of oxygen during mitosis phase of cell cycle, corresponding to (a) 15 hours, (b) 16 hours, (c) 17 hours and (d) 18 hours of cell cycle.	95
Figure 7.3 - Variation of glucose during interphase of cell cycle, corresponding to (a) 33 minutes, (b) 5 hours, (c) 9 hours and (d) 14 hours of cell cycle.	95
Figure 7.4 - Variation of glucose during mitosis phase of cell cycle, corresponding to (a) 15 hours, (b) 16 hours, (c) 17 hours and (d) 18 hours of cell cycle.	96
Figure 7.5 - (b)Oxygen and (c) glucose concentrations during cell cycle.	97
Figure 7.6 - Cellular growth during interphase at (a) 33 minutes, (b) 5 hours, (c) 9 hours and (d) 14 hours of cell cycle.	98
Figure 7.7 - Cellular growth during mitosis phase at (a) 15 hours, (b) 16 hours, (c) 17 hours and (d) 18 hours of cell cycle.	98
Figure 7.8 - After cell cycle, one cell result in two daughter cells (green and red).....	98
Figure 7.9 - Growth cell during all cell cycle using the exponential law. Both time and volume were normalized;.....	99

List of tables

Table 3.1 - Most popular types of cancer in United States [44].	46
Table 5.1 - Integration points coordinates and weights for triangular integration cells [209]......	60
Table 5.2 - Integration points coordinates and weights for quadrilateral integration cells' [209].....	60
Table 5.3 - Cell and medium properties used in the mathematical model [146]	69
Table 5.4 - Comparison between each growth laws created in this work (first line) and growth laws from literature (first column). "MM, 2009" corresponds to Mustafa Mir et al. 2011, "AT 2009" corresponds to Amit Tzur 2009 and "RK, 2013" corresponds to "R.Kafri 2013"	77
Table 6.1 - Computational costs between different time scales (time in each iteration).	80
Table 6.2 - Parameters analysed to compare regular and gradient mesh.	90
Table 7.1 - Parameters chosen for final analysis.....	93

Abbreviations and symbols

Abbreviation list

ATP	Adenosine Triphosphate
DNA	Deoxyribonucleic Acid
FAD	Flavin Adenine Dinucleotide
NAD	Nicotinamide Adenine Dinucleotide
NNRPIM	Natural Neighbour Radial Point Interpolation Method
RNA	Ribonucleic Acid
RPIM	Radial Point Interpolation Method

Symbols list

C_{O_2}	Oxygen concentration
C_{GL}	Glucose concentration
D_{O_2}	Oxygen diffusion
D_{GL}	Glucose diffusion
q_{O_2}	Oxygen consumption
q_{GL}	Glucose consumption

Chapter 1

Introduction

Cancer is the main cause of death in developed countries and the second in developing countries [1]. The incidence of cancer is increasing in developed countries resulting of: population aging and growth; smoking; physical inactivity; and non-balanced diets [1].

Presently, many researchers try to understand cancer's biology and mechanisms. Along the years, different types of cancer were discovered and it was concluded that several kind of tissues can have cancer. Researchers rapidly understood the difficulty of stopping the proliferation of cancer cells.

Due to the research activity, diagnostic tests and distinct treatments started to appear. Generally, the treatment depends on the diagnostic outcome:

- Surgery
- Chemotherapy
- Hormone therapy
- Targeted therapy
- Radiation therapy

The choice of the treatment depends largely on the type of cancer and the stage of the disease. It also depends on the health state of the patient, if the she/he wants to have children and/or other personal considerations [2].

Unfortunately, there is not a definitive cure for this disease, only diverse types of treatments that try to cure or delay the development of cancer. None of these treatments are really effective and they have side effects, in which patients become very fragile and limited.

Thus, it is necessary to create more incisive diagnoses and effective treatment options capable to reduce the treatment period and its side effects. Hence, this thesis aims to test a computational biomechanical meshless tool for the cellular proliferation of cancer cells. The tested software uses the RPIM, which is a precise and flexible meshless numerical method.

Numerical Methods

Similar to the Finite Element Method (FEM), meshless methods are discrete numerical methods that have been used on a large scale to solve problems from different scientific areas, such as mechanical engineering, astrophysics, fluid dynamics, economy and, more recently, biology. These phenomena are modelled by partial differential equations that need to be solved. However, those equations are frequently so complex that it is not possible to solve them using exact analytical techniques. Thus, discrete computational methods allow to obtain an approximate solution of the exact analytical solution [3].

1.1.1 - Finite Element Method

In numerical methods, FEM is the most popular because, as the literature shows, it can be applied to several science fields [4].

The approximation of the solution is done by dividing the problem domain into discrete simpler parts, called elements. The set of all the elements create a mesh in which is generated a relation between the elements [5]. After discretization of the problem, the field function of the domain is interpolated within each element in terms of an assumed approximation function (shape function). Lastly, the global domain equation system can be obtained by assembling each element's local equation system [5].

With the use of FEM in demanding computational mechanics fields, such as large deformations, complex geometries or fractures propagation, its limitations start to appear. These gaps are caused by building a mesh that hinders the treatment of discontinuities [6].

1.1.2 - Meshless Method

Meshless methods are an alternative approach to FEM, eliminating the necessity of the mesh. Meshless methods allow to discretize the problem domain using an unstructured nodal distribution and construct its interpolation functions using the concept of influence-domains instead of elements [6]. In addition, meshless methods allow to obtain more accurate variable fields (displacement, strain and stress fields).

Meshless method appeared in 1980 with the Generalized Finite Differences, by the application of the Finite Difference method into an arbitrary irregular mesh [6]. This work was followed by the Smoothed Particle Hydrodynamics Approach (SPH) in 1988, which was applied to model boundless astrophysical phenomena and flow dynamics. Then, SPH was improved, allowing to develop the Reproduced Kernel Particle Method (RKPM) [7].

Using distinct approximation techniques, different set of methods are obtained, such as the Diffuse Element Method (DEM), which has been afterwards modified and enhanced to the well-known element-free Galerkin method (EFGM) [7], [8]. The EFGM is a very precise and stable method, applied to both solids and fluid mechanics.

Along the years, other methods were developed, such as Petrov-Galerkin method (MLPG) [9], defined with local weak forms [20]; the method of the finite spheres (FSM) [10], considered as a special case of the MLPG; the Finite Point Method (FPM) [11] and the Radial Basis Function Method (RBFM), which used radial basis functions to approximate the variable fields [12]. RBFM is a ‘truly’ meshless method because it did not require an integration mesh and it used a strong formulation. However, all these methods have drawback: they use approximation functions instead of interpolation functions. This causes a problem, because approximation functions lack the delta Kronecker property [13], hinder the imposition of essential and natural boundary conditions.

Thus, to solve some of the limitations of approximation meshless methods, in the last years several meshless methods using interpolation functions were developed, such as Point Interpolation Method (PIM) [14], the Point Assembly Method [15], the Meshless Finite Element Method (MFEM) [16], the Natural Neighbour Finite Element Method (NNFEM) [17] or the Natural Element Method (NEM) [18]-[20].

From all these methods, PIM is the most attractive method, given the simplicity of its shape functions construction [13]. Additionally, PIM possesses the delta Kronecker property, allowing essential boundary conditions to be easily imposed. In order to improve PIM, Gaussian and multiquadratic radial basis functions were included in the formulation, originating the Radial Point Interpolation Method (RPIM) [21], [22].

Afterwards, RPIM combined with the natural neighbour concept, allowed the development of the Natural Neighbour Radial Point Interpolation Method (NNRPIM). The NNRPIM constructs its interpolation functions with a similar process to the RPIM and uses the natural neighbour interpolant concept to define nodal connectivity and create a background integration mesh. With this method, the interpolation functions are based in mathematical concepts, such as the Voronoï diagrams and the Delaunay tessellation [23].

1.2 - Mechanical models applied to cancer cells proliferation

The study of the mathematical models of cell biology using FEM began several years ago in the end of 20th century, although it was in the 21th century that this search line increase exponential [24].

In the late 90's, a work focus on tumour brain, developed a model of primary brain tumours that was applicable to a wide range of tumour types occurring within a variety of locations [24].

In the year 2000, a model was created to understand how epithelia and other planar collections of viscous cells might deform during events such as embryo morphogenesis and wound healing [25]. Zeng et al created a model of prostate cancer to improve the performance of prostate needle biopsy [26]. In 2005, a model of angiogenesis was created to understand cell proliferation and the factors that promote both [27]. Tumour necrosis and tissue invasion were studied via adaptive finite-element [28]. 3D growth of brain tumours was simulated as well as the invasion of glioblastomas in the brain and its mechanical interaction with the invaded structures. The model was compared to two magnetic resonance images to validate the created model [29]. Peterson et al. created a model for cell

proliferation and angiogenesis for 1D, 2D and 3D geometry in order to perform accurate and efficient simulations with a continuum-based tumour [30]. Brain tumour was modulated with FEM to understand the growth of abnormal cell concentration in a human subject at different positions [31]. Anotida et al. used those actin filaments to show cell expansion, cell contraction, cell translation and cell relocation [32]. Another model was done to solve a variety of cell pattern formation problems using details of cell shape, cell growth and shrinkage, cell birth and death, cell division and fusion [33]. After one year, Dong et al. proposed a mechanism of cellular growth controlled by the variation of the total energy on the volume and surface of the cells. The surface of each cell is divided by triangular elements and the nodal displacements determine the variation of the cellular surface and of the volume only when cells grow [34].

More recently, a methodology for lung tumour displacement was created to test the movement of the tumour during the breathing process [35]. It was possible for Mellal et al. to create a model for removal of tumours. The model showed a new method to control the direction of the temperature diffusion during thermal ablation [36]. In the current year, a finite element scheme for cancer invasion model was proposed. The model incorporates proliferation and haptotaxis effect of cancer cells. The numerical scheme is validated with numerical results took from literature [37].

Concerning meshless methods, there are few works related with tumour growth. One example is the research work from Dehghan and Mohammadi, in which a RBF collocation technique and the generalized moving least squares procedure are combined with a time dependent reaction-diffusion equations to describe a four-species tumour growth model. The results showed the ability of these techniques for solving the two and three-dimensional tumour growth equations [38].

1.3 - Objectives

Cancer cells have different characteristics and properties, comparing with healthy or normal ones, which allow the distinction between them. Those characteristics lead to specific mechanisms of growth, escaping death, getting nutrients and survival, which causes the cells to take hold of human organism, causing the death of many individuals.

Thus, the main goal of this work is to test a previous developed mathematical model of tumour growth, with the objective (in a near future) of predicting cancer evolution in the human body or *in vitro* experiments. With these models it will be possible to test drug efficiency, create new treatments and combine experiments with *in vitro* experiments.

1.4 - Thesis structure

This document was divided in 8 standard chapters in order to present the work developed in the dissertation, starting with the present introduction section, in which the numerical methods state-of-the-art and the objectives are presented.

The second chapter is about the literature review in order to introduce the topic. Here are presented the state-of-the-art concerning cell biology and cell cycle.

The third chapter explains how changes in cell biology lead to cancer.

The fourth chapter describes the types of mathematical models: discrete, continuum and hybrid models.

The fifth chapter introduces all methodologies used in this work. Starting with the numerical method (RPIM), which is fully presented and described in detail, together with reaction-diffusion model. The fifth chapter finishes with the developed growth laws.

The sixth chapter concerns the model validation, being useful to calibrate the several numerical parameters involved in the developed code.

The seventh one demonstrates the numerical results of this work obtained with the RPIM and the results are analysed and discussed.

This document ends with the eighth chapter in which conclusions and future works are presented.

Chapter 2

Cell biology

2.1 - Cell History

In biological science, it is fundamental to understand the molecular biology of cells.

First, it is important to know that cells are divided into two groups of cells: prokaryotic cells (

Figure 2.1), which lack a nuclear envelope, and eukaryotic cells, (Figure 2.3) which have a nucleus with genetic material that is separated from the cytoplasm. Prokaryotic cells are normally smaller and simpler than eukaryotic cells, their genomes are less complex, and they do not have cytoplasm organelles or cytoskeleton. Despite these differences, the two types of cells have the same basic molecular mechanisms in their lives, which indicate that all cells are descendent from a single primordial ancestor [52], [53]. It is reported that life started at least 3.8 billion years ago, approximately 750 million years after Earth was formed [52], [53].

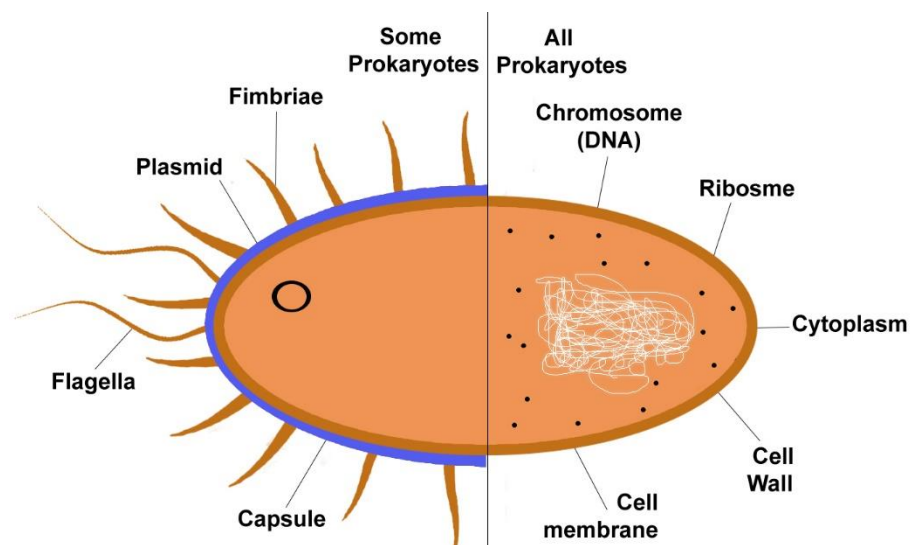


Figure 2.1 - Representation of a prokaryotic cell.

In eukaryotic cells, there are many compartments called organelles in which different metabolic activities occur, allowing these cells to function more efficiently [52], [53].

Investigations about eukaryotic and prokaryotic cells showed that organelles of eukaryotes are cells living inside others, a process known as endosymbiosis [52], [53]. That means that eukaryotic organelles probably evolved from prokaryotic cells living inside the ancestors of eukaryotes [52], [53] (Figure 2.2).

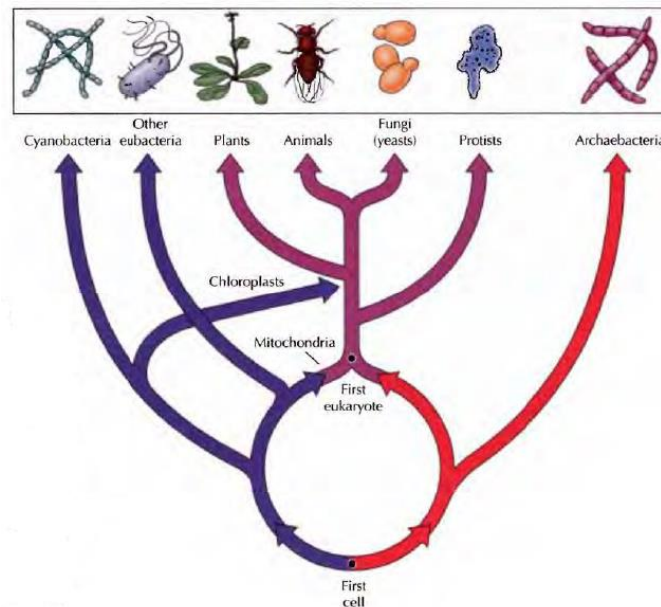


Figure 2.2 - Cells evolution. The current cells evolved from a prokaryotic ancestor [52].

In human cells, the organelle responsible for energy metabolism is the mitochondria, which generates most of the ATP (adenosine triphosphate) derived from the break-down of organic molecules. ATP is a molecule that stores energy that can be used in biological processes. The endoplasmic reticulum and the Golgi apparatus are responsible for sorting and protein transport destined for secretion, incorporation into the plasma membrane and into lysosomes. Besides this, they also synthesize lipids. Endoplasmic reticulum extends from the nuclear membrane to the cytoplasm and from this organelle, proteins are transported within small membrane vesicles to the Golgi apparatus. Another component of these cells is the cytoskeleton, which is a network of protein filaments along the cytoplasm. It determines the cell shape and the general organization of the cytoplasm. Cytoskeleton is also responsible for the movements of the cell, such as contraction of muscle cells, for the intracellular transport, positioning of organelles and for movements of chromosomes in cell division [52], [53].

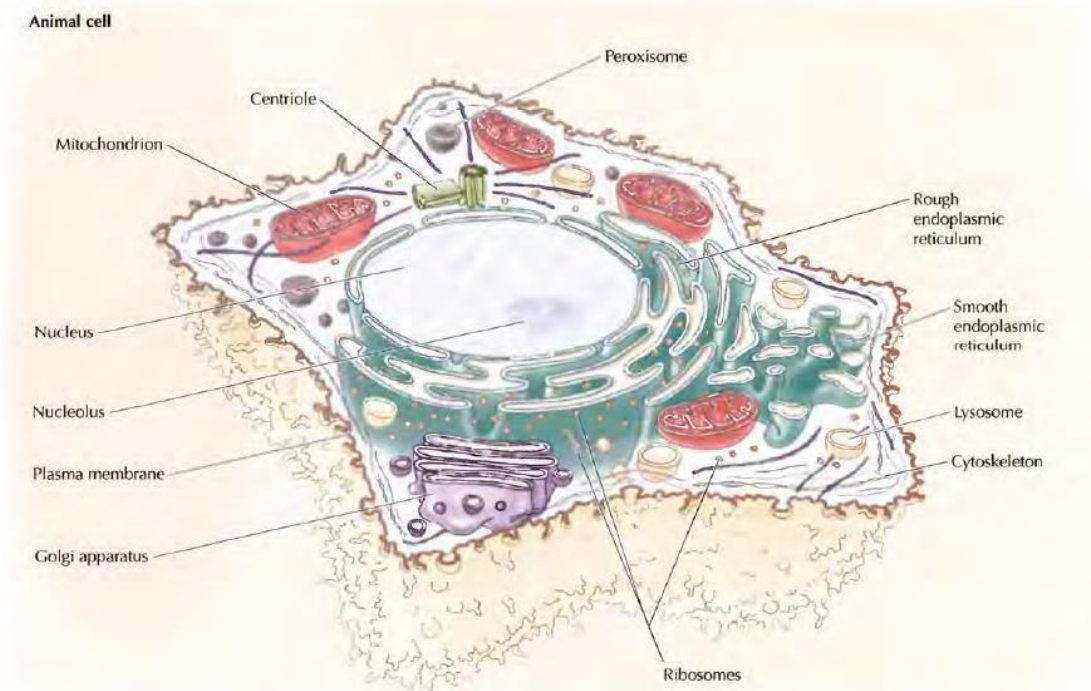


Figure 2.3 - Animal cell structure. Animal cells are surrounded by a plasma membrane and within there are a nucleus, a cytoskeleton and many cytoplasmic organelles [52].

2.2 - The nucleus

The nucleus is very important for storing the cell's genome and is the cell's control centre, because it is there that DNA replication, transcription and RNA processing (Figure 2.4) [52], [53].

It is the nuclear envelope that separates the contents of the nucleus from the cytoplasm, providing the structural framework of the nucleus. This separating is very important to prevent the passage of molecules between the nucleus and the cytoplasm, allowing to maintain the specific biochemical of this compartment. The nuclear pore complexes are the only channels that exist in the nuclear membrane which enables the regulated exchange of molecules between the nucleus and the cytoplasm, including the traffic of proteins and RNAs. Molecules can travel through the nuclear pore complex by two different mechanisms. Depending on molecule size, small molecules and some proteins (between 20 and 40 kD) pass freely through the pore in any direction by a process called diffusion. In contrast, macromolecules like most proteins and RNAs pass through by an active process in which macromolecules are recognized and selectively transported in a specific direction [52], [53].

The export of RNAs (mRNAs, rRNAs and tRNAs) is a critical and fundamental step in gene expression. Its transport is made by an active process, as already mentioned, which is an energy-dependent process [52], [53].

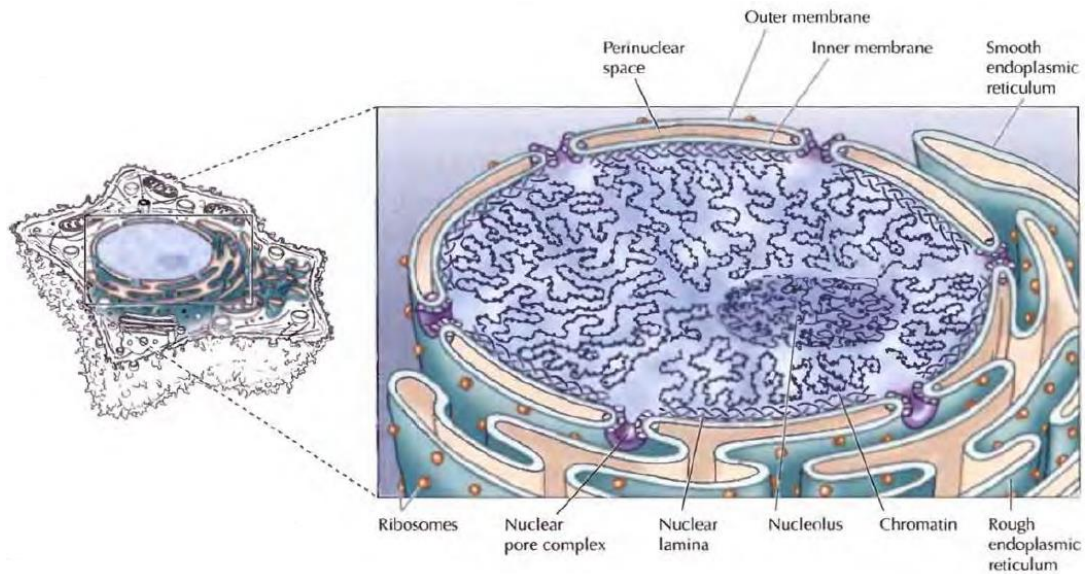


Figure 2.4 - Schematic of the nucleus structure [52].

The nucleus is surrounded by a nuclear envelope that consists in a complex structure of two concentric nuclear membranes, the inner and the outer nuclear membranes. These two membranes are very different and both important. The inner nuclear membrane transports specific proteins to the nucleus and the outer nuclear membrane is continuous with the endoplasmic reticulum, therefore its functionality is similar to the membranes of the endoplasmic reticulum and has ribosomes bound to its cytoplasm surface. The two membranes of the nucleus are connected by the nuclear pore complex [52], [53].

The nuclear lamina is a fibrous meshwork, essential to provide structural support to the nucleus, forming a lamina matrix. Connecting to this mesh, there is chromatin that corresponds to an organized large loop of DNA [52], [53].

Another nuclear body or component of the nucleus is the nucleolus. It is the place where rRNA transcription and processing occurs as well as aspects of ribosome assembly. Nucleolus is a ribosome production factory that is very important because cell require large number of ribosomes due to the protein synthesis [52], [53].

2.3 - The Composition of Cells

Cells are composed essentially by water (70%) and other components like inorganic ions and carbon-containing. The interactions between water and other constituents of the cell are very important and this is possible because water is a polar molecule. A molecule is polar when it has a positive and a negative charge. In water, hydrogen atoms have a positive charge and the oxygen has a negative charge, and, because of that, water molecules can establish hydrogen bonds between them or between other polar molecules and can interact with ions. All these molecules that interact with

water are soluble in water (hydrophilic). On the other hand, nonpolar molecules are poorly soluble and cannot interact with water (hydrophobic) [52], [53].

The organic molecules are unique constituents of cells and most of these organic compounds belong to one of these classes: carbohydrates, lipids, proteins and nucleic acids. Proteins, nucleic acid and carbohydrates are macromolecules formed by the joining of amino acids, nucleotides and simple sugars, respectively [52], [53].

Carbohydrates include simple sugars like glucose (major nutrients of cells) and polysaccharides that are storage forms of sugar and form structural components of the cell. Another important fact of carbohydrates is that they act as markers for a variety of cell recognition processes, adhesion of cells and transport of proteins [52], [53].

Lipids are the other major constituent of cells and they have three important functions in cells [52], [53]:

- Providing an important form of energy storage;
- Being the major components of cell membranes;
- Playing an important role in cell signalling as steroid hormones and as messenger molecules.

The simplest lipids are fatty acids (chains of hydrocarbon) and they can be divided in unsaturated fatty acids and in saturated fatty acids [52], [53].

Nucleic acids are the DNA and RNA that correspond to the principal informational molecules of the cell. Deoxyribonucleic acid (DNA) has a molecule that carries the genetic material, which is located in the nucleus in eukaryotic cells. Ribonucleic acid (RNA) participate in many cellular activities and according to the function RNA divided in [52], [53]:

- Messenger RNA (mRNA) carries information from DNA to the ribosomes for production of protein;
- Ribosomal RNA and transfer DNA have the function of protein synthesis.

Both DNA and RNA are polymers of nucleotides: adenine, guanine, cytosine, but DNA also has thymine and RNA has uracil. DNA is formed by a double-stranded molecule consisting of two polynucleotide chains in opposite directions. In contrast, RNA is formed by a single-stranded molecule [52], [53].

Each cell has several thousand different proteins which perform a big variety of functions. Concerning macromolecules, proteins are the most diverse and they have functions like [52], [53]:

- Serving as structural components of cells and tissues;
- Acting in the transport and storage of small molecules;
- Acting as defender against infections;
- Passing information between cells;
- Acting as enzymes.

2.4 - Cell Cycle

The study of cancer started a long time ago. Ward researched in many texts of ancient Greece, Egypt and Rome and he showed that the early physicians were capable of making a correct diagnosis and performing a therapy [54].

Interestingly, the research about cancer, its causes and cure, has not only helped cancer study but also a much wider area of medical knowledge, leading to discoveries about cell biology [55].

The most fundamental characteristic of cells and all living organisms is their self-reproduction. In cell cycle each parental cell divides into two daughter cells in the end of the cycle (Figure 2.5). These new cells can grow and also divide into two, giving rise to a new cell population formed by many cells that grow and divide themselves [52], [56]. So, consecutive cell cycles (where cell grow and divide) results in the development of a single fertilized egg into the approximately 10^{14} cells that represent the human body [52], [56].

The division of cells must be carefully regulated and coordinated with both cell growth and DNA replication to ensure the formation of intact genomes in all cells. However, there are defects in cell cycle regulation that cause abnormal proliferation of cancer cells, and, because of that, studies of the cell cycle and cancer have become closely interconnected [52], [56].

The main processes in cell cycle are: cell growth, DNA replication, distribution of the duplicated chromosomes to daughter cells and cell division. Cell growth is a continuous process and DNA is synthesized during one phase of the cell cycle [52], [56].

A typical eukaryotic cell cycle can be observed in human cells culture, which divides approximately every 24 hours. Interphase and mitosis are the two parts that form the cell cycle. Mitosis is the nuclear division and it means that in this phase occur the separation of daughter chromosomes and cell division. From 24 hours of cell cycle, only one hour is spent in mitosis; the rest of time is spent in interphase that corresponds to the period between two mitoses. During interphase, the cell grows, DNA is replicated and chromosomes are decondensed in the nucleus. All processes in this phase prepare cells to division (mitosis). During interphase, the growth is constant and the size in the end of interphase is twice the size in the beginning of the same phase. Although growth is a continuous process, there are checkpoints events that allow to divide interphase in three phases: G1, S and G2 [52], [56].

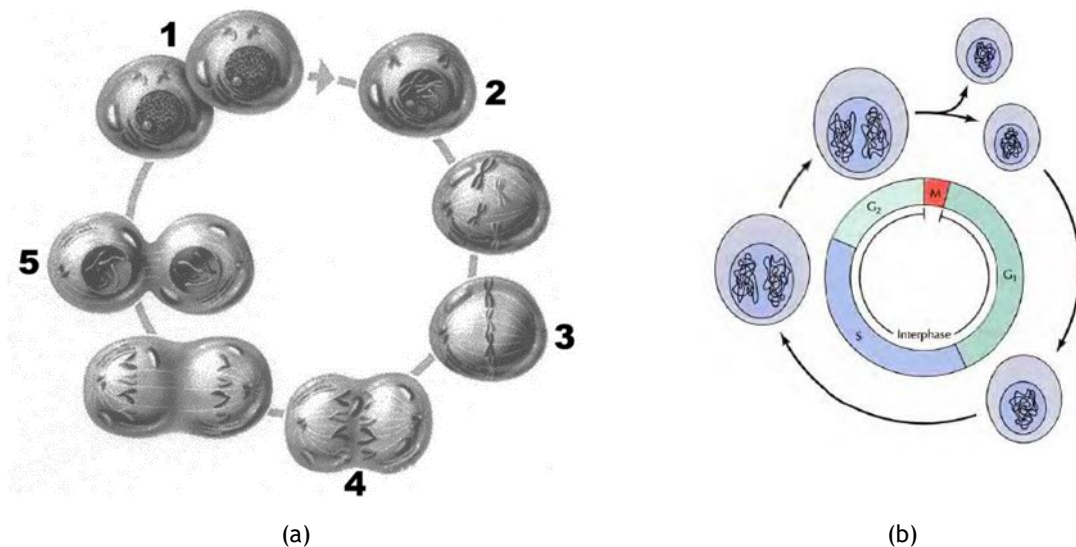


Figure 2.5 - a) Cell duplication (Mitosis) in five steps. It occurs to healthy and cancer cells, but in cancer cell it happen more times than in healthy cells[2]. b) Representation of four phases: G₁, S, G₂ and M [2].

When mitosis ends, G₁ phase (gap 1) is the following phase, which corresponds to the interval between mitosis and initiation of DNA replication. Here the cell is metabolically active and grows continuously. In S phase (synthesis) occurs DNA replication which is followed by the G₂ phase (gap 2) where cell continues to grow and proteins are synthesized in preparation for mitosis [52], [56].

Depending on cells type, cell cycle phases have different durations. For a typical proliferating human cell with a total cycle time of 24 hours, the G₁ is about 11 hours, S phase about 8 hours, G₂ phase about 4 hours and mitosis only 1 hour. However, other types of cells like budding yeasts can complete cell cycle in 90 minutes. In contrast, embryo cell cycle completes a cycle in 30 minutes, because cells do not grow and instead divide into progressively smaller cells. So, there is no G₁ or G₂ phase, only S phase and mitoses [52], [56] (Figure 2.6).

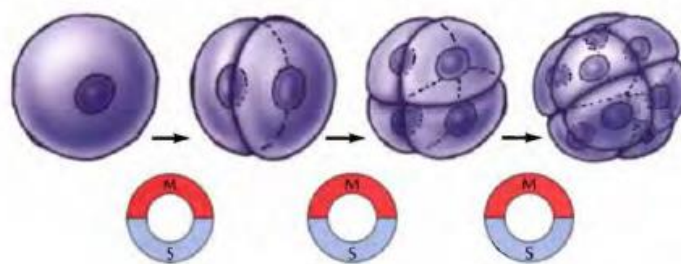


Figure 2.6 - Embryo cell cycle[52].

In adult animals, some cells stop dividing like nerve cells, and many other cells divide only occasionally to replace cells that have been lost because of injury or cell death as skin fibroblasts or liver cells. These types of cells exit G₁ to enter a quiescent stage called G₀, where cells remain metabolically active (low metabolism) but no proliferative unless they receive some specific

extracellular signals (Figure 2.7a). Other reason for cells to enter in G₀ is when growth factors are not available [52], [56].

Cell proliferation is regulated by several signals that act to inhibit cell cycle progression, like nutrients, growth factors and controllers of cell cycle. These controllers are called cell cycle checkpoints and they goal is to prevent the entrance into the next phase of the cell cycle until the events of the previous phase have been completed. There are four checkpoints [52], [56](Figure 2.7b):

- In G₁ phase to check if DNA is damaged;
- In S phase to check if there is unreplicated or damaged DNA;
- In the end of G₂ phase to check the same in S phase;
- In the end of M phase to check if there is chromosome misalignment.

If one of these errors occurs during the cell cycle, the cell is arrested in the corresponding phase to allow the error repair before the cell enters the next phase.

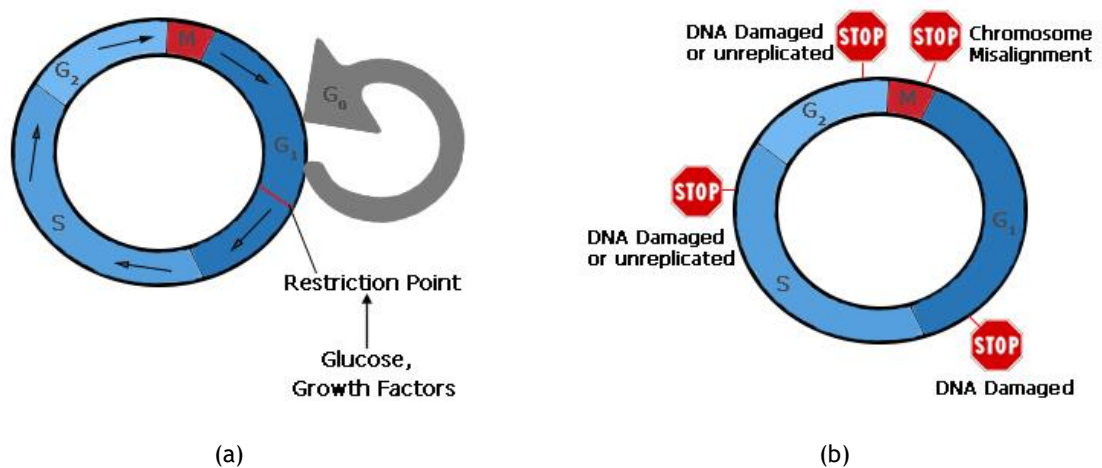


Figure 2.7 - (a) Cell reenter in G₁ phase due to the addition of growth factors. (b) Place of checkpoints on the cell cycle.

2.5 - Aerobic Respiration

Respiration is essential because all live cells of the body need oxygen and release carbon dioxide. Oxygen is obtained by pulmonary respiration and distributed along the cells, which is used in the final phase of a series of reactions in aerobic respiration. In this process, the energy is extracted from food molecules [57]. In human diet, glucose is the main carbohydrate, which is a sugar that is in the blood to insure all cells have energy. Glucose is so fundamental that it is present in all tissues. For example, it is an exclusive energy supply of red blood cells and brain [52], [58].

Aerobic respiration is divided in three phases [57]:

- Glycolysis is the anaerobic phase where glucose is broken in two pyruvic acid molecules by a process denominated oxidation (loss of electrons). In this step carbon dioxide and two

ATP molecules are released. Pyruvic acid enters in mitochondria where it reacts with coenzyme A to form acetyl-coenzyme A.

- Cycle of Krebs is a cycle where acetyl-coenzyme A reacts with oxaloacetate to originate citric acid. This is degraded by many enzymes to originate oxaloacetate. This molecule reacts with acetyl-coenzyme A and so on. During these reactions, many products are formed. Per glucose molecule 6 NADH_2 (nicotinamide adenine dinucleotide) molecules, 2 FADH_2 (flavin adenine dinucleotide) molecules, 2 ATP molecules and 4 CO_2 molecules are produced.
- The NADH_2 and FADH_2 are used in the breath chain or chemiosmosis. For each NADH_2 molecule in reaction with oxygen, ADP and phosphate occur the formation of 3 ATP molecules; for each FADH_2 molecule in reaction with the same compounds, originate 2 ATP molecules.

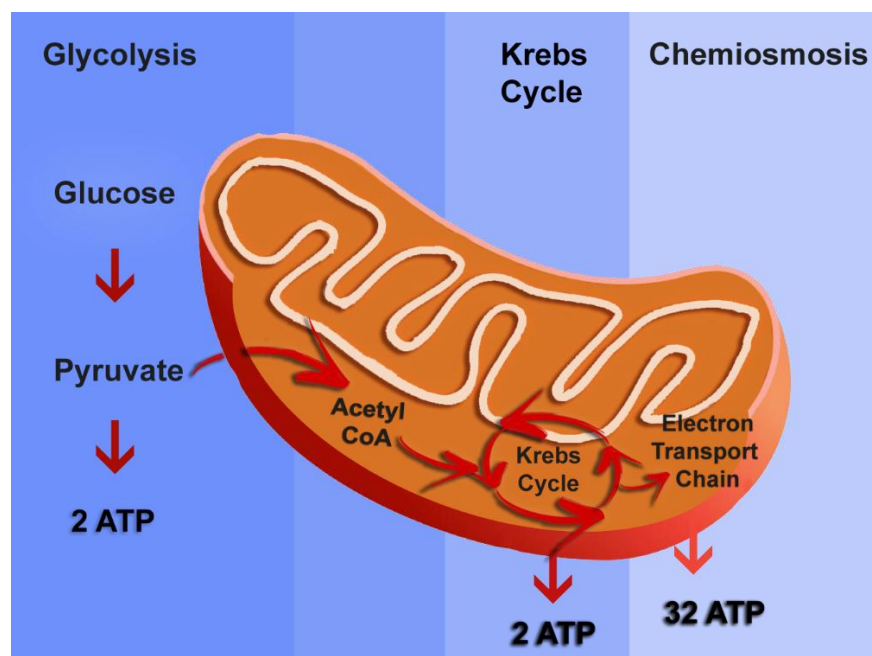
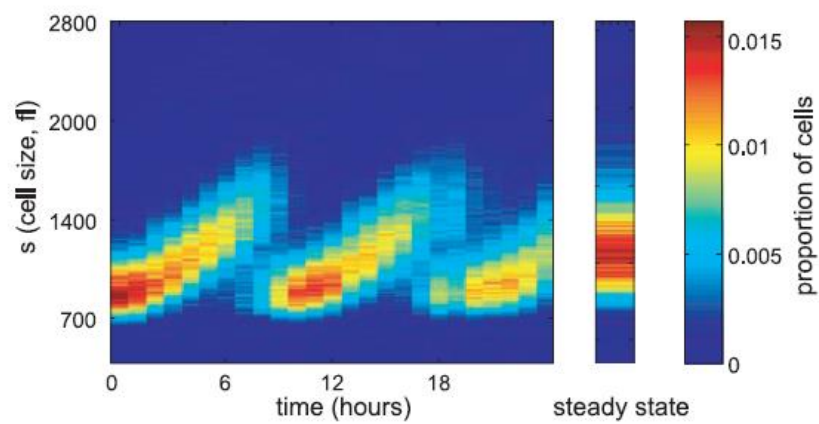


Figure 2.8 - Aerobic respiration steps inside and outside the mitochondria.

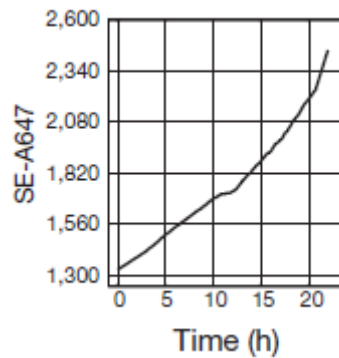
2.6 - Growth law

Determining the growth of single cells along cell cycle is a big challenge of contemporary cell biology. Cell size is a characteristic of cell physiology and pathology and because of that is important to understand how cell growth is regulated [21],[22]. In the past, it was assumed that the growth rate might be constant, leading to a linear increase in size, which does not imply the regulation required to maintain homeostasis [60]-[63]. Nowadays, it is known that growth rate is exponential [60]-[63].

There are many techniques that prove the relationship between growth rate and cell cycle phases and show the exponential growth. For example, Amit Tzur et al. calculate the dependence of growth rate with time using a method based on asynchronous population at steady state proposed by Collins and Richmond in 1962 [64], Figure 2.9(a). Other methodology was proposed by Ran Kafri et al. called ERA where authors calculated the dynamics of cell growth and cell cycle progression [59], Figure 2.9(b). Mustafa Mir et al. developed a new methodology in their laboratory called spatial light interference microscopy (SLIM), which combined with fluorescence imaging became a special method to study the cell cycle-dependent growth [60], Figure 2.9(c). All authors show that cell growth is exponential.



(a)



(b)

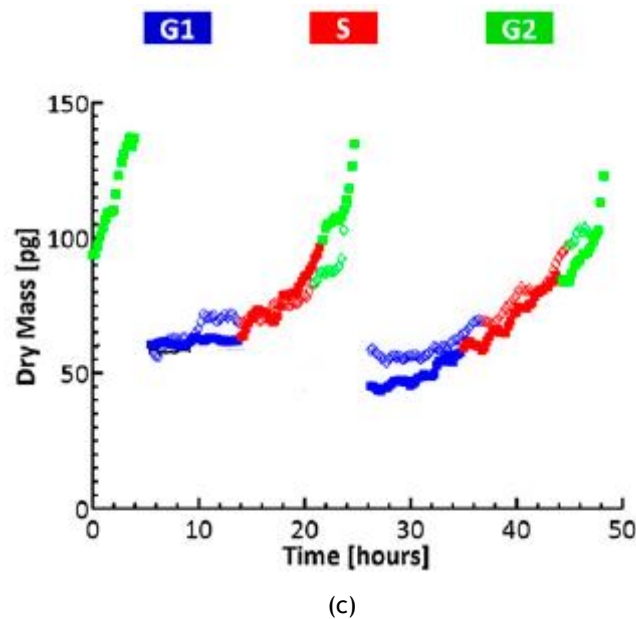


Figure 2.9 - (a) Measurements were done in cells from hour 0 to 24 to obtain the size distribution along 2.5 cycles [61]. (b) Measures of cells growth during cell cycle progression using ERA [59]. (c) Dry mass quantity during cell cycle.

2.7 - Cell Senescence

Cell division is limited even in ideal conditions of growth, so every cell has an intrinsically limited proliferation lifespan. When cells stop to divide, they enter in a quiescent state denominated senescence which is caused by a progressive cut of chromosome telomeres with each cell cycle. The replication process is incomplete and telomeres will shorten at each cell division [65], [66]. Telomeres are DNA sequences that are repeated at the ends of chromosomes [67]

Figure 2.10). The only way that prevents this event is by telomerase, which is an enzyme that adds the telomere at the chromosome end during cell division. However, most mammalian somatic tissues do not have telomerase and, therefore, cells enter in senescence. Because of that it was proposed that reduction of the telomeres could be a “clock” for cell division [67].

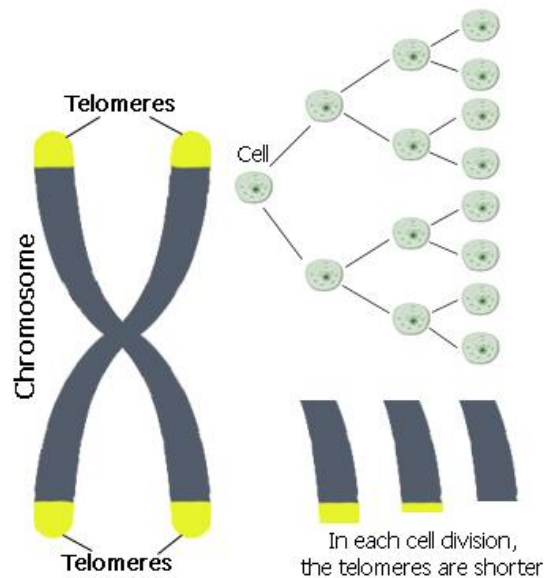


Figure 2.10 - Chromosomes lose their telomeres with each cell division until they stop to divide.

2.8 - Cell Death and Cell Renewal: Apoptosis and Necrosis

As previously mentioned, animal development begins with the rapid proliferation of embryonic cells, which then differentiate to produce many specialized types of cells that constitute adult tissues and organs.

Cells can die due to some unpredictable traumatic events, such as exposure to toxic chemicals and ultraviolet rays or as a result of normal physiological process of programmed cell death, which is preceded by a series of cellular changes known as apoptosis [52], [53] (Figure 2.11).

Apoptosis is also responsible to maintain constant the cell number in tissues and provides a defence mechanism by which damaged and dangerous cells can be eliminated. An example is DNA damage that induces programmed cell death and it may eliminate cells carrying potentially harmful mutations, which may lead to the development of cancer. Abnormalities of cell death are related with a variety of illnesses, including cancer, neurodegenerative disorders like Parkinson's and Alzheimer's disease and autoimmune disease. Therefore, programmed cell death plays a fundamental role in regulating the associations between cells in tissues. Apoptosis consists in a set of events that occur in order and it is regulated by specific genes [52], [68]:

- Cellular shrinkage;
- Condensation of the nuclear chromatin;
- Rupture of the cortex and bleb formation;
- DNA fragmentation;
- Cytoplasmic vacuolisation;
- Cell lysis.

All components of the cell are encapsulated in autophagosomes and they travel through the cytoplasm until they find a lysosome to merge with it, forming an autolysosome. Then the components inside are degraded [52], [53].

For a long period, necrosis was considered to be a cell death that occurs only by accident in response to physicochemical aggressions. However, new research show the existence of multiple pathways of regulated necrosis, which is a cell death process controlled genetically and results in cellular leakage characterized by cytoplasmic granulation and organelle and/or cellular swelling [68], [69] (Figure 2.11). The cell membrane rupture and the components (not functional) of the cells are released into cytoplasm, causing inflammatory reactions in neighbouring tissues in order to eliminate death tissues and to perform tissue reparation. The digestion is made in cytoplasm by two processes: autolyse (destruction by the action of enzymes of the cell itself) and heterolysis (enzymes derivated from leukocytes or white blood cell) [52], [53].

Necrosis can be caused by microorganisms, virus, chemical agents and others or may occur when apoptosis is blocked [68].

Another difference between the two process of death is the intracellular ATP levels: high ATP levels enable apoptosis and low ATP levels favour necrosis [70].

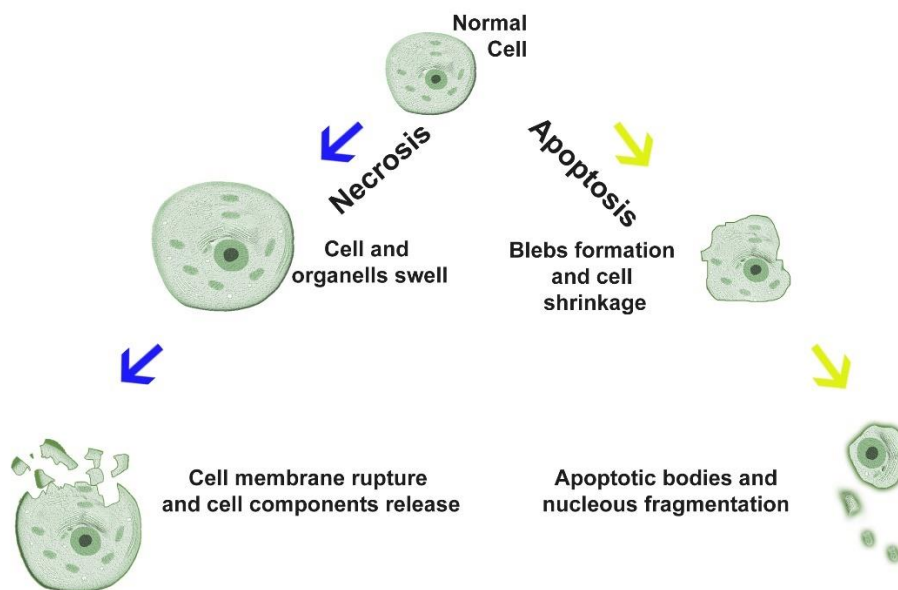


Figure 2.11 - Main differences between apoptosis and necrosis.

Chapter 3

Cancer

Cancer is a result of defects in the regulatory mechanisms that govern normal cell behaviour. Processes such as proliferation, differentiation and survival of individual cells are carefully regulated in multicellular organisms to maintain the organism healthy. However, this regulation is lost in cancer cells, which grow and divide uncontrolled and can spread throughout the body and interfere with the function of normal tissues and organs (Figure 3.1). These problems in cancer cells are the result of accumulated abnormalities in cell regulatory systems and it is why it is possible to distinguish cancer from normal cells. In cell cycle, cancer cells divide faster, because checkpoints have problems, so they continue to divide when they should not [52], [53]. For example, there are several problems in genes that promote proliferation (oncogenes), apoptosis (tumor suppressor genes) and, furthermore, regulatory signals may be ignored by these cells. These changes can be inherited from the individual's parents or they can appear during the individual's lifetime, as a result of errors that occur when cells divide or due to DNA damage. DNA damage can be caused by environmental exposures like chemicals in tobacco smoke and radiation (ultraviolet rays from the sun) [2], [71].

Therefore, in cancer cells the normal process of growing and dying is malfunctioning and that is why cells become more and more abnormal, old or damaged instead of dying [2], [72]. Cells proliferate and avoid death, changing their microenvironment to favour their survival, which may lead to migration and metastasize in regions far from the primary tumour (process called metastatic cancer). It may kill the host due to physical obstruction or organ malfunction. Additional mutations and epigenetic changes within an abnormal cell population may also cause a different subgroup of cells that differ in their characteristics. Cells proliferate out of control and form microscopic nodules, however, they do not have access to the vascular network. So, they receive nutrients and growth factors via diffusion through the healthy tissue. Most cancerous tumours form solid tumours, which are masses of tissues. However, some cancers (such as blood cancer) generally do not form solid tumours [2], [72], [73].

Cancer cells have a specific characteristic that helps them to proliferate *ad eternum*. They reactivate telomerase that prevents cells to enter in senescence and maintains cancer cells viability [74], because telomerase prevents DNA damage activation responses and cell arrest (cell cycle stop) [75], [76].

There are other important differences between healthy and cancer cells [2], [52]:

- Healthy cells are specialized, which means that cells mature into very distinct cell types with specific functions. Cancer cells are less specialized, because they are blocked at an early stage of differentiation, which is consistent with their continued active proliferation;
- Cancer cells ignore signals to stop dividing or to begin apoptosis;
- Cancer cells can influence healthy cells, molecules and blood vessels that surround and feed a tumour. For example, cancer cells can induce healthy cells to form blood vessels that will supply tumours with oxygen and nutrients and remove waste products from tumours.
- Cancer cells can also evade the immune system, organs, tissues and specialized cells, such as cells that protect the body from infections. They are also able to hide themselves from the immune system, and avoid destruction.
- Cancer cells are less adhesive due to few cell surface adhesion molecules, which allows them to invade and metastasize.

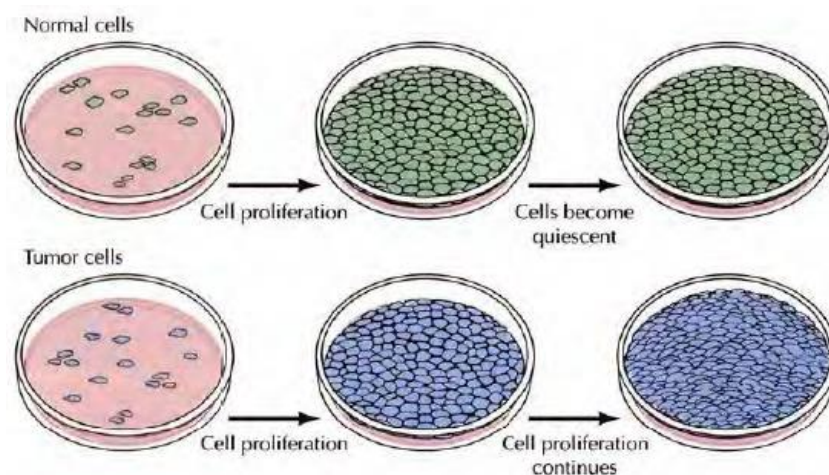


Figure 3.1 - In culture, normal cells proliferate until they reach a finite cell density at which point cells stop to divide and enter in G0 (quiescent). However, tumour cells continue to proliferate independent of the number of cells [52].

3.1 - Socioeconomic

Cancer is the main cause of death in developed countries and the second one in developing countries [1]. The incidence of cancer is increasing in developed countries resulting of: aging and growth population; smoking; physical inactivity; and non-balanced diets [1]. These facts are proven

in a report on worldwide cancer rates by the World Health Organization's International Agency for Research on Cancer [39] which shows that North America leads the world in the rate of cancers diagnosed, followed by Western Europe, Australia and New Zealand. Other study published in Australian Institute of Health and Welfare (1999) demonstrates that it is expected that one in three men and one in four women will be directly affected by cancer in the first 75 years of life [40]. Currently it is estimated that 29% of male and 25% of female die due to cancer[40]

In the United Kingdom, for example, cancer is the cause of one in four deaths and 160,000 people die because of this disease every year [40].

However, cancer not only affects individuals but also their families and the economy. In 2015 a study showed that over half of people who are adults under the age of 65 will be diagnosed with cancer at some point in their lifetime [41].

Nowadays, many investigations conclude that both cancer incidence and cancer mortality are related to socio-economic status. The incidence of most cancer types is higher among people from more deprived areas than least deprived groups [42] (Figure 3.2).

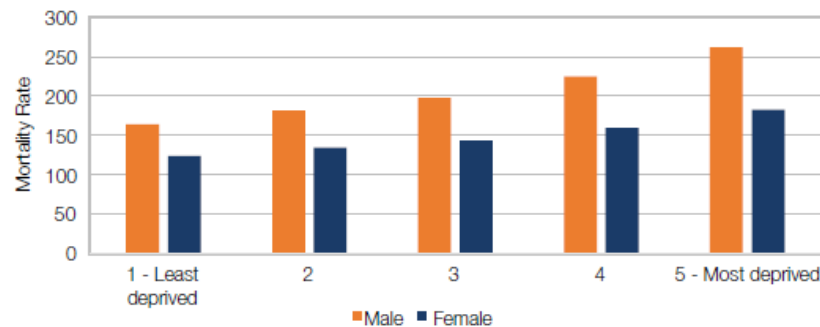


Figure 3.2 - Cancer mortality rates by deprivation quintile[42].

Depending on age and gender, different types of cancer can appear. For example, leukaemia, brain tumours and lymphomas are the most common in children, while in women appear more frequently cancer of the ovaries, uterus and cervix and in men cancer of the testis. However, breast, lung, bowel and prostate cancers are the most common in adults over the age of 50 and they correspond to more than half the cancer incidence [40]. Cancer incidence has increased over the years due to population ageing, since cancer is more common among older age groups [40].

Cancer has a huge impact on people's lives, not only physically but also emotionally. Physically, treatments can result in fatigue, nausea, constipation, diarrhoea, hair loss, infection, scarring and weight loss [42]. Emotionally because diagnosis is often faced with shock, followed by fear, sadness, while other people feel anger and bitterness, or loneliness and isolation [42].

As Figure 3.3 shows, cancer affects the economy of a country due to many reasons.

First, there are many patients who die because of it and this removes many productive workers from the job market [43].

Second, there are the consequences of non-fatal cancers. When people are diagnosed with cancer, they leave their jobs because of treatments and recuperation. The majority of these people do not return to work or work in part time, because of the after effects of cancer and cancer treatments. Patients live with pain, fatigue, mental health problems and also health problems as a result of chemotherapy or radiation therapy [43]. These changes may reduce a cancer survivor's economic productivity, which makes the patient's life difficult [42].

Third, the direct medical costs (total of all health care costs) by the Agency for Healthcare Research and Quality for cancer is approximately [44]:

- 50 % for hospital outpatient or doctor office visits;
- 35% for inpatient hospital stays;
- 11% for prescription drugs.

Besides the effect on the country, most patients suffer economic problems in their lives because of their physical conditions and medical treatment. As already mentioned, patients do not work or work less, so they earn less money but need more money for treatments [43]. Also, uninsured patients and those from ethnic minorities are more likely to discover cancer at a later stage, when treatment can be more extensive, more costly and less successful [44].

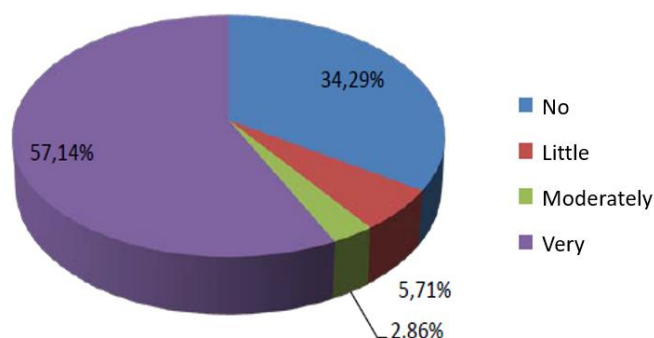


Figure 3.3 - Answer for the question if cancer (physical condition and treatment) lead to financial problems [44].

Many factors can influence the incidence of cancer which explains why some individuals have and others don't. Excluding the biology effect, Simpson and Brown showed that racial and social inequalities may affect the lifestyle choices which can lead to overweight, lack of breastfeeding, poor diet and lack of exercise. All these life options can increase the probability of cancer appear in these people [45].

Depending on race and financial situation, people have better living conditions have the possibility to detect cancer in an early stage and have more treatments available. However, a study showed that

women with higher income and education levels have a higher risk to have breast cancer because of their life style [46]-[48] (Figure 3.4):

- Have their first child at a later age;
- Use menopausal hormone therapy;
- Have fewer children;
- Drink alcohol.

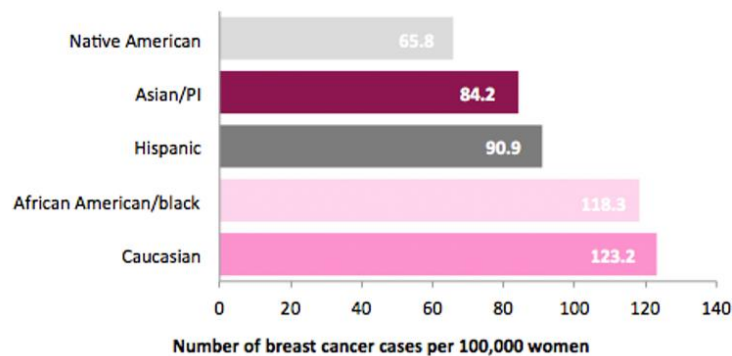


Figure 3.4 - Incidence of breast cancer by race 2006-2010 [1].

A very important help for patients with cancer and their families is a psychological support during all treatment and recuperation. This is essential to minimize the high rates of psychopathological disorders that make the recovery process very difficult. According to many scientific articles, it was verified that besides contributing to increase life quality of patients, it also helps in [49], [50]:

- Decreasing in clinical recovery time;
- Better control perception of cancer;
- Decreasing somatizations (effect of transferring to the body a psychological problem);
- Bigger indices of fight cancer;
- Decreasing in polymedication;
- Decreased rates of depressive and anxious disorders.

All these factors can increase the survival time of the patient by stimulating the immune system function. Therefore, psychological support can be a strong therapeutic ally of extreme importance.

This support is also fundamental for families of patients with cancer. For example, when a parent of a child has cancer, the child will feel alone and sad, because the parent won't be able to give appropriate attention to the child. Children do not understand some behaviours and attitudes that need to be explained to the children by someone qualified [51].

3.2 - Types of Cancer

The abnormal proliferation characteristic in cancer exists in different kinds of cells in the body, so there are more than a hundred different types of cancer (Table 3.1) [52], [53]. They differ in their behaviour and response to treatment. The principal question in cancer pathology is if tumour is malignant or benign. The first are cancerous tumours, which means they can spread into or invade nearby normal tissues. Then as tumours grow, some cancer cells can break off and travel to distant places in the body through the blood or the lymph system (which contains a collection of vessels that carry fluid and immune system cells) and form new tumours far from the original tumour. Benign tumours do not spread to distant body sites, nor invade normal tissues, but they can be quite large. An example is the common skin wart. When they are removed, they usually do not grow again whereas malignant tumours sometimes do [2], [52], [73].

Table 3.1 - Most popular types of cancer in United States [44].

<i>Cancer site</i>	<i>Cases per year</i>	<i>Deaths per year</i>
<i>Prostate</i>	232.100 (16.9%)	30.400 (5.3%)
<i>Breast</i>	212.900 (15.5%)	40.900 (7.2%)
<i>Lung</i>	172.600 (12.6%)	163.500 (28.7%)
<i>Colon/rectum</i>	145.300 (10.6%)	56.300 (9.9%)
<i>Lymphomas</i>	63.700 (4.6%)	20.600 (3.6%)
<i>Bladder</i>	63.200 (4.6%)	13.200 (2.3%)
<i>Skin (melanoma)</i>	59.600 (4.3%)	7800 (1.4%)
<i>Uterus</i>	51.200 (3.7%)	11.000 (1.9%)
<i>Kidney</i>	36.200 (2.6%)	12.700 (2.2%)
<i>Leukemias</i>	34.800 (2.5%)	22.600 (40.%)
<i>Pancreas</i>	32.200 (2.3%)	31.800 (5.6%)
<i>Subtotal</i>	1103.800 (80.4%)	410.800 (72.1%)
<i>All sites</i>	1373.000 (100%)	570.000 (100%)

Malignant and benign tumours are classified according to where they appear, this means, type of cells and organ. For example, erythroid leukemias arise from precursors of erythrocytes or red blood cells and fibrosarcomas from fibroblasts [52], [53].

Most cancers can be classified into three main groups: carcinomas, sarcomas and leukemias or lymphomas. Carcinomas are malignancies of epithelial cells and represent approximately 90% of human cancers; sarcomas are rare in humans and are solid tumours of connective tissues like muscle, bone, cartilage and fibrous tissue. Leukemias and lymphomas correspond approximately 7% of human

malignancies and appear in blood-forming cells (leukemia) and in immune system cells (lymphoma) [52], [53].

3.3 - The development of Cancer

Tumour clonality, which is the development of tumours from single cells that proliferate abnormally, is one of the fundamental features of cancer [52] (Figure 3.5).

At the cellular level, cancer involves processes like mutation and selection of cells with progressively increasing capacity for proliferation, invasion, metastasis and survival. So, the first step is tumour initiation that results from a genetic alteration leading to abnormal proliferation of cells, forming a population of clones. Tumour progression continues with mutations that occur within cells of the tumour population, conferring selective advantage to the cell, such as rapid growth. In this step, there is a process called clonal selection where some clones from tumour cells have characteristics that confer advantage in relation to the other tumour cells, so they grow faster, have better properties of metastasis and invasion. Therefore, tumours become more rapid-growing and increasingly malignant [52].

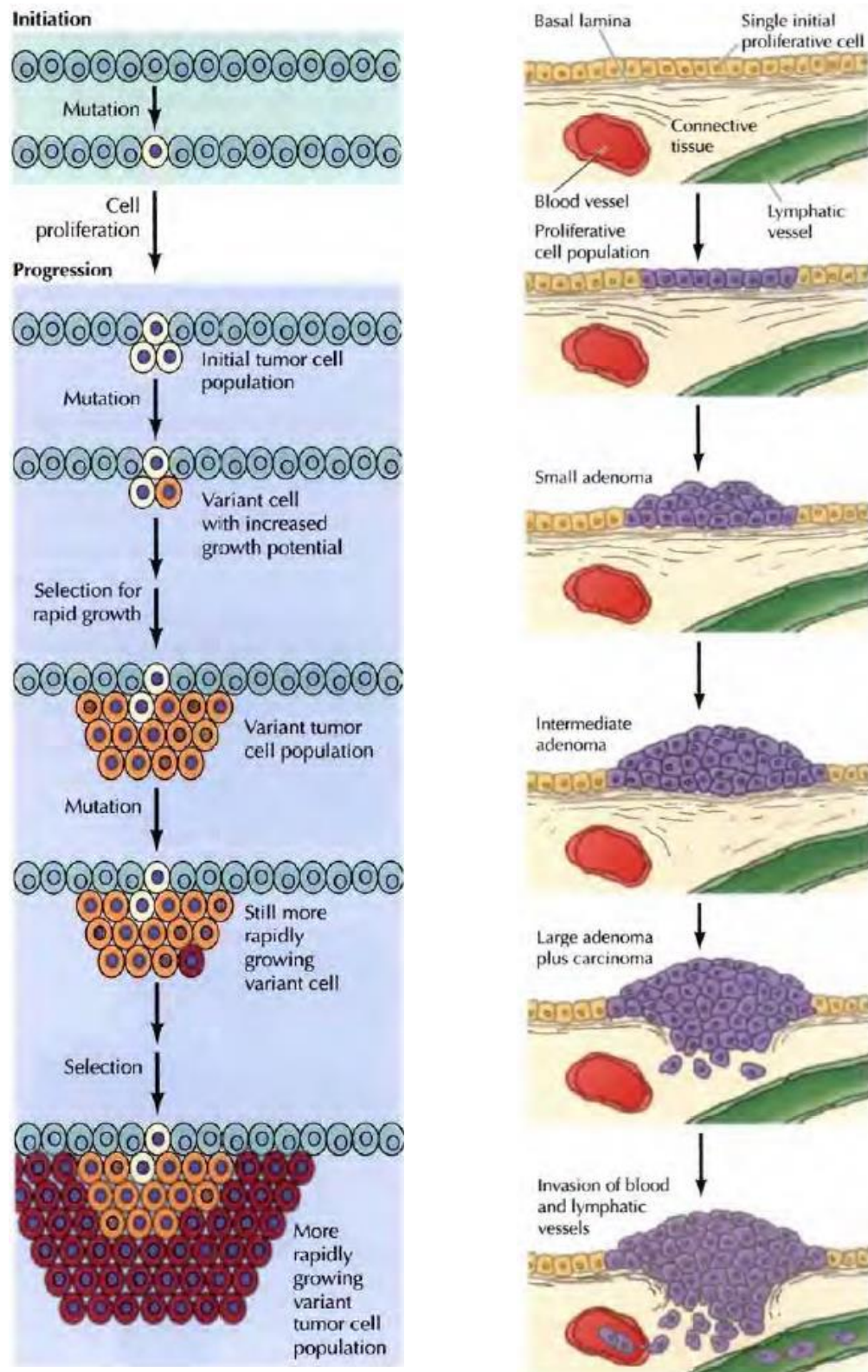


Figure 3.5 - Evolution and progression of a tumour [52].

3.4 - Tumours Growth

The aspects that tumor growth involve are [77]:

- Rapid cancer cell proliferation that lead to tumor solid formation;
- Metabolic activity in which cells consume nutrients like oxygen and glucose and result byproducts;
- Mechanical interactions between tumor mass, the extracellular matrix (ECM) and surrounding tissues;
- Formation of new tumor colonies due to cell migration.

The number of tumour cells increase in the nodules and their accumulation may cause acute and chronic lack of oxygen, which leads to hypoxia, and lack of nutrients, such as glucose leading to hypoglycemia, and accretion of metabolites, such as lactic acid that leads to acidosis [78]-[81]. Due to these effects, cells under stressful conditions may induce angiogenesis by release of pro-angiogenic growth factors, such as vascular endothelial growth factor (VEGF) (Figure 3.6). When this happens, the tumour can grow larger and, as a consequence, the neo capillaries can be used to send cancer cells to the blood flow, leading to the formation of a tumour in another part of the body (metastasis) [52], [53].

The tumor-induced microvasculature exacerbates hypoxia, hypoglycemia and acidosis, because, unlike the normal vasculature, the new blood vessels tend to be highly disorganized and poorly functional [82], [83], leading to an unequal distribution of oxygen and nutrients [84], [85]. These conditions increase the risk of cancer spreading through the body [86]-[90] and can select for apoptosis-resistant tumour cells, which induces the formation of blood vessels, increasing invasiveness [78], [91]-[98].

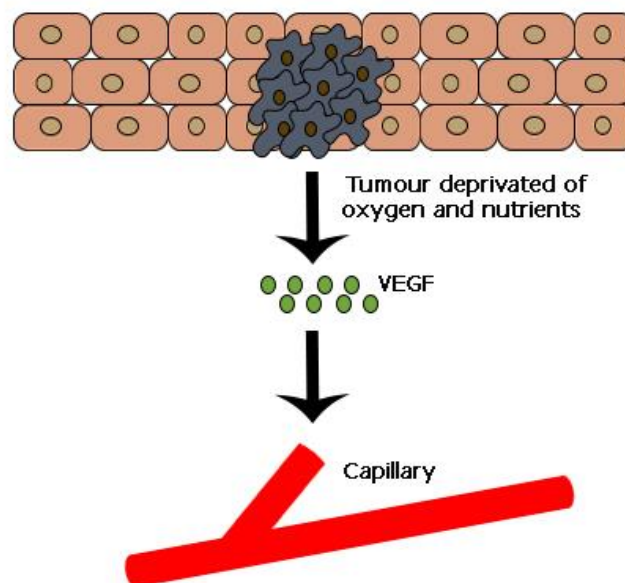


Figure 3.6 - VEGF is secreted by cells deprived of nutrients, leading to the formation of new capillaries, improving blood supply.

3.5 - Causes of Cancer

Carcinogen is the name given to substances that cause cancer. The development of malignancy is a complex multistep process but there are many factors that may affect the probability that cancer will develop like radiation, chemicals and viruses [52], [53].

Some agents such as radiation and some chemical carcinogens (unbalanced diets, drugs and environmental substances) act by damaging DNA and inducing mutations. Some examples are solar ultraviolet radiation, related with skin cancer, carcinogenic chemicals in tobacco smoke related with lung cancer and aflatoxin that is a potent liver carcinogen [52], [53].

Another way to contribute to cancer development is stimulating cell proliferation instead of mutation induction. This stimulation is made by tumour promoters that facilitate the proliferation of cell population during early stages of tumour development. Examples are hormones and some viruses [52], [53].

Unfortunately, there is not a definitive cure for this disease, only diverse types of treatment that try to cure or delay cancer development. So, they have a significant potential to enhance quality of life and increase life-expectancies. Nevertheless, none of these treatments are really effective and they have side effects. There are many types of treatments that could be used depending on the diagnostic tests. It could be recommended one or more treatment options, such as [52], [53]:

- Surgery
- Chemotherapy
- Hormone therapy
- Targeted therapy
- Radiation therapy

The choice of treatment depends largely on the type of cancer and the stage of the disease, and on the patient's health, if the patient wants to have children and/or other personal considerations [2].

Dynamics between molecular- and tissue-scale in a tumor can have unexpected effects on invasion and outcome of therapy. Invasion is a problem to resection (surgery for partial or total extraction of an organ) and treatment, because it can be very difficult to define optimal mass removal due to the complexity to estimate the tumor margin and invasion potential. An example of an unexpected effect in outcome of therapy is the anti-angiogenic therapy that should lead to tumor regression [99]-[102]. However, it may also exacerbate hypoxia [103] and cause tumour fragmentation, cancer cell migration and tissue invasion [104]-[109],[110]-[118].

3.6 - Selection of Cell Line

In cell culture it is important to use cells or tissues that are similar to reality, so spheroids, which are spherical aggregates of tumour cells that are identical to the nodules on solid tumors [119]-[121],

can be developed in the lab [122]. Spheroids can develop central necrosis, like tumour nodules, so they can be a useful model which provides information about the metabolites penetration on tissues and how they influence cell death [119].

There are three phases that describe these biological structures. First phase is characterized by the aggregation of single cells, creating small agglomerates that grow quasi-exponentially [121], [123]. This growth continues until a specific volume. At this point of the spheroid growth, cells are in different stage of the cell cycle, resulting in an accumulation of G1-like cells at the centre and periphery cells proliferate [121], [122], [124], [125]. This difference leads to a progressive reduction of the growth rate that lead to a second phase of growth [121], which is characterized by a linear expansion of the spheroid diameter with time [126], [127]. In last phase, as the spheroid grows and becomes larger, its growth progressively slows down until it reaches a maximum diameter [125], [128]. This special growth of the spheroids is a consequence of the diffusion and consumption of nutrients, such as oxygen and glucose, as well as growth factors [129], [130] and inhibitory factors produced by live or dead cells [130], [131]. All these steps belong to the avascular growth phase (Figure 3.7), after which comes the tumor vascular growth phase. It is in the vascular growth phase that the tumour invade other tissues and depend on their ability to create new blood vessels [132].

Other characteristic of malignant growth of spheroids is their tissue structure disorganization, abnormal blood vessel development and insufficient vascular supply. Because of that, these cancer cells have physical, chemical and nutritional stresses [133].

Like all tumours, spheroid metabolism and proliferation are dependent on oxygen and glucose concentration and pH, so cells stop growing when exposed to extreme hypoxia [134]-[136], glucose deprivation [137], and low pH levels [138].

Glucose deprivation in cells is associated with quiescence, synthesis of stress proteins, decreasing glucose metabolism and increasing oxygen consumption rates [137], [139]-[142]. In the same way when oxygen concentration decreases, glucose consumption rate increases. In necrotic region the concentration of oxygen can be zero [143]-[145].

Thus, for this numerical study it was selected one of the most used tumour spheroid in cancer research - the multicellular tumour spheroids of the EMT6/Ro mouse mammary tumour cell line [146]. For the EMT6/Ro cell line, the normal culture conditions are: culture medium is BME (basal medium Eagle) with 5,5 mM of glucose [146].

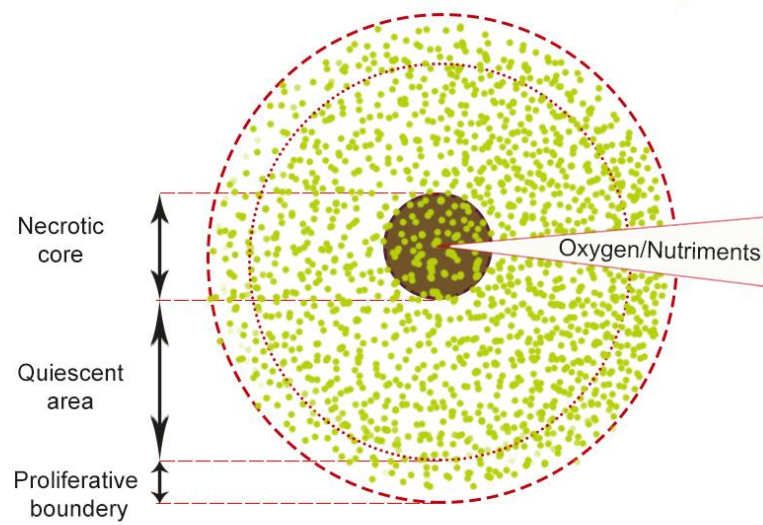


Figure 3.7 - Division of a spheroid according to its healthy state due to availability of oxygen and nutrients. From the periphery to the centre, the concentration of oxygen and nutrients available decreases and consequently cell's ability to proliferate decreases also.

Chapter 4

Mathematical models

Nowadays, in cancer research, it is usual to use new techniques from molecular biology that are capable to produce information very important. However, to improve these discoveries it is essential to use mathematical models that provide approximated insights of critical parameters controlling the system dynamics [147].

Mathematical models have the potential to explain the causes of solid tumour invasion and metastasis and can help to understand the experimental and clinical observations. *In vitro* experiences take a long time and involve complex numerous experiments. Alternatively, mathematical models, which describe different aspects of solid tumour growth, have the advantage to prevent excessive experimentation and provide biologists with complementary information about the mechanisms that may control the development of solid tumors [148]. Besides that, modelling and simulation have also the goal to minimize patient suffering and maximize treatment effectiveness by the development of individualized therapy protocols. For these reasons, experimentalists and clinicians are becoming increasingly interested in mathematical modelling as a good counterpart, recognizing that medical techniques and experimental approaches are often unable to resolve problems alone [149].

To concretize these goals is important to know that there are more than 100 types of cancer, each with many subtypes, and all cancers develop a common set of basic characteristics [149]:

- Self-sufficiency in growth signals;
- Insensitivity to anti-growth signals;
- Evasion of apoptosis;
- Limitless replicative potential;
- Sustained angiogenesis;
- Tissue invasion and metastasis.

There are many mathematical models to study the various phases of cancer progression [132], [150]-[173] and they are divided based on how the tumour tissue is represented: discrete cell-based models and continuum models. Both approaches provide important contributes to cancer-related processes, so the complexity of cancer and the interactions among the cell- and tissue-level can be described using a continuum-discrete (hybrid) approach, relating the molecular and cellular scales to the tumour scale [58], [169], [174].

4.1 - Discrete Model

Discrete modelling has been particularly useful in recent years in studies of carcinogenesis, genetic instability, natural selection and interactions of individual cells with each other and the microenvironment, because individual cells are tracked and updated according to a specific set of biophysical rules [175]. With this models, it is also possible to study biological cell characteristics of a specific population, like response to therapy and in studies of immunology. Discrete models are divided in two types: lattice-based and lattice-free. The first describes the dynamics of discrete tumour cells as automata on a grid whose states are controlled by a set of deterministic or probabilistic rules [175]. Lattice-free describes the actions of discrete cells in arbitrary locations and their interactions [175]. The disadvantage is the computational cost that increases with the number of cells modelled, limiting these methods in the spatial and temporal scales. For example, it is not possible to use discrete approach when the spheroid tumour of 1 mm^3 contains several thousand of cells [175].

Nevertheless, the literature describes discrete models that include a discrete-continuum approach related with substrate concentration like oxygen and glucose. In these models, the species concentrations are described using continuum approach and cell components are assumed as discrete [152], [154], [155], [176]-[183].

4.2 - Continuum Model

Continuum methods are used in larger scale systems, because they treat tumours as a collection of cells, where densities and volume fractions of cells are described. Individual cells and some components are not tracked and variables of the model might contain cell volume fractions and cell substrate concentrations such as oxygen, nutrient and growth factors. Comparing with discrete modelling, continuum model parameters may be easier to obtain, analyze, control and can be more accessible through laboratory experimentation. Therefore, these models are indicated at the tissue scale where gross tumour behaviour might be quantified. However, these models are not appropriate for modelling individual cells and discrete events. An example of the importance of these methods is

when studying the effect of genetic, cellular and microenvironment characteristics on overall tumour behaviour.

Traditional works normally use ordinary differential equations to model tumours as a homogeneous population and partial differential equation restricted to a spherical geometry [130], [184]. When the model aims to simulate avascular tumours, growth is modelled as a function of cell substrate concentration, normally oxygen [175]. Many recent models incorporate cell movement, through diffusion [185]-[192], convection [54], [193]-[196] and chemo/haptotaxis [189], [195]. Many interactions with the microenvironment like nutrients limitations or inhibitory factor to growth [197]-[201] and models with strong cell-cell interactions [202], [203] were also studied.

4.3 - Hybrid Model

Hybrid model combines both continuum and discrete models in order to link the subcellular- and cellular-scales to the tumour scales and provide a more realistic model. This means that substances such as oxygen, nutrient, growth factors, drug and certain tissue features can be described as continuum fields in the tumour microenvironment, while individual discrete elements such as cells and parts of cells evolve in response to local conditions such as substance concentration. The advantage of this method is the potential to combine the best features of both discrete and continuum models.

In the literature it is possible to find two research works of hybrid model [58], [204] showing a new approach to tumour modelling using simultaneously continuum and discrete approaches. For discrete cell a lattice-free model is used. The parameters used for discrete cells were: chemotaxis (cell motion in consequence of a chemical stimulus), haptotaxis (directional mobility or growth cells like proliferation and migration) and two cells cannot be in the same position in space. Continuum volume fractions induce velocity and cell fight against the continuum description for nutrients [58], [204].

Chapter 5

Methods

This chapter describes physical phenomenon under study and the numerical technique used by the software tested in this work.

5.1 - Meshless Method: RPIM

The nodal discretization can be regular or irregular, which has a direct effect on the numerical analysis outcome because, generally, an irregular discretization has a lower accuracy. However, when it is predictable that some location will generate higher stress, that location should be enriched with a higher number of nodes. So, as a good practice, one should only increase the nodal densities in domain areas in which higher stresses are expected [205] (Figure 5.1).

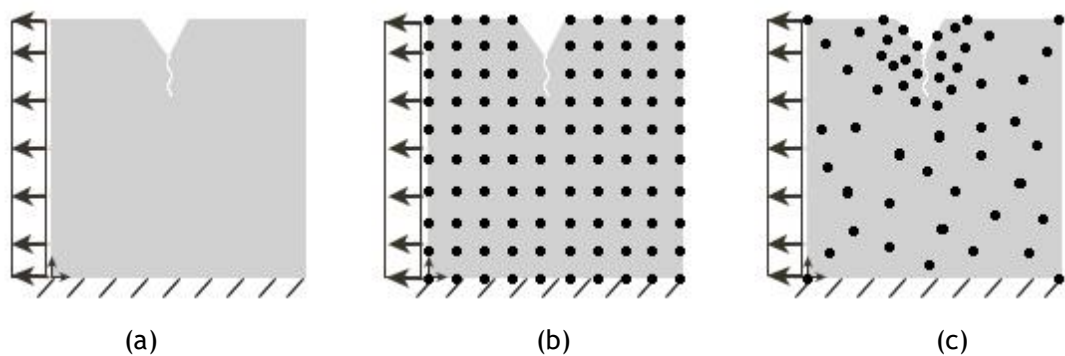


Figure 5.1 - (a) Problem domain with the essential and natural boundaries applied. (b) Regular nodal discretization. (c) Irregular nodal discretization.

After discretization, it is necessary to obtain the nodal connectivity. In FEM, to obtain the nodal connectivity it is used the element mesh, in which the nodes belonging to the same element interact directly between themselves and the boundary nodes interact with the boundary nodes of nearby

elements. In meshless methods the connectivity is provided by the overlapping of influence-domains, when it comes to RPIM.

The next step is the numerical integration. A background integration mesh is constructed, which can be nodal dependent or independent. Using nodal dependent mesh, it is necessary to implement a stabilization method in order to achieve accurate results although this increases the computational cost [206]-[208]. However, the only information required by this method is the spatial location of the nodes. Finally, it is possible to obtain the field variables under study by using either approximation or interpolation shape functions. In RPIM, the interpolation shape function is based on the combination of radial basis functions with polynomial basis functions.

5.1.1 - Influence-domain and nodal connectivity

Regarding the nodal connectivity, influence-domains can have a fixed or variable size. Variable size influence-domains ensure that every node's influence-domain contains the same number of nodes, allowing the shape functions to have the same degree of complexity in the entire domain. The literature recommends using between $n=[9, 16]$ nodes inside the influence-domain for two-dimensional (2D) problems [8], [9], [14], [21]. The density of the nodal discretization does not influence the number of nodes inside the influence-domain [205] (Figure 5.2).

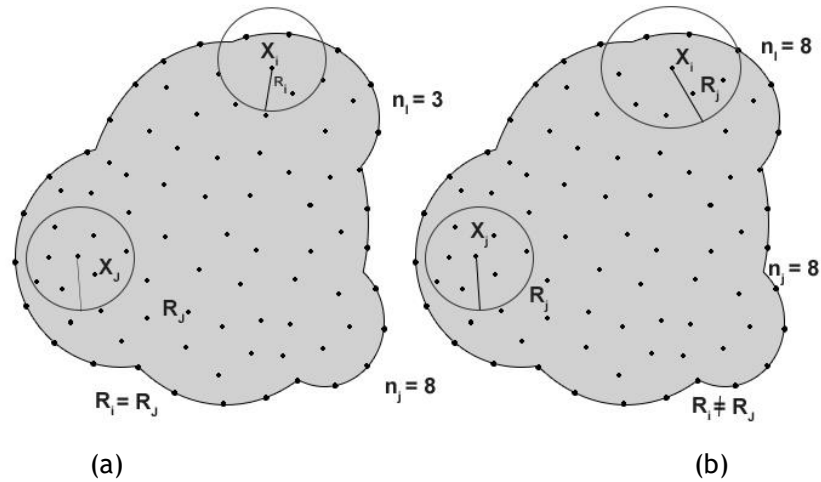


Figure 5.2 - (a) Fixed size circular influence-domain. (b) Variable size circular influence-domain.

5.1.2 - Numerical integration

The integro-differential equations governing the studied problem are integrated using the Gauss-Legendre integration scheme. A background mesh can be constructed using quadrilateral or triangular integration cells, as seen in Figure 5.3 a) and b), or using a background cell-mesh, larger than the problem domain, which is filled with integration points, as shown in

Figure 5.3 c). However, the integration points outside the problem domain have to be eliminated from the computation.

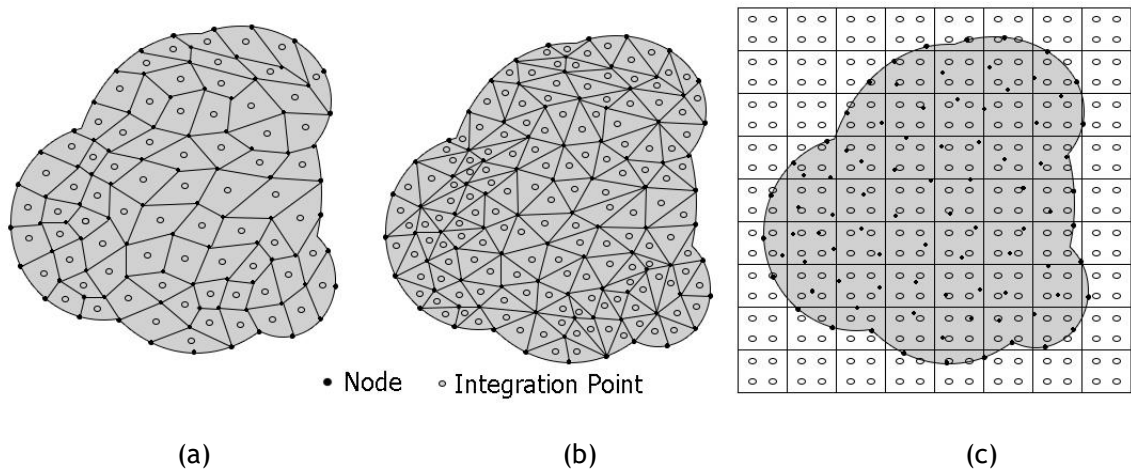


Figure 5.3 - a. Quadrilateral integration cell background mesh with 1 integration point. b. Triangular integration cell background mesh with 1 integration point. c. Quadrilateral grid background mesh with 2x2 integration points.

As it is possible to see in

Figure 5.3, the integration cells of the background mesh can be triangular (b) or quadrilateral (a and c) and inside of each one, integration points are distributed as shown in Figure 5.4.

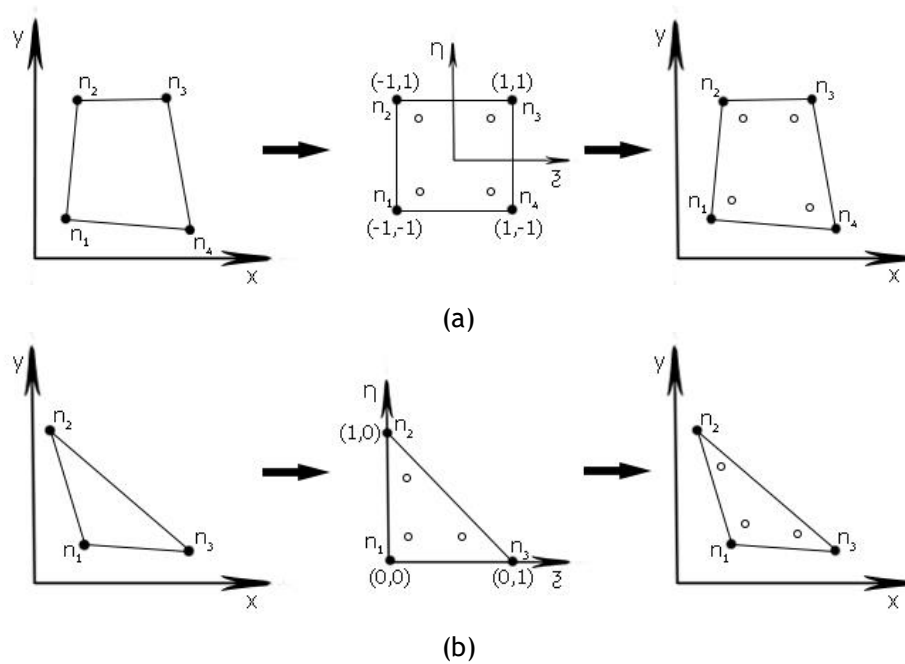


Figure 5.4 - (a) Transformation of the initial quadrilateral integration cell into an isoparametric square shape and application of the 2x2 quadrature point rule followed by the return to the initial quadrilateral shape. (b) Transformation of the initial triangle integration cell into an isoparametric triangle shape and application of the 3-point quadrature point rule followed by the return to the initial triangle.

The isoparametric integration points have different location and weights if the element is triangular or quadrilateral, as you can see in the following Table 5.1 and Table 5.2.

Table 5.1 - Integration points coordinates and weights for triangular integration cells [209].

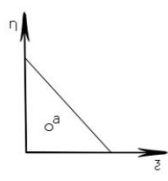
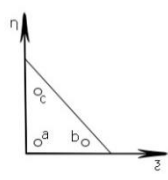
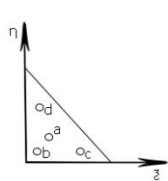
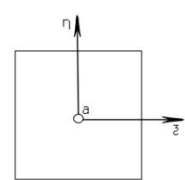
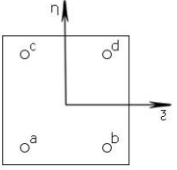
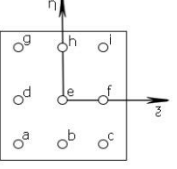
Points	ξ	η	Weight	Representation
<i>a</i>	$\frac{1}{3}$	$\frac{1}{3}$	$\frac{1}{2}$	
<i>a</i>	$\frac{1}{6}$	$\frac{1}{6}$	$\frac{1}{6}$	
<i>b</i>	$\frac{2}{3}$	$\frac{1}{6}$	$\frac{1}{6}$	
<i>c</i>	$\frac{1}{6}$	$\frac{2}{3}$	$\frac{1}{6}$	
<i>a</i>	$\frac{1}{3}$	$\frac{1}{3}$	$\frac{27}{96}$	
<i>b</i>	$\frac{1}{5}$	$\frac{1}{5}$	$\frac{25}{96}$	
<i>c</i>	$\frac{3}{5}$	$\frac{1}{5}$	$\frac{25}{96}$	
<i>d</i>	$\frac{1}{5}$	$\frac{3}{5}$	$\frac{25}{96}$	

Table 5.2 - Integration points coordinates and weights for quadrilateral integration cells' [209].

Points	ξ	η	Weight	Representation
<i>a</i>	0	0	4	
<i>a</i>	$-\frac{1}{\sqrt{3}}$	$-\frac{1}{\sqrt{3}}$	1	
<i>b</i>	$+\frac{1}{\sqrt{3}}$	$-\frac{1}{\sqrt{3}}$	1	

c	$-\frac{1}{\sqrt{3}}$	$+\frac{1}{\sqrt{3}}$	1	
d	$+\frac{1}{\sqrt{3}}$	$+\frac{1}{\sqrt{3}}$	1	
a	$-\sqrt{\frac{3}{5}}$	$-\sqrt{\frac{3}{5}}$	$\frac{25}{81}$	
b	0	$-\sqrt{\frac{3}{5}}$	$\frac{40}{81}$	
c	$+\sqrt{\frac{3}{5}}$	$-\sqrt{\frac{3}{5}}$	$\frac{25}{81}$	
d	$-\sqrt{\frac{3}{5}}$	0	$\frac{40}{81}$	
e	0	0	$\frac{64}{81}$	
f	$+\sqrt{\frac{3}{5}}$	0	$\frac{40}{81}$	
g	$-\sqrt{\frac{3}{5}}$	$+\sqrt{\frac{3}{5}}$	$\frac{25}{81}$	
h	0	$+\sqrt{\frac{3}{5}}$	$\frac{40}{81}$	
i	$+\sqrt{\frac{3}{5}}$	$+\sqrt{\frac{3}{5}}$	$\frac{25}{81}$	

Now the Cartesian coordinates of the integration points can be obtained using known isoparametric interpolations functions.

$$x = \sum_{i=1}^m N_i(\xi, \eta) \cdot x_i$$

$$y = \sum_{i=1}^m N_i(\xi, \eta) \cdot y_i \quad (5.1)$$

in which, m is the number of nodes defining the element and x_i and y_i are the Cartesian coordinates of the integration cells nodes.

For triangles

$$\begin{aligned} N_1(\xi, \eta) &= 1 - \xi - \eta \\ N_2(\xi, \eta) &= \eta \\ N_3(\xi, \eta) &= \xi \end{aligned} \quad (5.2)$$

For quadrilaterals:

$$N_1(\xi, \eta) = \frac{1}{4}(1 - \xi)(1 - \eta)$$

$$\begin{aligned}
N_2(\xi, \eta) &= \frac{1}{4}(1 - \xi)(1 + \eta) \\
N_3(\xi, \eta) &= \frac{1}{4}(1 + \xi)(1 + \eta) \\
N_4(\xi, \eta) &= \frac{1}{4}(1 + \xi)(1 - \eta)
\end{aligned} \tag{5.3}$$

The integration weight belonging to the integration point is obtained by multiplying the isoparametric weight, of the integration point with the inverse of the Jacobian matrix determinant of the respective integration cell.

$$[J] = \begin{pmatrix} \frac{\partial \mathbf{x}}{\partial \xi} & \frac{\partial \mathbf{x}}{\partial \eta} \\ \frac{\partial \mathbf{y}}{\partial \xi} & \frac{\partial \mathbf{y}}{\partial \eta} \end{pmatrix} \tag{5.4}$$

The differential equation integration is done using,

$$\int_{-1}^1 \int_{-1}^1 f(x) dx dy = \sum_{i=1}^m \sum_{j=1}^m \omega_i \omega_j f(x) \tag{5.5}$$

where ω_i and ω_j is the weight in each direction of the integration point \mathbf{x} .

5.1.3 - Shape functions

Shape functions used by RPIM are based on a combination of radial basis functions with polynomial functions [21], [22]. One of the major advantages of both these method's shape functions is that they possess the Kronecker delta property, meaning that they are interpolating shape functions.

Considering a function $u(\mathbf{x}_I)$, defined in a certain influence-domain and discretized by a set of n distinct nodes. At an interest point \mathbf{x}_I , the function $u(\mathbf{x}_I)$ can be defined as,

$$u(\mathbf{x}_I) = \sum_{i=1}^n R_i(\mathbf{x}_I) a_i(\mathbf{x}_I) + \sum_{j=1}^m p_j(\mathbf{x}_I) b_j(\mathbf{x}_I) = \mathbf{R}^T(\mathbf{x}_I) \mathbf{a} + \mathbf{p}^T(\mathbf{x}_I) \mathbf{b} \tag{5.6}$$

which can be written as:

$$u(\mathbf{x}_I) = \sum_{i=1}^n R_i(\mathbf{x}_I) a_i(\mathbf{x}_I) + \sum_{j=1}^m p_j(\mathbf{x}_I) b_j(\mathbf{x}_I) = \{\mathbf{R}^T(\mathbf{x}_I), \mathbf{p}^T(\mathbf{x}_I)\} \begin{Bmatrix} \mathbf{a} \\ \mathbf{b} \end{Bmatrix} \tag{5.7}$$

where $R_i(\mathbf{x}_I)$ is the radial basis function (RBF), $p_j(\mathbf{x}_I)$ is the polynomial basis function, n is the number of nodes inside the influence-domain of the interest point \mathbf{x}_I and $a_i(\mathbf{x}_I)$ and $b_j(\mathbf{x}_I)$ are non-constant coefficients of $R_i(\mathbf{x}_I)$ and $p_j(\mathbf{x}_I)$ respectively. Thus, these vectors can be represented as,

$$\mathbf{a}^T(\mathbf{x}_I) = [a_1(\mathbf{x}_I), a_2(\mathbf{x}_I), \dots, a_n(\mathbf{x}_I)]$$

$$\mathbf{b}^T(\mathbf{x}_I) = [b_1(\mathbf{x}_I), b_2(\mathbf{x}_I), \dots, b_m(\mathbf{x}_I)]$$

$$\mathbf{R}^T(\mathbf{x}_I) = [R_1(\mathbf{x}_I), R_2(\mathbf{x}_I), \dots, R_n(\mathbf{x}_I)]$$

$$\mathbf{p}^T(\mathbf{x}_I) = [p_1(\mathbf{x}_I), p_2(\mathbf{x}_I), \dots, p_m(\mathbf{x}_I)] \quad (5.8)$$

The RBF use has the following general form:

$$R_{ij} = (r_{ij}^2 + c^2)^p \quad (5.9)$$

where c and p are shape parameters which, accordingly to the literature, should be considered as $c=0.0001$ and $p=0.9999$ in order to maximize the method's performance [205] and r_{ij} is the Euclidian norm between the integration point \mathbf{x}_I and a certain node \mathbf{x}_j ,

$$r_{ij} = \sqrt{(x_i - x_j)^2 + (y_i - y_j)^2} \quad (5.10)$$

The polynomial basis functions used have the following monomial terms,

$$\mathbf{p}^T(\mathbf{x}_I) = [1, x, y, x^2, xy, y^2, \dots] \quad (5.11)$$

This leads to the following possible polynomial bases, for the 2D problem,

$$\begin{aligned} \text{Null basis} - \mathbf{x}^T &= \{x, y\}; \mathbf{p}^T(\mathbf{x}) = \{0\}; m = 0 \\ \text{Constant basis} - \mathbf{x}^T &= \{x, y\}; \mathbf{p}^T(\mathbf{x}) = \{1\}; m = 1 \\ \text{Linear basis} - \mathbf{x}^T &= \{x, y\}; \mathbf{p}^T(\mathbf{x}) = \{1, x, y\}; m = 3 \\ \text{Quadratic basis} - \mathbf{x}^T &= \{x, y\}; \mathbf{p}^T(\mathbf{x}) = \{1, x, y, x^2, xy, y^2\}; m = 6 \end{aligned} \quad (5.12)$$

The polynomial term must however satisfy the following requirement, in order to guarantee a unique approximation,

$$\sum_{i=1}^n p_j(\mathbf{x}_i) a_i = 0, \quad j = 1, 2, \dots, m \quad (5.13)$$

The function can be written in matrix form,

$$\begin{bmatrix} \mathbf{R} & \mathbf{p} \\ \mathbf{p}^T & \mathbf{0} \end{bmatrix} \begin{Bmatrix} \mathbf{a} \\ \mathbf{b} \end{Bmatrix} = \begin{Bmatrix} \mathbf{u}_s \\ \mathbf{0} \end{Bmatrix} = \mathbf{G} \begin{Bmatrix} \mathbf{a} \\ \mathbf{b} \end{Bmatrix} \quad (5.14)$$

And solving the equation:

$$\begin{Bmatrix} \mathbf{a} \\ \mathbf{b} \end{Bmatrix} = \mathbf{G}^{-1} \begin{Bmatrix} \mathbf{u}_s \\ \mathbf{0} \end{Bmatrix} \quad (5.15)$$

Finally, the shape function is expressed as:

$$\mathbf{u}(\mathbf{x}_I) = \{\mathbf{R}^T(\mathbf{x}_I), \mathbf{p}^T(\mathbf{x}_I)\} \mathbf{G}^{-1} \begin{Bmatrix} \mathbf{u}_s \\ \mathbf{0} \end{Bmatrix} = \boldsymbol{\varphi}(\mathbf{x}_I) \mathbf{u}_s \quad (5.16)$$

in which $\boldsymbol{\varphi}(\mathbf{x}_I)$ is the shape function vector defined by

$$\boldsymbol{\varphi}(\mathbf{x}_I) = \{\mathbf{R}^T(\mathbf{x}_I), \mathbf{p}^T(\mathbf{x}_I)\} \mathbf{G}^{-1} = [\boldsymbol{\varphi}_1(\mathbf{x}_I), \boldsymbol{\varphi}_2(\mathbf{x}_I), \dots, \boldsymbol{\varphi}_n(\mathbf{x}_I)] \quad (5.17)$$

RPIM shape functions are interpolating, since they respect the Kronecker delta property,

$$\boldsymbol{\varphi}_i(\mathbf{x}_j) = \begin{cases} \mathbf{1}, & i = j, \quad j = 1, 2, \dots, n \\ \mathbf{0}, & i \neq j, \quad j = 1, 2, \dots, n \end{cases} \quad (5.18)$$

which means they pass through every single node within the influence-domain, in opposition to approximation shape functions. Thus, interpolation shape functions permit to easily impose the

essential and natural boundary conditions, using direct imposition methods, reducing the computational cost.

5.2 - Reaction-diffusion model

Diffusion is a transfer phenomenon that can describe the distribution of a chemical species in equal concentrations in space over time [210], [211].

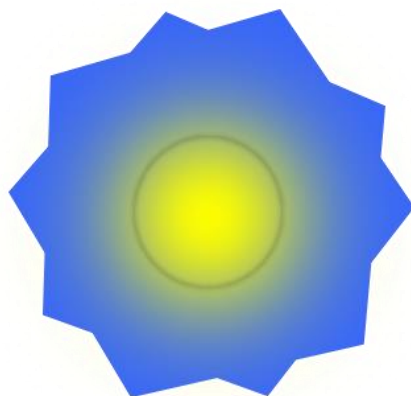
Chemical species can be chemically dissolved in a solvent or one component in a gas mixture (oxygen in air). Diffusion occurs when the initial concentration of the species is different in distinct domain locations, its mean that if one region possesses a larger species' concentration than another region, mass transfer will occur until an uniform concentration between two regions is achieved [210], [211].

The thermal motion of molecules is the force that allows diffusion, because at temperatures above zero, molecules are always in movement. This happens due to their kinetic energy and when molecules collide with each other, their motion become randomized [210], [211].

5.2.1 - Oxygen and Glucose Diffusion on Human Body

Oxygen and glucose are moving and changing direction in human vessels causing diffusion to the cells because of the statistics of this movement [210], [211].

This kind of situation occurs also in experiments with cells *in vitro*, in which the cells are in a specialized plate with medium at specific oxygen concentration (C_{O_2}) and glucose concentration (C_{GL}). The image below shows an example of different concentration between a cell (circle) and the medium (around circle) (Figure 5.5). It is in the medium that the concentration is higher and, after some time, diffusion leads to a uniform concentration between them [210], [211].



(a)



(b)

Figure 5.5 - (a) The cell (circle) in yellow represents low concentration and the medium in blue represents high concentration. (b) Due to diffusion, the concentration will be the same in circle and surround medium.

Next image shows with arrows the initial concentration (size of the arrow) and the direction of the molecules. As their motion is random, oxygen and glucose move equally in all directions from any region [210], [211] (Figure 5.6).

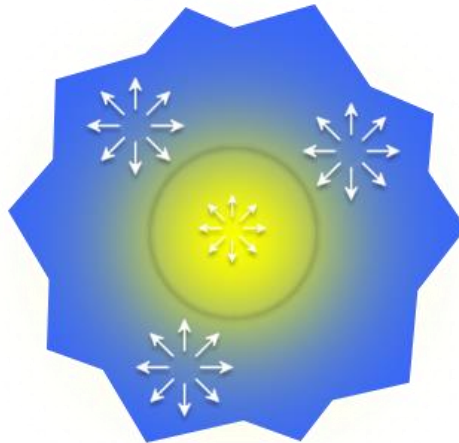


Figure 5.6 - The arrows show the directions that molecules can take and the initial concentration in both sites.

When the concentration is the same in the two regions, it means that the number of molecules that are moving in opposite directions is the same. However, in the boundary, where the concentration is different, there will be more molecules moving from the medium to the cell. This happens because there are more molecules in the medium than in the cell [210], [211] (Figure 5.7).

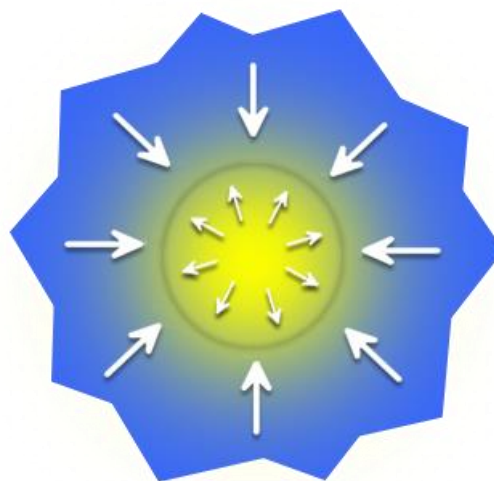


Figure 5.7 - Preferential movement of the molecules in the boundary between the cell and the medium. There are more molecules pass from the medium to the cell than the other way around.

Once the concentration is equal, the molecules are still moving but now the number of molecules that cross the boundary are the same. If the conditions are maintained, there is no statistical driving force and molecules do not accumulate in any region [210], [211].

It is possible to describe the diffusion phenomenon using continuous partial differential equations. This effect was elucidated by Albert Einstein in 1905 [212]. The partial differential equations used to model diffusion problems can include Fick's law (convection-diffusion equation) or methods more complex when it is used concentrated mixtures such Maxwell-Stefan diffusion [210], [211].

The velocity of diffusion varies between molecules depending on the diffusion coefficient that is specific for each molecule. Diffusion coefficient is the rate of the diffusion process [210], [211].

It is possible to obtain a steady-state diffusion where the concentration is different between two regions, as in the example of the cell and the medium. This happens when there is a constant supply of material and a steady concentration will be attained but not a uniform concentration [210], [211].

5.2.2 - Diffusion Coefficient and Fick's Laws

Diffusion flux is given by Fick's first law depending on the diffusion coefficient, which is the property translating the interaction of the solute with the solvent. It is similar to the property of thermal diffusivity that occurs in heat transfer [210], [211]:

$$N_i = -D_i \nabla c_i \quad (5.19)$$

Where i is a specie, N_i is the molar flux ($\text{mol m}^{-2} \text{s}^{-1}$), D_i is the diffusion coefficient ($\text{m}^2 \text{s}^{-1}$), c_i is the concentration (mol m^{-3}) and ∇ is the gradient operator [210], [211].

So,

$$D_i \equiv \frac{|N_i|}{|\nabla c_i|} \quad (5.20)$$

Additionally, based in the continuity equation for mass [210], [211]:

$$\frac{\partial c_i}{\partial t} + \nabla \cdot N_i = 0 \quad (5.21)$$

It is possible derive Fick's second law [210], [211]:

$$\frac{\partial c_i}{\partial t} = D_i \nabla^2 c_i \quad (5.22)$$

From this, it is possible to conclude that D_i is a constant, only true for diluted solutions. This is normally assumed for diffusion in solids, chemicals diffusion in diluted solution (water or other liquid solvents) and diffusion of diluted species in the gas phases (oxygen in air) [210], [211].

Diffusion of molecules dissolved in liquids is slower than dissolved in a gas, so diffusion in liquids is dominated by convection. The units of diffusion coefficient are area per time ($\text{m}^2 \text{s}^{-1}$) in SI units [210], [211].

Analysis of Fick's second law show that, in diffusive processes, there is a relation between the elapsed time and the square of the length in which diffusion takes place [210], [211].

5.3 - Algorithm scheme

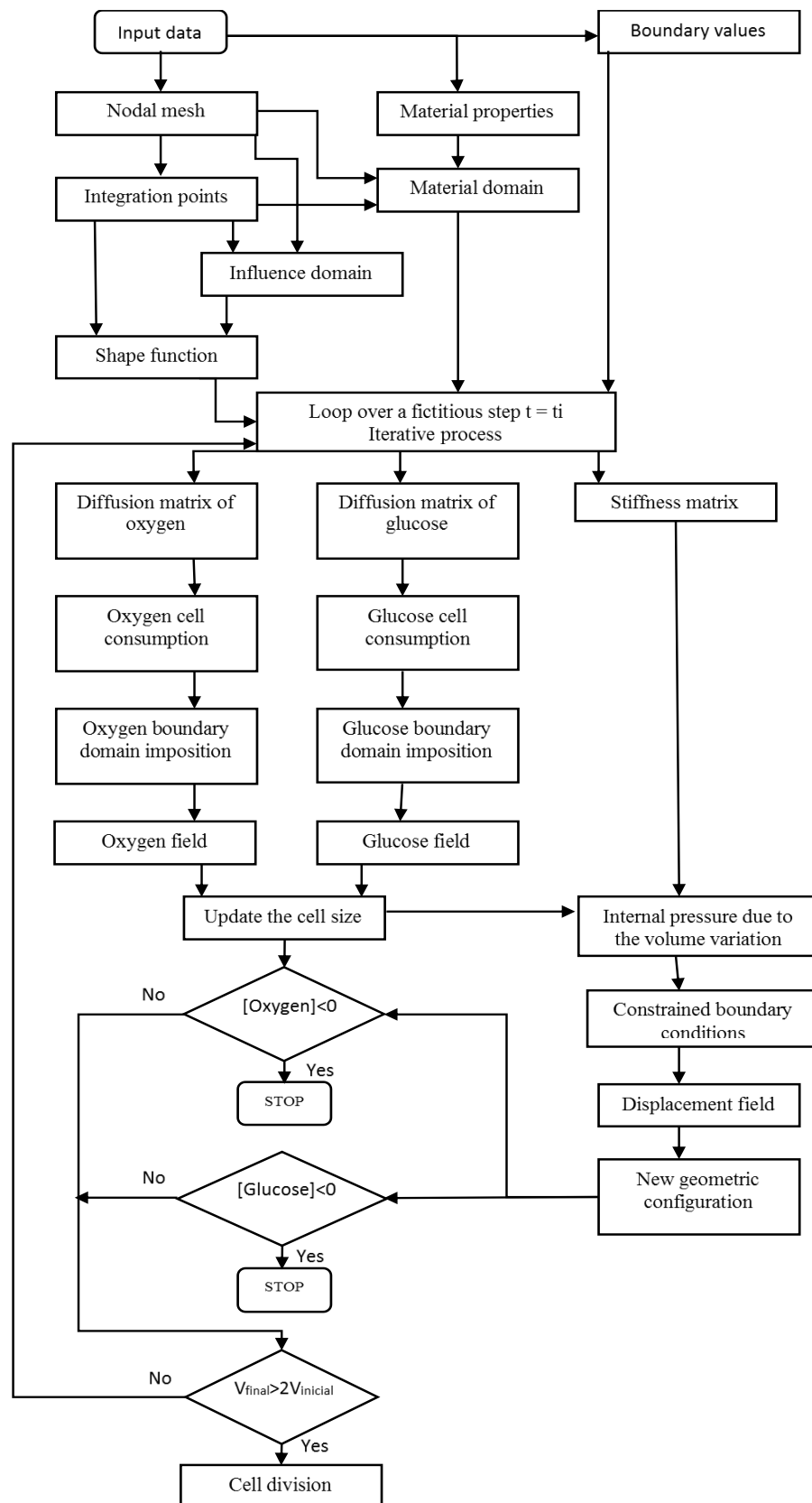


Figure 5.8 - General representation of the algorithm used by the RPIM software tested in this work.

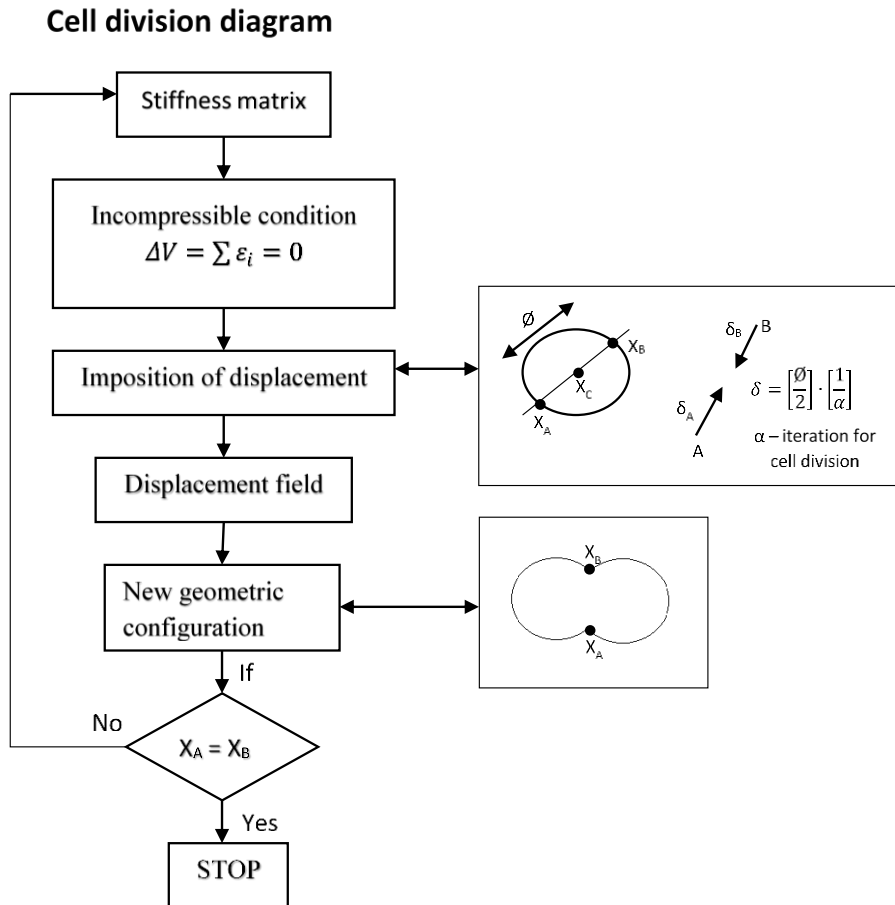


Figure 5.9 - General representation of the algorithm for the simulation of the cell division. This algorithm is contained into the block “Cell division” of the general algorithm presented in figure 6.8.

The algorithm represented in Figure 5.8, shows all steps of the tested RPIM software.

First, the user has to input all information required by the code (‘input data’ block Figure 5.8), such as: Domain dimensions; Divisions along xx and yy ; Cell size (diameter and area); Number of maximum iterations; Cell and medium properties: diffusion coefficients and C_{O_2} and C_{GL} .

In this work, it was consistently considered the following dimensions: $1000 \mu\text{m} \times 1000 \mu\text{m}$ by the xx and yy axes. For the cell it was considered a diameter of $100 \mu\text{m}$, corresponding to a typical size. The cell and medium properties are shown in a Table 5.3.

Table 5.3 - Cell and medium properties used in the mathematical model [146]

	Local	Diffusion coefficient ($\mu\text{m}^2/\text{s}$)	Concentration ($\text{mol}/\mu\text{m}^2$)
Oxygen	Cell	2000	3.5×10^{-16}

Medium		3030	3.5×10^{-16}
Glucose	Cell	500	2.75×10^{-14}
Medium		925	2.75×10^{-14}

From the 'input data' data in Figure 5.8, the software builds the nodal mesh, sets the material properties and identifies the boundary values. Regarding the mechanical properties of the homogenized medium, it was considered 1 Pa for the elasticity modulus and 0.45 for coefficient of Poisson.

Boundary values describe the natural boundary and the essential boundary. In the essential boundary the software applies a periodic boundary condition (double mirror) in all edges.

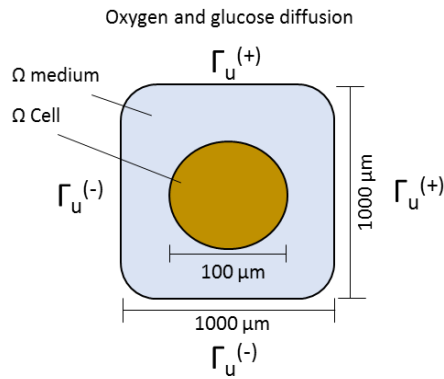


Figure 5.10 - Scheme of the cell and medium domain and the periodic boundary condition. Molecules of oxygen and glucose can movement from one boundary $\tau_u^{(+)}$ to $\tau_u^{(-)}$ and vice versa.

The background integration mesh is obtained using square integration cells coming from a regular lattice. The linear dimension of the edges of the square integration cells is double of the medium nodal distance. Inside each integration cell, Gauss-Legendre quadrature points are distributed.

Afterwards, it is possible to define the material domain, which identifies the medium domain and the cell domain (material domain box). The influence domain is built using the nodal mesh and the integration points. The used software possesses a routine that generates the domain of influence for each integration point. Then, another routine build the shape functions.

Using all this information, the software enters into an iterative loop assuming fictitious time step iterations.

During each iteration, the diffusion matrix for oxygen and for glucose is obtained, the consumption of oxygen (q_{O_2}) and glucose (q_{GL}) is calculated and the oxygen and glucose at the boundary domain is imposed. In the end, the software allows to obtain the C_{O_2} and C_{GL} field. Then, using the structural mechanics block (Figure 5.8), the internal pressure due to the volume variation is determined and the consequent new nodal configuration is obtained.

As cell grows, if its volume is larger than the double of the initial volume, the software enters to cell division block, represented in Figure 5.9. Here, the cell is prevented from growing. The used RPIM software selects two points in opposite position and move them in opposition directions in order to meet each other. When two points are in the same position, cell is divided in two daughter cells and the program stops.

5.4 - Discrete Equation System

In this work two distinct phenomena are applied: the mechanics for solids and structures and the chemical diffusion in homogeneous medium [213]. Thus, both formulations should be represented as discrete equation systems, in order to obtain a final numerical solution, as the algorithm in Figure 5.8.

5.4.1 - Chemical diffusion

The chemical diffusion can be numerically simulated as a field problem. The approach used to derive meshless methods equations in chemical diffusion problems is a general approach to solve partial differential equations using the meshless methods [213]. The general form of system equations of 2D linear steady state field problems can be given by the following general form of the Helmholtz equation,

$$D_x \frac{\partial^2 \phi}{\partial x^2} + D_y \frac{\partial^2 \phi}{\partial y^2} - g\phi + Q = 0 \quad (5.23)$$

Being ϕ the field and D_x , D_y , g and Q constants whose physical meaning is different for different problems. In this work, D_x and D_y will represent the diffusion coefficients along dimension x and y , respectively, g will be the matrix of chemical diffusibility but in this work will be neglected ($g = 0$) since there are not convection effects and Q will be concentration of the studied substance. Using the weighted residual approach it is possible to formulate the meshless system equations from equation [213]:

$$[K_D + K_g]\Phi - q = 0 \quad (5.24)$$

where,

$$K_D = \int_A B_G^T D B_G dA \quad (5.25)$$

Being,

$$B_G = \begin{bmatrix} \frac{\partial \phi}{\partial x} \\ \frac{\partial \phi}{\partial y} \end{bmatrix} = \begin{bmatrix} \frac{\partial \phi_1}{\partial x} & \frac{\partial \phi_2}{\partial x} & \dots & \frac{\partial \phi_n}{\partial x} \\ \frac{\partial \phi_1}{\partial y} & \frac{\partial \phi_2}{\partial y} & \dots & \frac{\partial \phi_n}{\partial y} \end{bmatrix} \quad (5.26)$$

and

$$\mathbf{D} = \begin{bmatrix} D_x & 0 \\ 0 & D_y \end{bmatrix} \quad (5.27)$$

Additionally,

$$\mathbf{K}_g = \int_A g \boldsymbol{\varphi}^T \boldsymbol{\varphi} dA \quad (5.28)$$

and

$$\mathbf{q} = \int_A Q \boldsymbol{\varphi}^T dA \quad (5.29)$$

Thus, solving equation (5.24) assuming D_x and D_y as the oxygen and glucose diffusion coefficient, respectively and Q as the species consumption, will allow to obtain the final medium species concentration Φ .

5.4.2 - Solid mechanics

Consider a closed domain Ω bonded by Γ . The equilibrium equations are expressed by: $\nabla \boldsymbol{\sigma} + \mathbf{b} = 0$, where ∇ is the gradient vector, $\boldsymbol{\sigma}$ the Cauchy stress tensor and \mathbf{b} the set of external forces applied to the body. Applying the Galerkin weak form, the following expression is obtained,

$$\mathbf{0} = \int_{\Omega} \delta \boldsymbol{\varepsilon}^T \boldsymbol{\sigma} d\Omega - \int_{\Omega} \delta \mathbf{u}^T \mathbf{b} d\Omega - \int_{\Gamma} \delta \mathbf{u}^T \mathbf{t} d\Gamma \quad (5.30)$$

where \mathbf{t} is the vector of external forces applied to the natural boundary Γ , $\boldsymbol{\varepsilon}$ is the strain vector and \mathbf{u} is the displacement field vector. The strain vector for the 2D case can be represented as,

$$\boldsymbol{\varepsilon} = \mathbf{L}\mathbf{u} = \begin{bmatrix} \frac{\partial}{\partial x} & 0 \\ 0 & \frac{\partial}{\partial y} \\ \frac{\partial}{\partial y} & \frac{\partial}{\partial x} \end{bmatrix} \begin{bmatrix} u \\ v \end{bmatrix} = \begin{bmatrix} \frac{\partial u}{\partial x} \\ \frac{\partial v}{\partial y} \\ \frac{\partial u}{\partial y} + \frac{\partial v}{\partial x} \end{bmatrix} \quad (5.31)$$

In this work only small deformations and elasto-static assumptions are considered. Therefore, with the Hooke Law it is possible to obtain the stress field $\boldsymbol{\sigma} = \mathbf{C}\boldsymbol{\varepsilon}$, being \mathbf{C} the material constitutive matrix, which can be obtained inverting the compliance elasticity matrix,

$$\mathbf{C}_{plane\ stress} = \begin{bmatrix} \frac{1}{E_{11}} & -\frac{\nu_{21}}{E_{22}} & 0 \\ -\frac{\nu_{12}}{E_{11}} & \frac{1}{E_{22}} & 0 \\ 0 & 0 & \frac{1}{G_{12}} \end{bmatrix}^{-1} \quad (5.32)$$

or

$$\mathbf{C}_{plane\ strain} = \begin{bmatrix} \frac{1 - \nu_{31}\nu_{13}}{E_{11}} & -\frac{\nu_{21} + \nu_{31}\nu_{23}}{E_{22}} & 0 \\ -\frac{\nu_{12} + \nu_{32}\nu_{13}}{E_{11}} & \frac{1 - \nu_{32}\nu_{23}}{E_{22}} & 0 \\ 0 & 0 & \frac{1}{G_{12}} \end{bmatrix}^{-1} \quad (5.33)$$

being E_{ij} the elasticity modulus, ν_{ij} material Poisson coefficient and G_{ij} the distortion modulus in material direction i and j . Equation (5.30) leads to,

$$\mathbf{K}\mathbf{U} - \mathbf{f}_b - \mathbf{f}_t = \mathbf{0} \quad (5.34)$$

Being,

$$\mathbf{K} = \int_{\Omega} \mathbf{B}^T \mathbf{C} \mathbf{B} d\Omega \quad (5.35)$$

Which is very similar with equation (5.24). However, in this case D is given by equation (5.32) or equation (5.33) and the deformation matrix \mathbf{B} is obtained with,

$$\mathbf{B} = \begin{bmatrix} \frac{\partial \varphi_1}{\partial x} & 0 & \frac{\partial \varphi_2}{\partial x} & 0 & \dots & \frac{\partial \varphi_n}{\partial x} & 0 \\ 0 & \frac{\partial \varphi_1}{\partial y} & 0 & \frac{\partial \varphi_2}{\partial y} & \dots & 0 & \frac{\partial \varphi_n}{\partial y} \\ \frac{\partial \varphi_1}{\partial y} & \frac{\partial \varphi_1}{\partial x} & \frac{\partial \varphi_2}{\partial y} & \frac{\partial \varphi_2}{\partial x} & \dots & \frac{\partial \varphi_n}{\partial y} & \frac{\partial \varphi_n}{\partial x} \end{bmatrix} \quad (5.36)$$

Regarding the force vectors,

$$\mathbf{f}_b = \int_{\Omega} \mathbf{H} \mathbf{b} d\Omega \quad \text{and} \quad \mathbf{f}_t = \int_{\Gamma} \mathbf{H} \mathbf{t} d\Gamma \quad (5.37)$$

Being $\mathbf{b} = \{b_x \ b_y\}^T$ and $\mathbf{t} = \{t_x \ t_y\}^T$. Matrix \mathbf{H} is defined as,

$$\mathbf{H} = \begin{bmatrix} \varphi_1 & 0 & \varphi_2 & 0 & \dots & \varphi_n & 0 \\ 0 & \varphi_1 & 0 & \varphi_2 & \dots & 0 & \varphi_n \end{bmatrix} \quad (5.38)$$

Solving the equation system represented in equation (5.34), it is possible to obtain the displacement field, allowing to update the new domain of the cell.

5.5 - Developed growth law

Based on the experimental observation described in chapter 2, section 2.7, a set of expressions were developed to simulate the cell growth. It was developed and tested a linear law and, in addition, several other exponential laws. To create the expressions to obtain the volume (V_f) of the cell in the end of each iteration, the follow parameters were used: initial volume (V_i) of the cell of 100 μm ,

division time (t_d - time that cell take from initializing cell division until originating two cells) of 16 hours and the time corresponding to each iteration (t_i). Thus, using these three parameters, the following expression were created:

$$V_f = V_i \cdot \left(1 + \frac{t_i}{t_d}\right) \quad (5.39)$$

$$V_f = V_i \cdot \left[2 \cdot \frac{e^{\frac{t_i}{t_d}}}{e} - \left(\frac{2}{e} - 1\right) \cdot \left(1 - \frac{t_i}{t_d}\right)\right] \quad (5.40)$$

$$V_f = V_i \cdot \left[2 \cdot \frac{e^{\frac{t_i}{t_d}}}{e} - \left(\frac{2}{e} - 1\right) \cdot \left(1 - \frac{t_i}{t_d}\right)\right]^n \cdot \frac{1}{2^n} \cdot \frac{t_i}{t_d} \cdot V_i \quad (5.41)$$

Equation (5.39) is a linear law, meaning that the cell grows in the same way during its whole cell cycle. Equation (5.40) is an exponential law, meaning that the cell grows slower in G1 and faster in G2 (phases of cell cycle). However, the deceleration that occur in G1 and the peak growth in G2 were not sufficiently represented by equation (5.40). Therefore, the equation (5.41) was developed, which allows to choose the inclination of the curve with parameter n . It was tested $n = 2, 3, 5$ e 10 . All curves were compared with literature data referred in chapter 2, section 2.7. After normalizing the t_i (division between actual time and total time) and V_f (\tilde{v} - division between actual volume and V_i) the following graphs were built. Figure 5.11 (a), (c) and (e) show the relation between data from literature and linear and exponential curves. Figure 5.11 (b), (d) and (f) show the relation between data from literature and exponential curves with different n . In order to have quantitative comparisons, it was calculated an average ($\bar{\varepsilon}$) between the difference of the two volumes (volumes from the literature data, \tilde{v}_i^{ref} , and experimental volumes, \tilde{v}_i^{exp}).

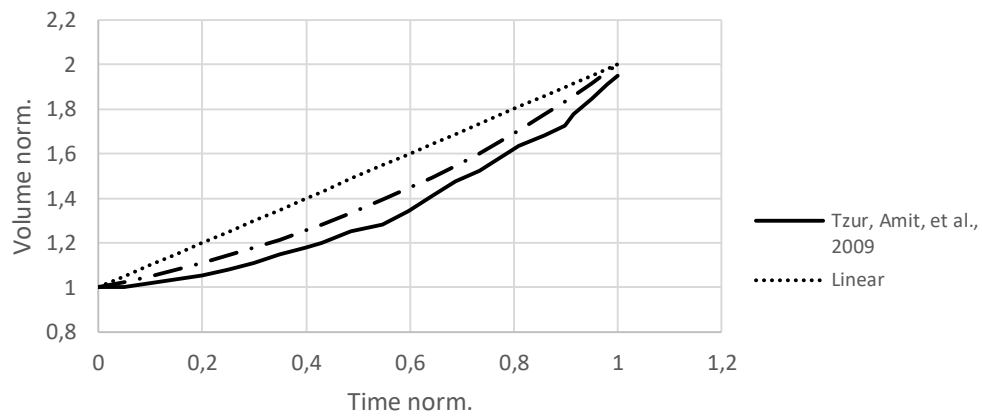
$$\bar{\varepsilon} = \frac{\sum_{i=1}^{n_t} |\tilde{v}_i^{ref} - \tilde{v}_i^{exp}|}{n_t}$$

Being n_t the total of compared values. Thus, for each time t_i of the experimental data, it was reported the corresponding volume \tilde{v}_i^{ref} . Then, time t_i was inserted in expression (5.39) or (5.40) or (5.41), the theoretical volume for that time t_i was obtained, \tilde{v}_i^{exp} .

The information obtained from this calculus is in

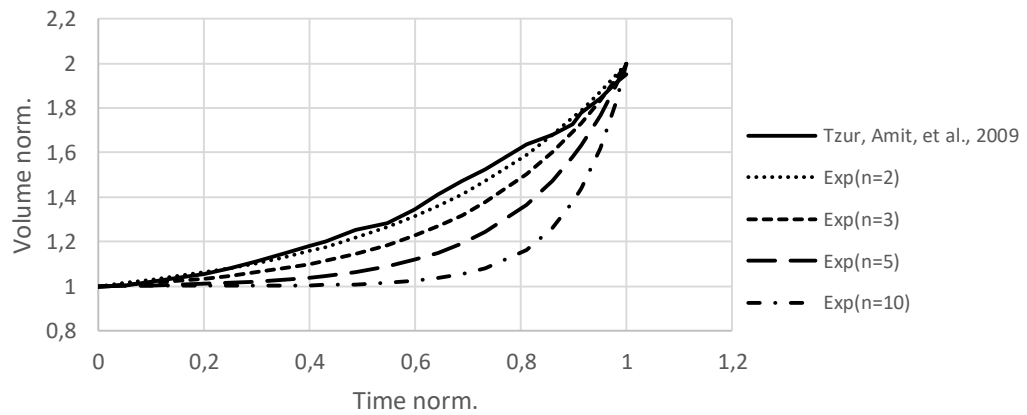
Table 5.4, which presents the average difference between the values obtained with experimental observation (coming from three distinct experimental observations) and the corresponding values coming from the developed theoretical expressions.

Analysis of growth laws



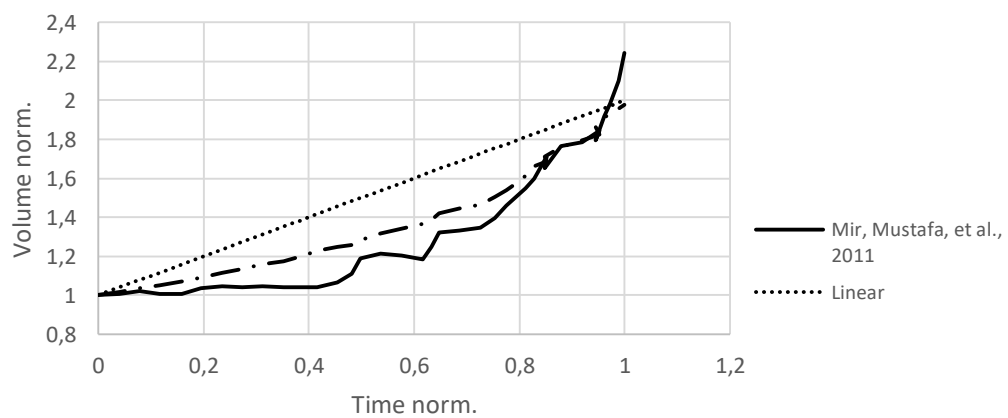
(a)

Analysis of growth laws



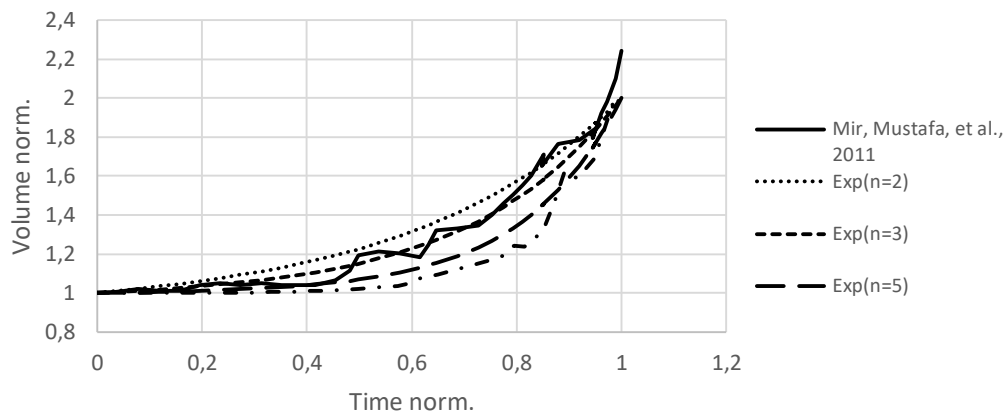
(b)

Analysis of growth laws



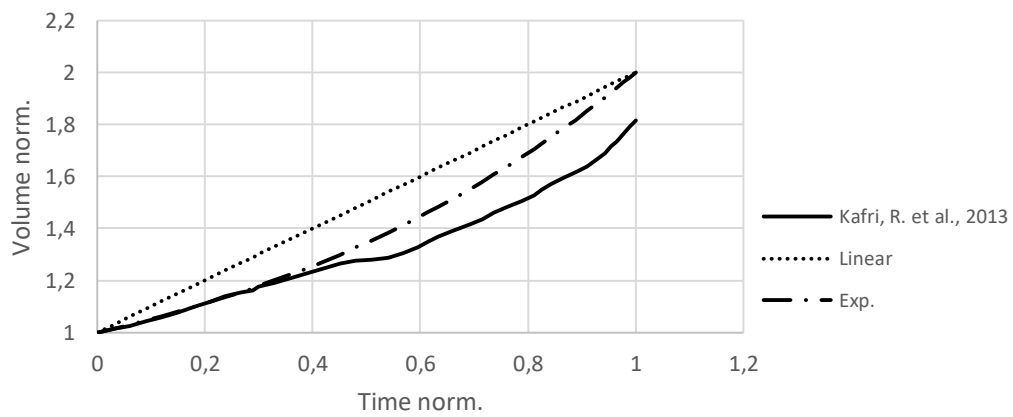
(c)

Analysis of growth laws



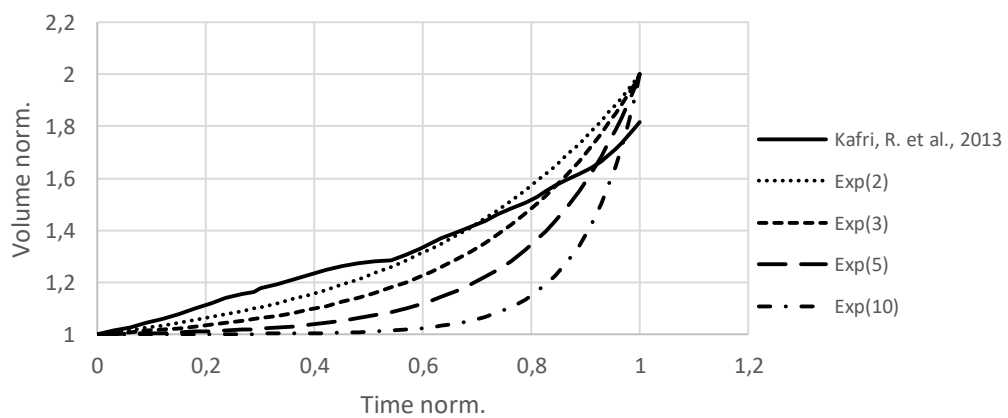
(d)

Analysis of growth laws



(e)

Analysis of growth laws



(f)

Figure 5.11 - Comparison between data from literature and new ones formed with growth laws created in this work.

Table 5.4 - Comparison between each growth laws created in this work (first line) and growth laws from literature (first column). “MM, 2009” corresponds to Mustafa Mir et al. 2011, “AT 2009” corresponds to Amit Tzur 2009 and “RK, 2013” corresponds to “R.Kafri 2013”

	Linear	Exp	Exp(n=2)	Exp(n=3)	Exp(n=5)	Exp(n=10)
AT, 2009	0.1603	0.0675	0.0242	0.0653	0.1305	0.2102
MM, 2011	0.2315	0.1376	0.0643	0.0437	0.0965	0.1901
RK, 2013	0.1934	0.0984	0.0679	0.0899	0.1396	0.2103

Analysing the graphs and the table, the growth laws more appropriate are Exp(n=2) and Exp(n=3) because they produce the smallest average difference in relation to the experimental observations. Therefore, in this work, the cell was forced to grow following equation (5.41) with n=2.

Chapter 6

Model Validation

In order to validate the available RPIM software it is necessary to verify the adequacy of several numerical parameters. The optimization of such parameters will allow to reduce the computational cost without losing accuracy. Thus, in this section it was studied: the influence of the size of the time scale (t_s); the convergence of the used numerical approach; the optimal number of nodes inside the influence domain; and the optimal Gauss-Legendre quadrature scheme (background integration mesh).

6.1 - Time scale

Time scale is a term created to define the time corresponding to each iteration of the used software. It is used to calculate the t_i in section 5.5 (developed growth law), using the following expression: $t_i = t_s \cdot n_{it}$, where t_i is the time corresponding to each iteration, t_s is the time scale and n_{it} is the corresponding iteration. When the value of t_s is modified, t_i is also changed. From the expression, increasing t_s the time corresponding to each iteration will be higher and the total number of iteration will be smaller.

In order to understand how results vary according to time scale, several time scales was chosen: 1, 2, 6, 10, 20, 60, 100, 200, 600, 1000, 2000 and 6000 seconds per each iteration. For example, the time scale 100 seconds means that each iteration corresponds to 100 seconds.

The analysis was performed using a regular nodal discretization with 1089 for the problem domain, an integration scheme of 2x2 per integration cell and 17 nodes in each influence domain.

It was verified that time scales of 1, 2 and 6 seconds lead to an inadmissible computational cost. The overall computational time was beyond acceptable (more than 24 hours, which is larger than the real division time: 16 hours). Furthermore, the time scales 10, 20 and 60 presented heavy

computational cost, which would increase the overall validation process. Therefore, the analyses considering time scales of 1, 2, 6, 10, 20 and 60 seconds were abandoned.

The time scale of 100 seconds is the lowest time scale value that allows to perform completely the analysis from the beginning (single cell) up to the complete cell division (two daughter cells).

So, it was compared all time scales with 100 seconds through the expressions: $\Delta_{ts,O_2} = \frac{C_{O_2(ts)} - C_{O_2(100)}}{C_{O_2(100)}}$ and $\Delta_{ts,GL} = \frac{C_{GL(ts)} - C_{GL(100)}}{C_{GL(100)}}$ where Δ_{ts,O_2} and $\Delta_{ts,GL}$ are relative differences between the concentrations of oxygen or glucose, $(C_{O_2(ts)}, C_{GL(ts)})$, obtained with an analysis using time scale, t_s , and the same concentrations, $(C_{O_2(100)}, C_{GL(100)})$, obtained for an analysis performed with the time scale of 100 seconds, t_{100} . Figure 6.2 shows the results of these comparisons for oxygen in (a) and for glucose in (b). If the results of higher time scales are similar to the results of time scale 100, it will be possible to perform the analysis with higher time scales, obtaining the same results as time scale $t_s=100$. Therefore, reducing significantly the computational cost. In fact, differences between them are all insignificant, and it was chosen the time scale of 2000 seconds that have a difference of 6.0×10^{-8} to oxygen and -1.0×10^{-8} to glucose.

In Table 6.1 and Figure 6.1 are shown the computational costs in seconds for each time scale (Table 6.1) and in minutes for a complete analysis (Figure 6.1). The ‘computational cost’ is the time that the analysis takes to complete a full cell cycle. As already mentioned, time scale is the time chosen for each iteration of the used software; real iteration time is the time that in fact one iteration take to be complete. Analysis time is the total time of the program obtained by multiplication of real time iteration and the number of iterations. Therefore, it is possible to observe that with larger time scales, the used software requires less time to finish the analysis.

Table 6.1 - Computational costs between different time scales (time in each iteration).

Time scale (s)	Real iteration time (s)	Analysis time (min)
100	9.30	163.37
200	9	79.05
600	8.80	25.81
1000	8.50	15.02
2000	8.30	7.33
6000	8.20	2.50

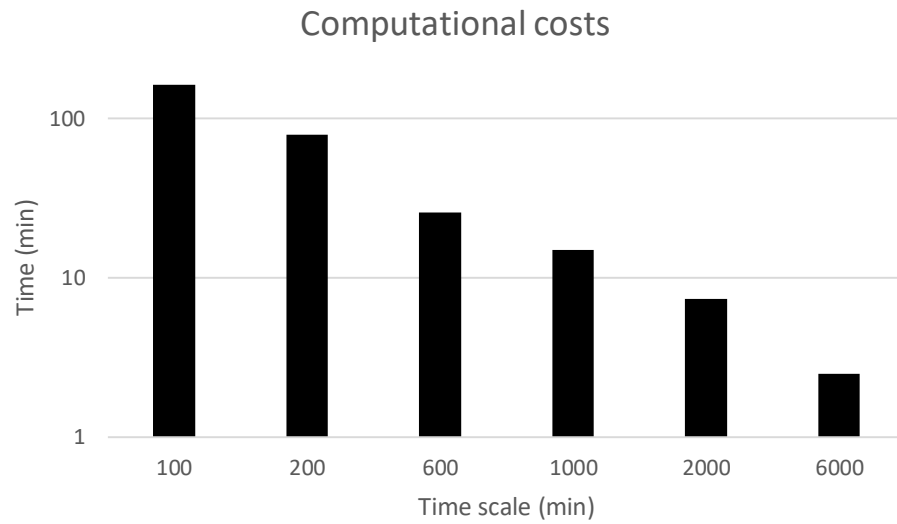
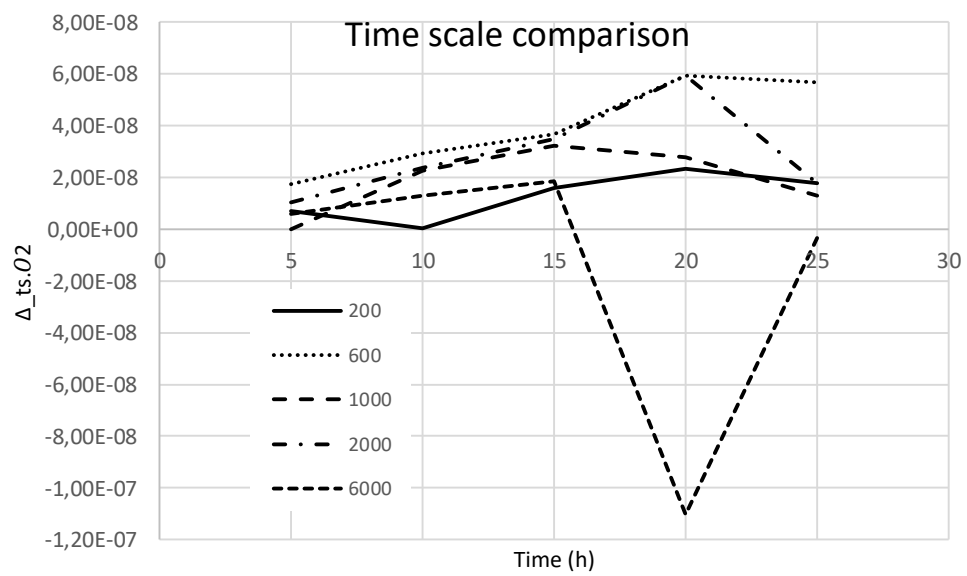
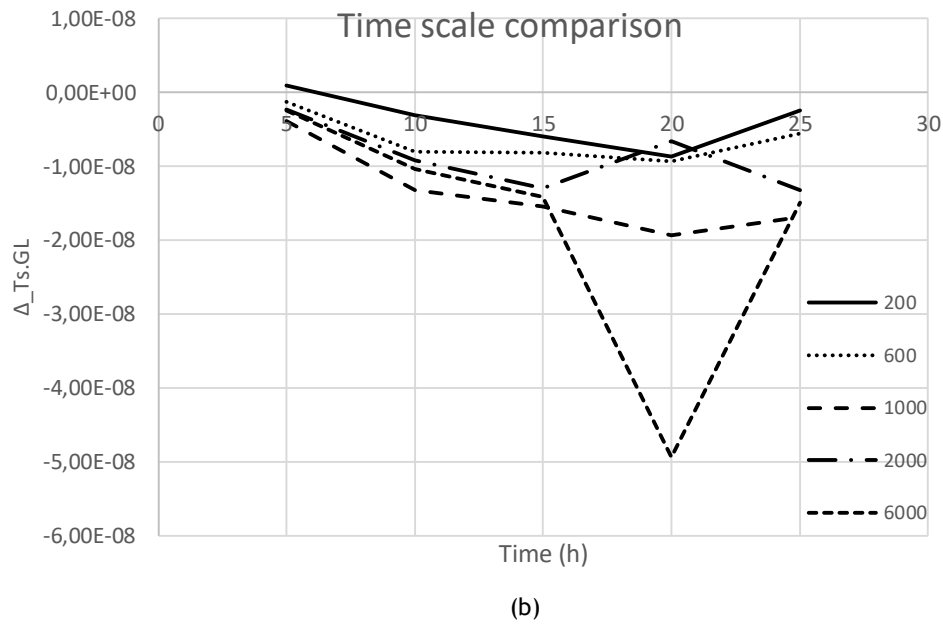


Figure 6.1 - Computational costs between each time scale chosen in logarithmic scale.



(a)



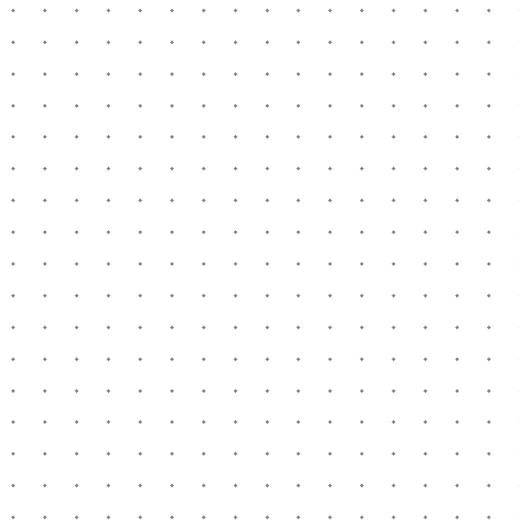
(b)
Figure 6.2 - Time scale of 100 seconds comparing with 200, 600, 1000, 2000 and 6000 seconds. (a) Δ_{O_2} and (b) Δ_{GL} .

6.2 - Convergence study

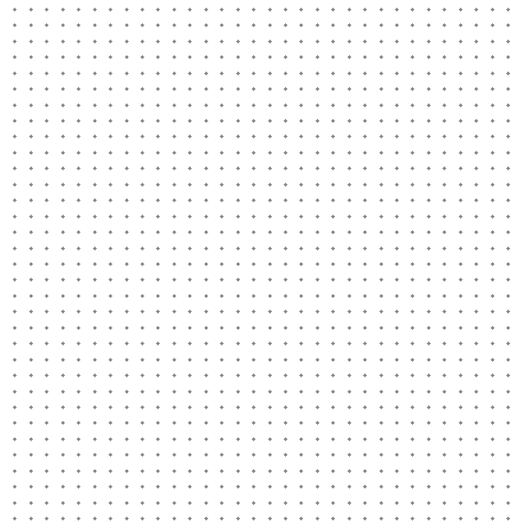
The study performed in this section will allow to understand if the methodology produces a convergent solution, according with the variation of the number of nodes discretizing the problem domain. The methodology is convergent if the obtained solution tends to the same value when the nodal mesh is increased in density (following a quadratic rule).

The number of nodes is related to the number of divisions along x and y in the problem domain. Therefore, 16x16 divisions will generate 289 (17x17) nodes discretizing the problem domain. So, increasing the number of divisions, the number of nodes will be higher. Based on that, it was decided to test a number of divisions of 16x16 - 289 nodes, 32x32 - 1089 nodes and 64x64 - 4225 nodes.

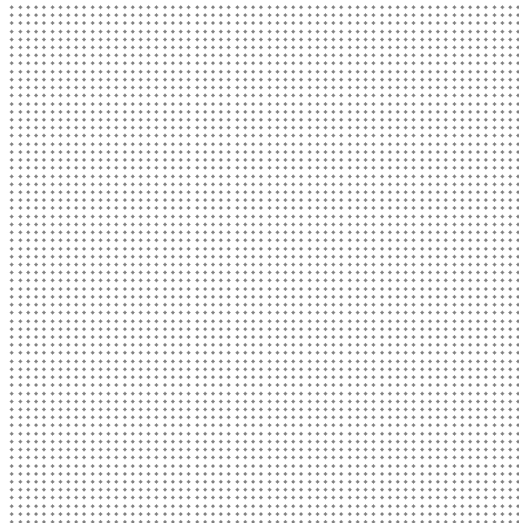
Nodal mesh is regular along the problem domain as shown in Figure 6.3.



(a) 16x16



(b) 32x32

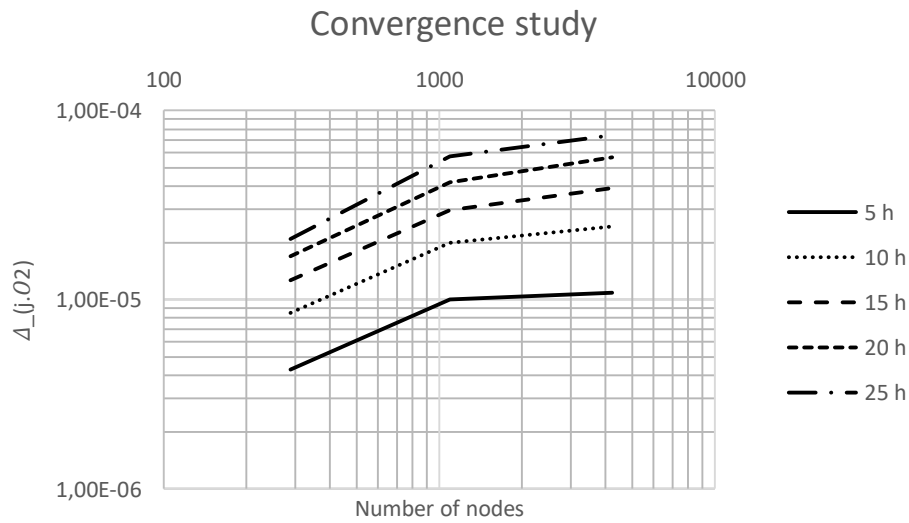


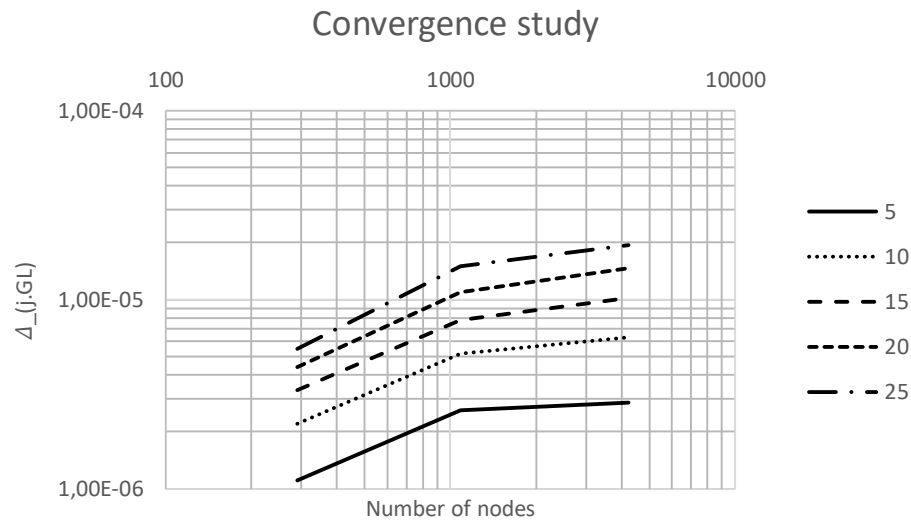
(c) 64x64

Figure 6.3 - Nodal discretization of a regular mesh. (a) 16x16 - 289 nodes, (b) 32x32 - 1089 nodes and (c) 64x64 - 4225 nodes.

The analysis was performed using a time scale of 600 seconds, an integration scheme of 2x2 and 17 nodes in each influence domain.

Since the developed cell growth algorithm is iterative, and therefore, nonlinear, it is important to understand the performance of the code during the analysis. Therefore, for each nodal discretization (289, 1089 and 4225 nodes) it was captured the C_{O_2} and C_{GL} in distinct time steps, corresponding to 5, 10, 15, 20 and 25 hours. The results for C_{O_2} and C_{GL} are presented in Figure 6.4(a) and Figure 6.4(b), respectively and the results are obtained using the expressions: $\Delta_{j,O_2} = \frac{C_{O_2(j)} - C_{O_2(i)}}{C_{O_2(i)}}$ and $\Delta_{j,GL} = \frac{C_{GL(j)} - C_{GL(i)}}{C_{GL(i)}}$, where Δ_{j,O_2} and $\Delta_{j,GL}$ correspond to the relative difference between the concentrations of oxygen and glucose obtained in iteration j ($C_{O_2(j)}$, $C_{GL(j)}$) and the initial concentrations ($C_{O_2(i)}$, $C_{GL(i)}$). Figure 6.4 show the obtained values of Δ_{j,O_2} and $\Delta_{j,GL}$ (captured in distinct iterative steps j) for distinct nodal meshes. It is possible to visualise that the solution tends to a hypothetical convergent final value, which will be very close to the value obtained with the nodal mesh of 4225 nodes. Regardless the iteration step (time step) in which the solution is captured, the corresponding convergence path is perceptible. Thus, it is understandable that, using nodal meshes with a total number of nodes higher than 4225 will allow to produce results very close to the final converged solution.





(b)

Figure 6.4 - Convergence study to decide the best number of nodes to use. The values were obtained in the end of 5, 10, 15, 20 and 25 hours. (a) Δ_{Cs,O_2} and (b) $\Delta_{Cs,GL}$. Both axis are in logarithmic scale.

6.3 - Influence domain study

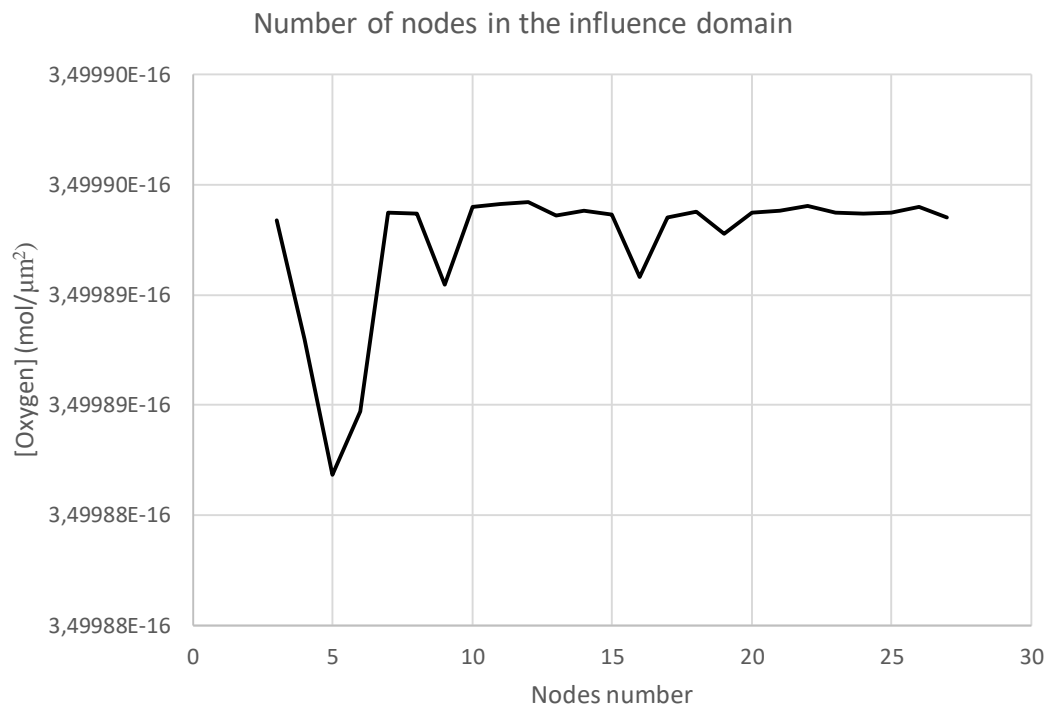
The study performed in this subsection aims to obtain the optimal number of node inside each influence domain. In order to determine the optimal number of nodes inside the influence domain, several analysis should be performed, each one using a distinct value for the number of nodes inside of each influence domain. Then, the solution of each analysis should be compared with a reference solution and a polynomial functions should be adjusted to the obtained scattered data. The minimum of those functions represents the optimal number of nodes inside each influence domain.

Therefore, in this work, several number of nodes in each influence domain was tested, from 3 to 27. The analysis was performed using a time scale of 600 seconds, an integration scheme of 2x2 and 1089 nodes discretizing the problem domain.

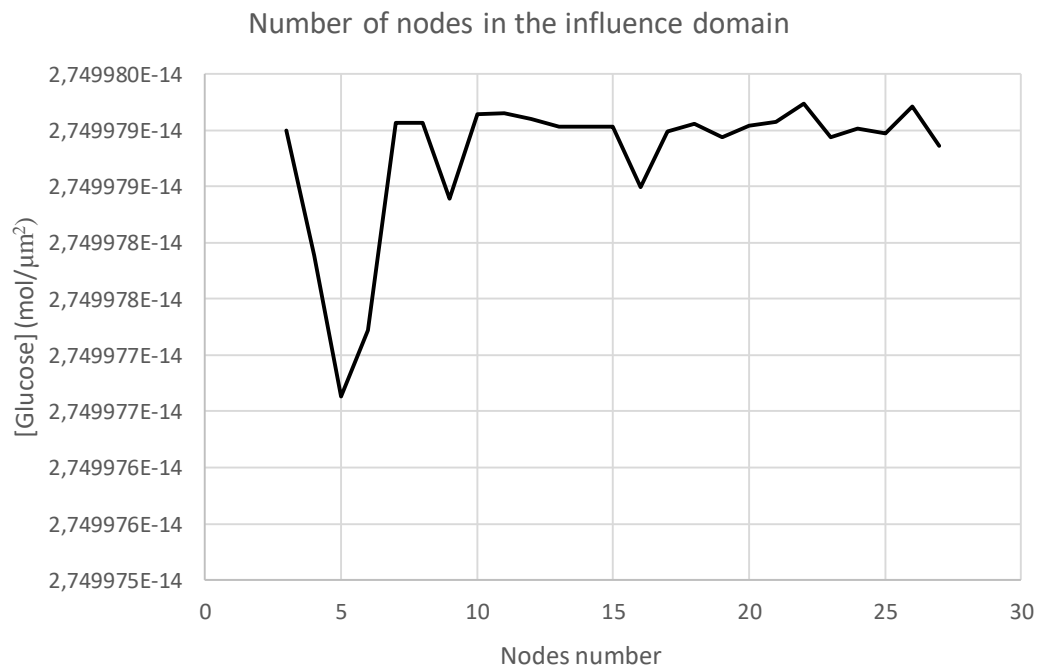
The oxygen and glucose concentrations in the middle of the computational analysis, Figure 6.5, and again in the end of the analysis, Figure 6.6 were reported. Figure 6.5 and Figure 6.6 show that both concentrations vary according to the number of nodes inside each influence domain, showing some peaks until 16 nodes. Thus, for this range values, this instability does not allow to decide with confidence the best value for the number of nodes inside the influence domain. However, it is possible to visualize that after 16 nodes de solutions tend to stabilize, showing very small variations with the variation of the number of nodes inside each influence domain.

Therefore, 17 nodes were selected as the optimal number of nodes inside each influence domain. Notice that from this value beyond the solution does not experience large variations. In addition,

since the increase of the influence domain size increases the computational cost, it is preferable to use the lowest possible number of nodes inside the influence domain.

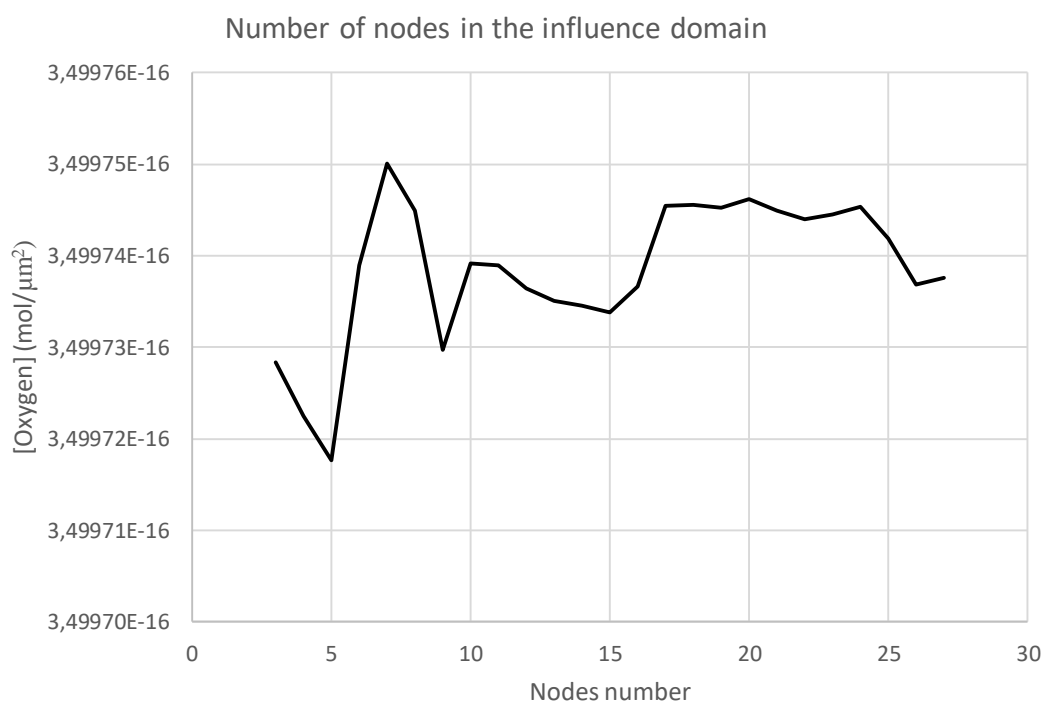


(a)

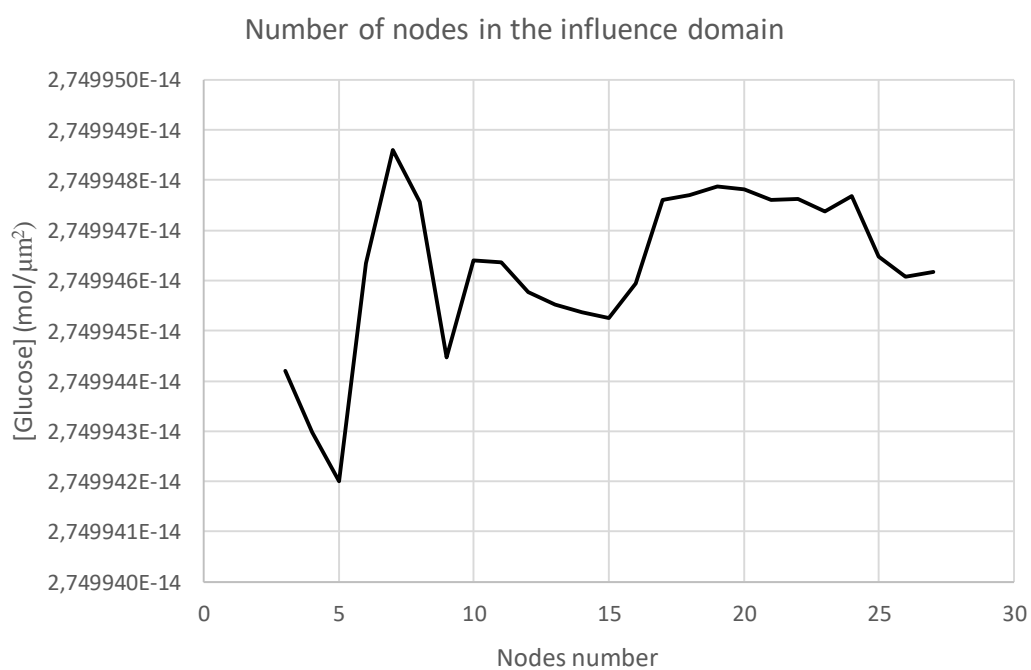


(b)

Figure 6.5 - Comparison between the number of nodes in the influence domain in the middle of the program, relatively to oxygen in (a) and to glucose in (b).



(a)



(b)

Figure 6.6 - Comparison between the number of nodes of the influence domain in the last iteration, relatively to oxygen in (a) and to glucose in (b).

6.4 - Integration scheme

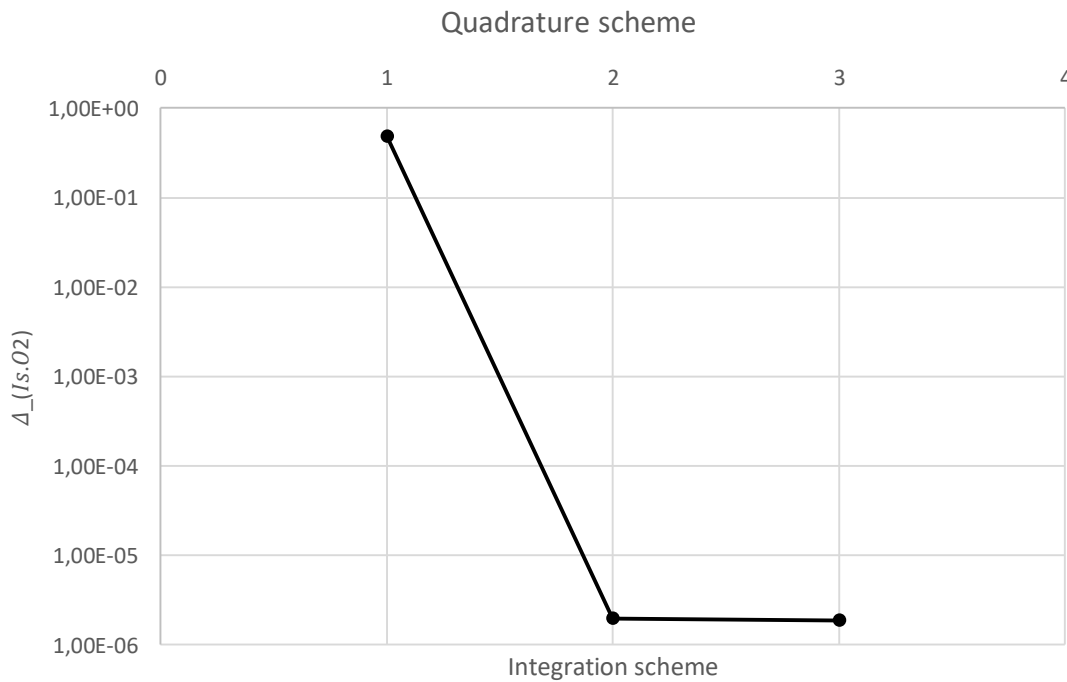
In this subsection the integration scheme was analysed. Thus, square integration cells were obtained from a background lattice, in which each edge of the squares is equal to the double of the average nodal distance. Inside of each integration cell, it is possible to distribute integration points following the Gauss-Legendre quadrature scheme, as already mentioned in Chapter 5.

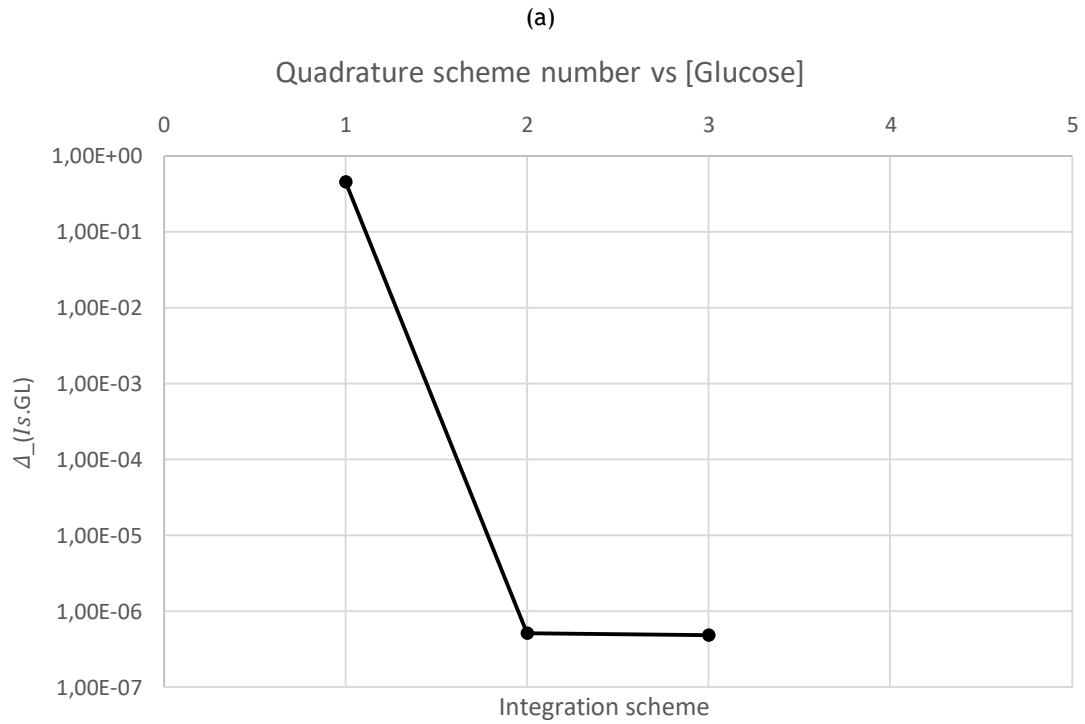
Here, four integration schemes were tested for each integration cell: 1x1, 2x2, 3x3 or 4x4.

Theoretically, increasing the number of integration points inside each integration cell will lead to an increase in accuracy of the solution. However, it will also increase the computational cost. Therefore, it is necessary to find an optimal integration scheme, capable to deliver an accurate solution within an acceptable computational cost.

The analysis was performed using 1089 nodes discretizing the domain problem, a time scale of 600 seconds and 17 nodes in each influence domain.

Then, the integration scheme of 4x4 with all others was compared with the following expressions: $\Delta_{Is.O2} = \frac{C_{O2(Is)} - C_{O2(i)}}{C_{O2(i)}}$ and $\Delta_{Is.GL} = \frac{C_{GL(Is)} - C_{GL(i)}}{C_{GL(i)}}$, where $\Delta_{Is.O2}$, $\Delta_{Is.GL}$ represent the relative difference between the final oxygen and glucose concentrations obtained for each integration scheme, $C_{O2(Is)}$, $C_{GL(Is)}$, and $(C_{O2(i)}, C_{GL(i)})$ are the final concentrations of oxygen and glucose for the 4x4 integration scheme. Figure 6.7 presents the results of the previous expressions, in which it is possible to visualize that the quadrature scheme of 1x1 produces results very distant from the ones obtained with an integration scheme of 4x4 (the difference value is approximately 1.0), while using integration scheme of 2x2 and 3x3 it is possible to obtain lower differences (approximately 1.0×10^{-6}). Therefore, a quadrature scheme of 2x2 for further analysis was selected.





(b)

Figure 6.7 - Comparison between integration scheme of 4x4 and 1x1, 2x2 and 3x3. (a) Δ_{I_s, O_2} and (b) $\Delta_{I_s, GL}$.

6.5 - Gradient mesh

Considering a nodal discretization of 4225 nodes (64x64 divisions) permits to obtain accurate results, however it also represents a very high computational cost. Therefore, it is necessary to find an alternative discretization procedure to reduce the computational cost and, at the same time, maintain or increase the accuracy of the solution.

Since the cell will be placed at the centre of the domain, it is suggested that this centre region is discretized with a higher density, and then, in neighbouring regions, the discretization density will smoothly start to reduce. Thus, the gradient nodal distribution presented in Figure 6.8 is proposed.

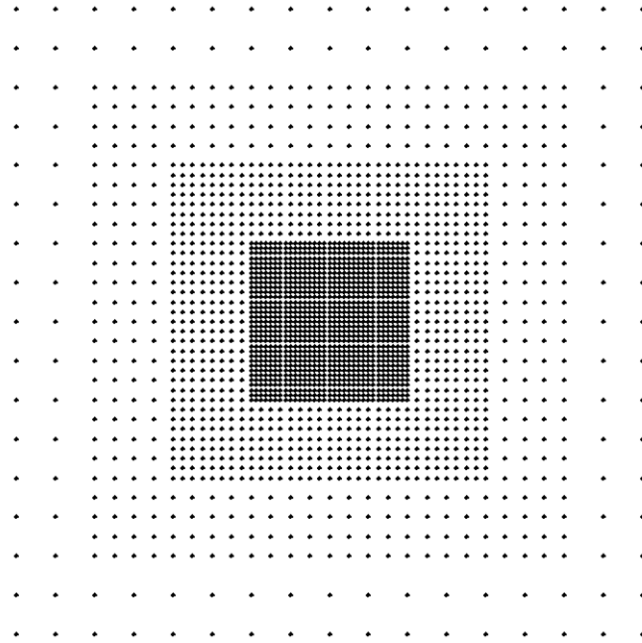


Figure 6.8 - Gradient mesh increasing the number of divisions in the centre and consequently the number of nodes.

In order to understand the efficiency of using a gradient mesh, some comparison studies were performed, in which the solutions obtained with the previously presented regular nodal distributions are compared with the proposed gradient mesh. The following parameters in Table 6.2 were defined: domain size (μm), thickness (μm), number of division/number of nodes in the problem domain, number of nodes in the influence domain, quadrature scheme and time of each iteration.

Table 6.2 - Parameters analysed to compare regular and gradient mesh.

Mesh	Domain size (μm)	Thickness (μm)	N° nodes inf.domain	Quadrature scheme	Time scale (s)	N° nodes discretizing the problem domain
Regular	1000x1000	5000	17	2	2000	1089 4225 16641
Gradient	1000x1000	5000	7	2	2000	2040

Thus, using the parameters in Table 6.2 the variation of volume along time for each analysis was obtained. In order to present clearly the results, the volume was normalized following the expression: the cell's volume at each iteration is divided by the initial volume of the cell.

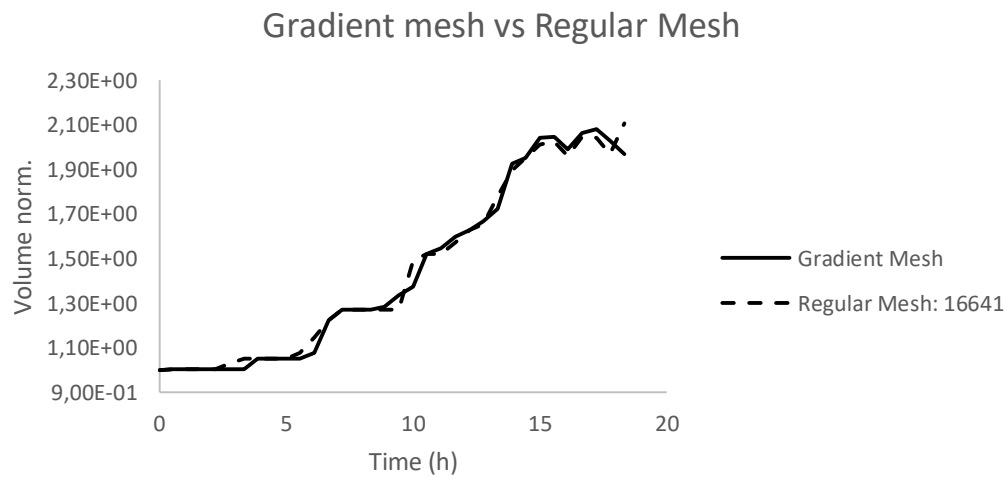
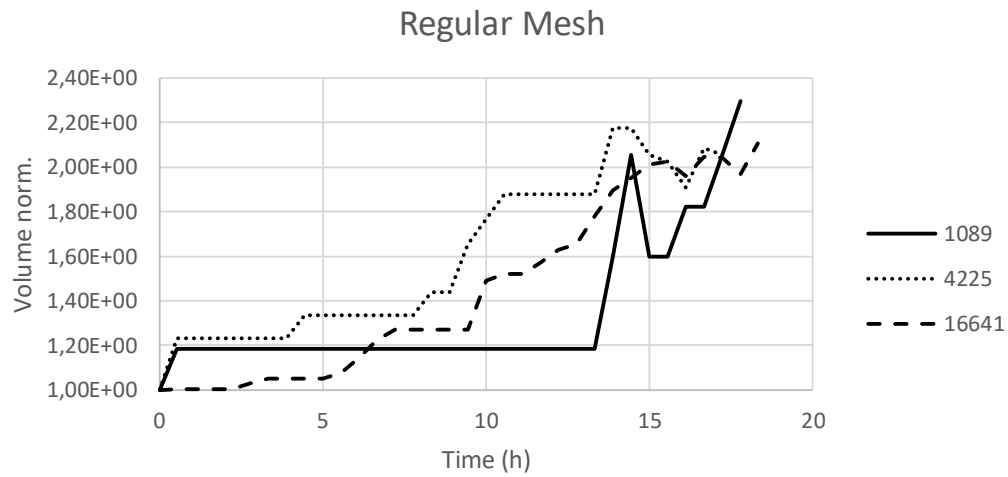


Figure 6.9 - Comparison between different meshes: (a) only between different regular meshes; (b) between the best divisions using regular mesh with gradient mesh.

Figure 6.9 (a) compares the volume variation obtained with distinct regular nodal distributions and Figure 6.9 (b) compare a regular mesh using 128x128 divisions with the proposed gradient mesh. Here, it is possible to conclude that both have a similar increase of cell volume and so the gradient mesh is the best option because this gradient mesh decreases the time consumption and the computational costs, maintaining the good results. The computational costs used in this comparison are presented in the Figure 6.10.

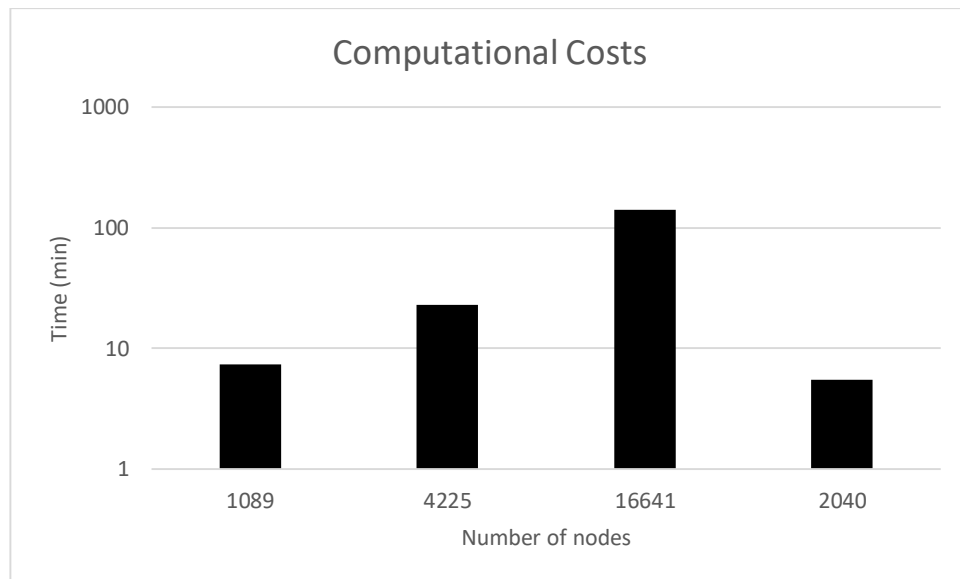


Figure 6.10 - Computational costs between the number of nodes in logarithmic scale.

As it is possible to see, regular mesh using 128x128 divisions (16641 nodes) take too much time to be conclude: 2 hours. A gradient mesh using only 2040 nodes give the same results of regular mesh using 128x128 divisions, but take 5.5 minutes, which show that a gradient mesh is a big advantage.

Chapter 7

Results and Discussion

In this section, it is possible to visualize the results of the study of tumour growth and cell cycle using the RPIM software.

Several tests were performed with the objective of showing the performance of the used software. Since the literature shows that cell growth is exponential, the used software allows to select the type of growth using the expressions previously presented. All results showed a cell cycle duration in an acceptable range of hours, less than 20 hours [214][215] which demonstrate cell cycle in cancer cells is faster than healthy ones.

As previously described, mitosis correspond to 5% of the entire cell cycle. Thus, to capture the mitosis progression with high accuracy, the time steps during mitosis were reduced by 20%. This way, it is possible to study the cell growth using a time scale of 2000s and when the cell starts the mitosis, the time scale is reduced to 400s. The model validation, the results were obtained using the parameters summarized in the following Table 7.1. Only 7 nodes were used in influence domain instead of 17, because 7 nodes are enough in gradient mesh.

Table 7.1 - Parameters chosen for final analysis.

Mesh	Domain size (μm)	Thickness (μm)	Number of nodes discretizing the problem domain	Nº nodes inf.domain	Quadrature scheme	Time scale (s)
Gradient	1000x1000	5000	2040	7	2	2000

In Figure 7.1, Figure 7.2, Figure 7.3 and Figure 7.4 are presented the C_{O_2} and C_{GL} in the medium during cell cycle: interphase and mitosis. The colours represent the concentration: oxygen decreased from $3.5e^{-16}$ to $3.4996e^{-17}$ [mol/cm^3] and glucose $2.75e^{-14}$ to $2.7499e^{-14}$ [mol/cm^3].

Figure 7.5 shows the decrease of C_{O_2} and C_{GL} [mol/cm^3] in the medium along time from the initiation of program until the cell divides in two daughter cells.

In Figure 7.6 and Figure 7.7 is observed the cell growth and cell division until it originate two independent cells.

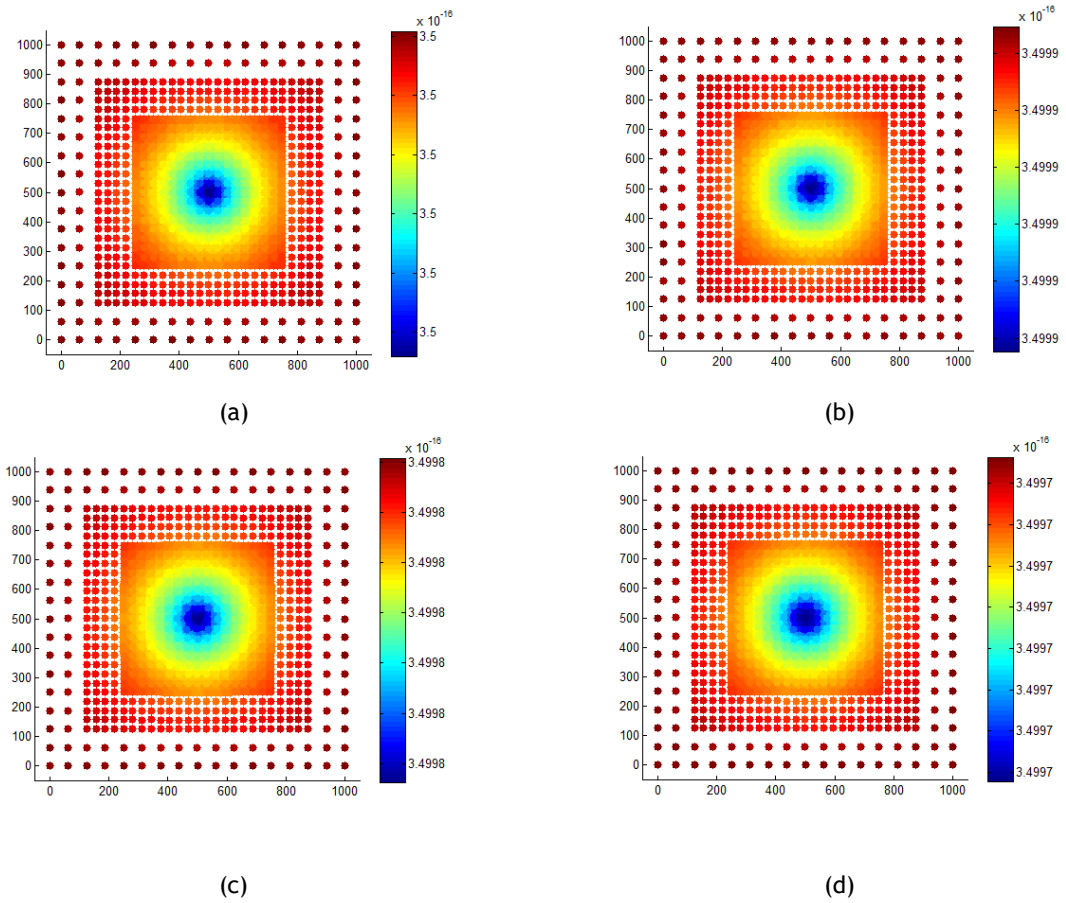
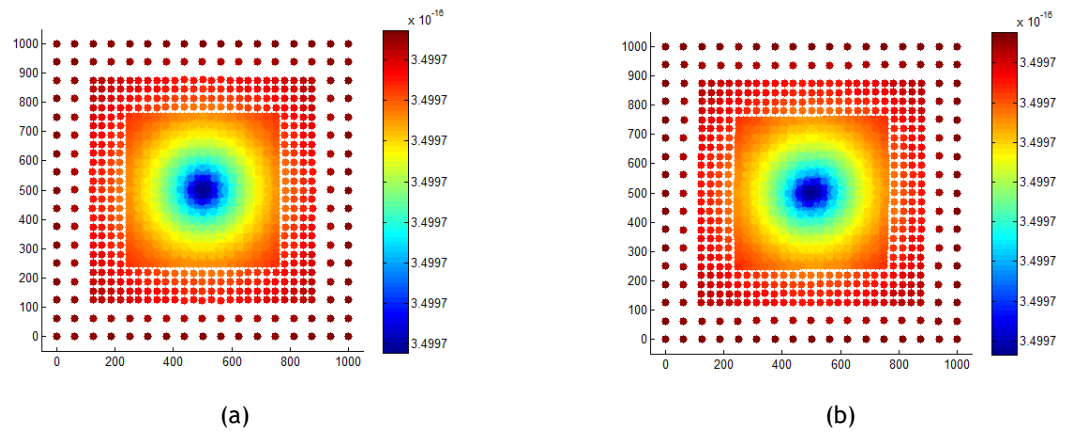
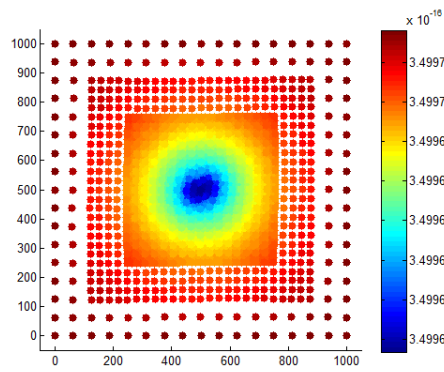
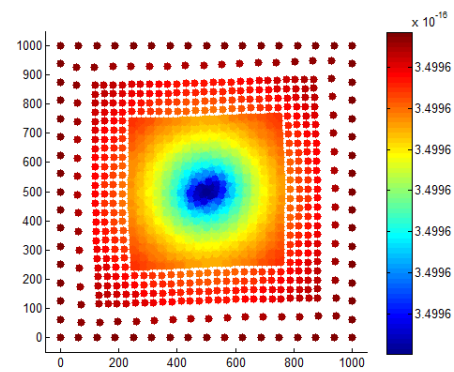


Figure 7.1 - Variation of oxygen during interphase of cell cycle, corresponding to (a) 33 minutes, (b) 5 hours, (c) 9 hours and (d) 14 hours of cell cycle.



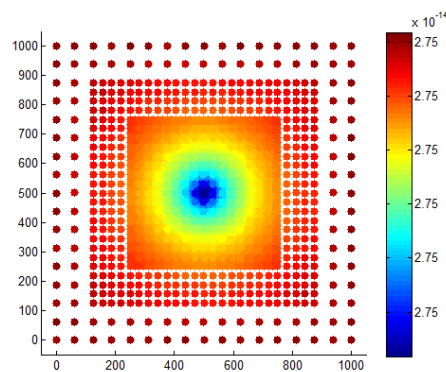


(c)

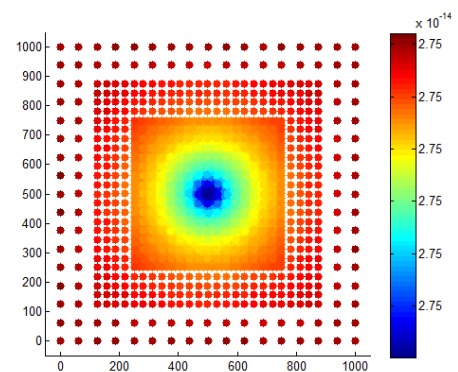


(d)

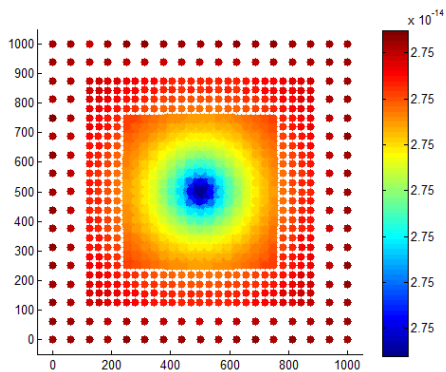
Figure 7.2 - Variation of oxygen during mitosis phase of cell cycle, corresponding to (a) 15 hours, (b) 16 hours, (c) 17 hours and (d) 18 hours of cell cycle.



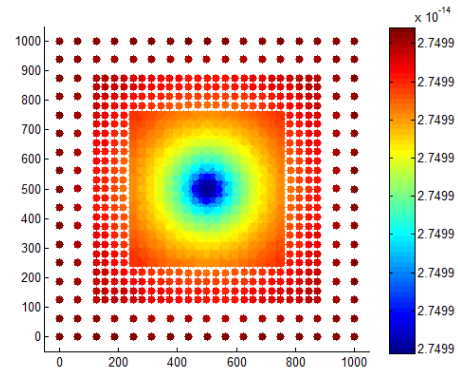
(a)



(b)



(c)



(d)

Figure 7.3 - Variation of glucose during interphase of cell cycle, corresponding to (a) 33 minutes, (b) 5 hours, (c) 9 hours and (d) 14 hours of cell cycle.

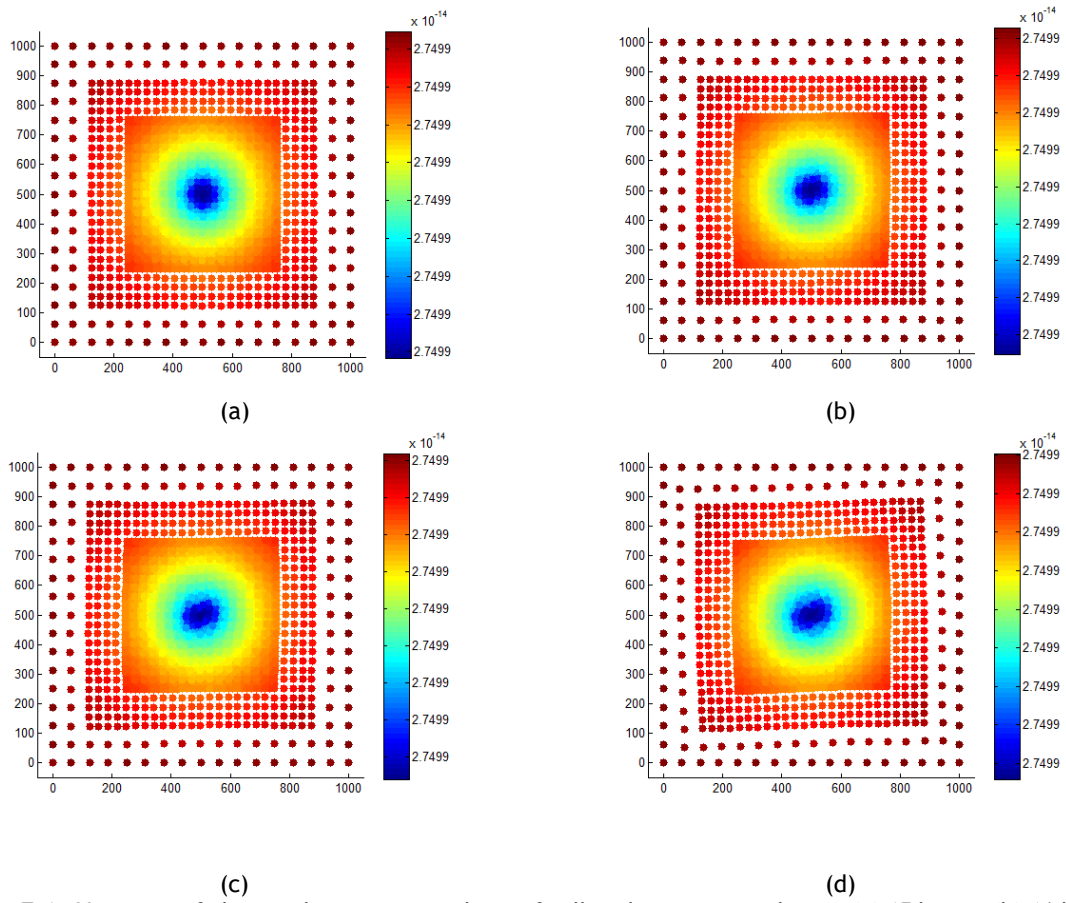
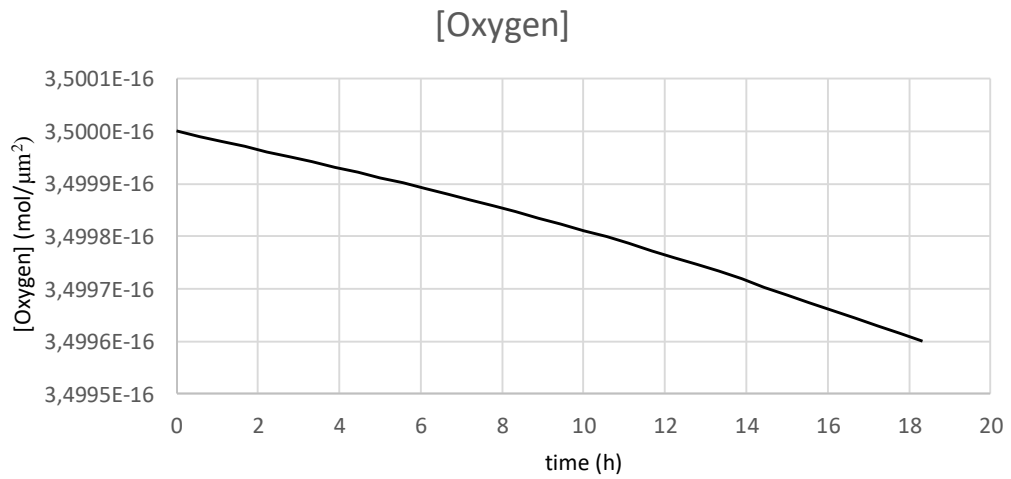


Figure 7.4 - Variation of glucose during mitosis phase of cell cycle, corresponding to (a) 15 hours, (b) 16 hours, (c) 17 hours and (d) 18 hours of cell cycle.



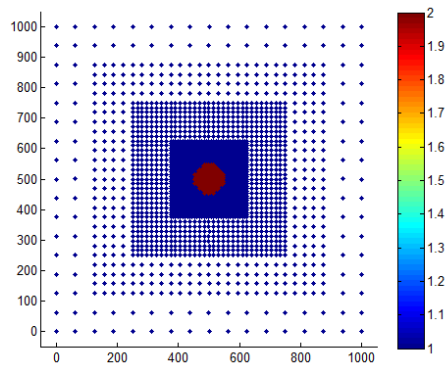
(a)



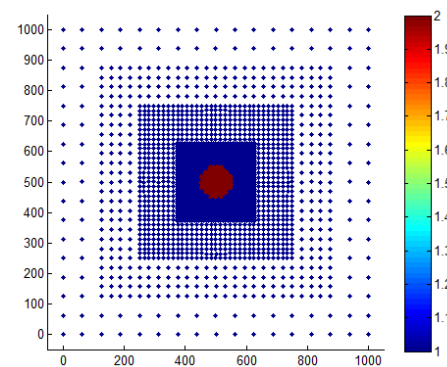
(b)

Figure 7.5 - (b)Oxygen and (c) glucose concentrations during cell cycle.

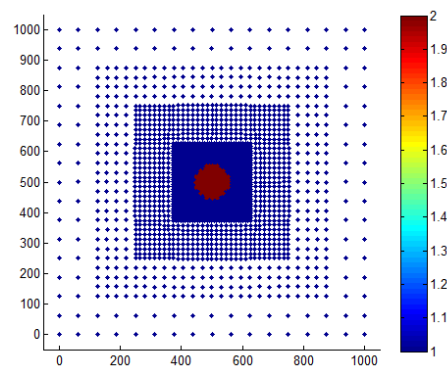
From the results, it is possible to visualize that the oxygen and glucose concentration decrease at the same rate. These results corroborate the consumption rates described in the literature [146] and both concentrations can be used for a higher number of cells as occur *in vitro* experiences.



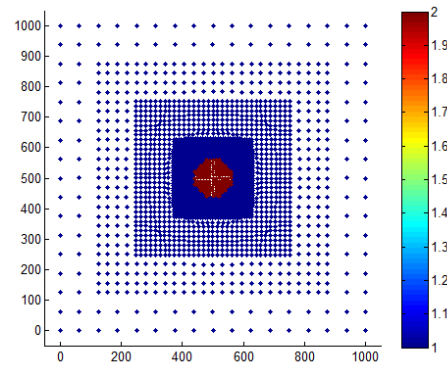
(a)



(b)



(c)



(d)

Figure 7.6 - Cellular growth during interphase at (a) 33 minutes, (b) 5 hours, (c) 9 hours and (d) 14 hours of cell cycle.

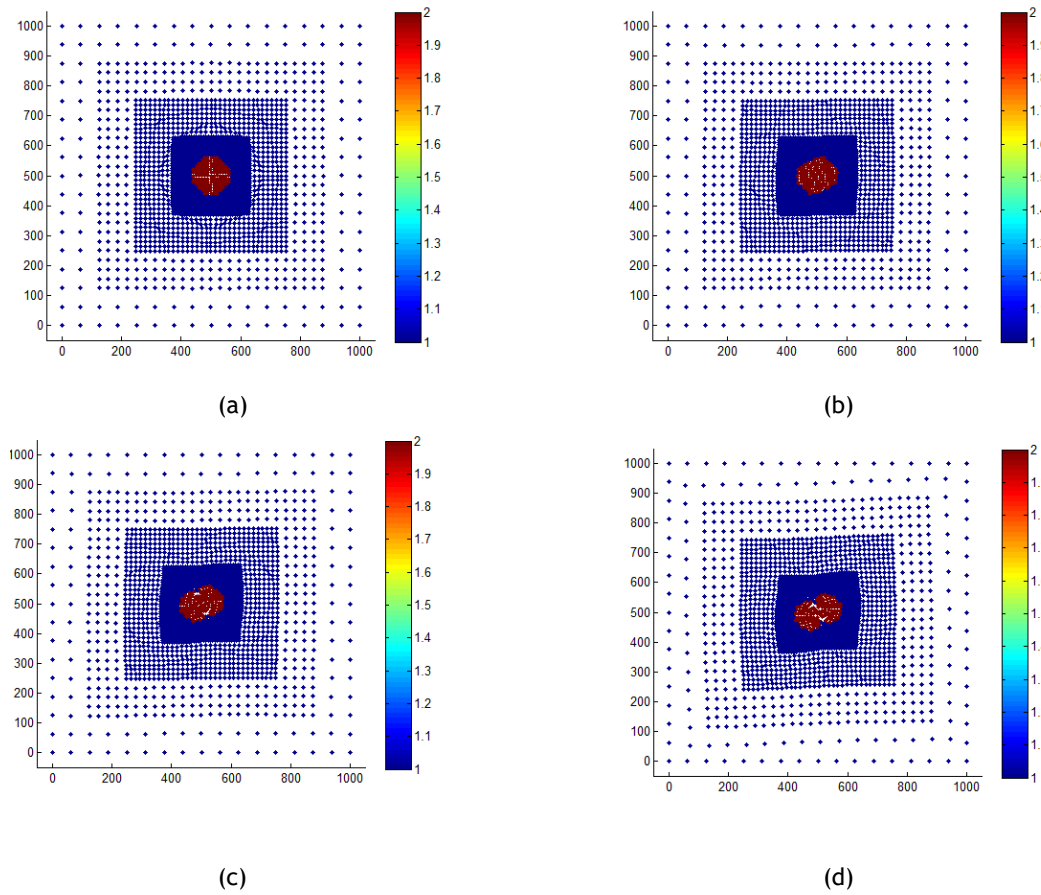


Figure 7.7 - Cellular growth during mitosis phase at (a) 15 hours, (b) 16 hours, (c) 17 hours and (d) 18 hours of cell cycle.

The final iteration of the program shows the two cells in different colours (green and red) with the nodal mesh reorganized (Figure 7.8).

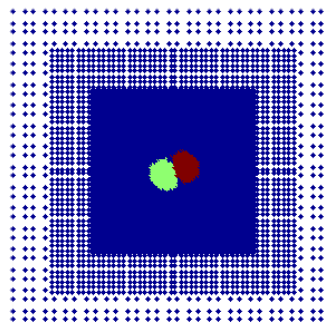


Figure 7.8 - After cell cycle, one cell result in two daughter cells (green and red).

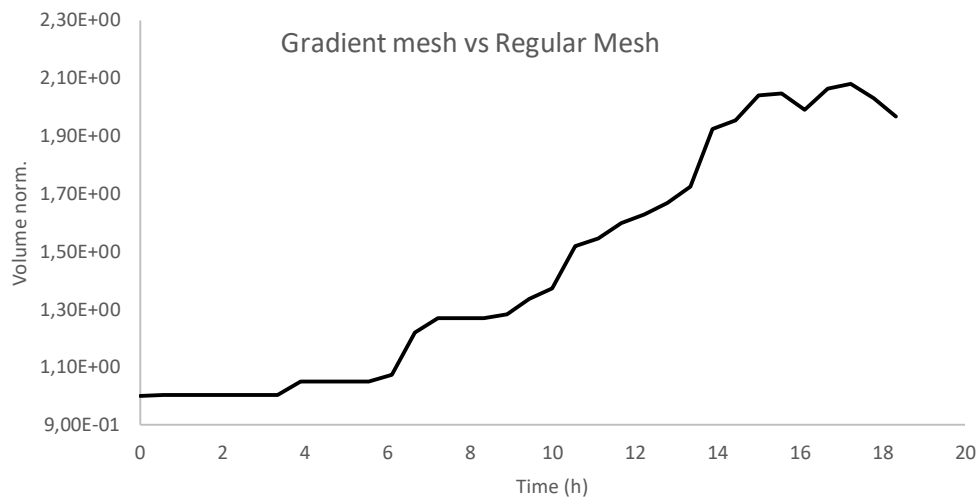


Figure 7.9 - Growth cell during all cell cycle using the exponential law. Both time and volume were normalized;

In Figure 7.6 and Figure 7.7 it was possible to isolate interphase from mitosis in cell cycle. In the used software it is possible to understand when interphase stops and when mitosis starts, and, besides that, it was possible to visualize the shape changes during interphase (growth) and mitosis (elongation and division in two cells). It was also possible to finish the cell cycle and obtain two daughter cells. In Figure 7.9 is represented the growth law obtained with the program and is the same that was validated before.

The repetition of the dividing process will allow in the near future to predict the cellular division of multiple cell at the same time and, thus, predict the evolution of a cell population.

The time it takes for the cell to reach twice the initial size corroborates the literature that claims that cancer cells can divide in less than 24 hours, depending on type of cancer cell [52], [56]. Here, cancer cells take 20 hours to divide with an exponential growth, which is less than 24 hours.

Chapter 8

Conclusions and Future Works

Mathematical models are useful to complement the experimental investigation, with the possibility to obtain better results. They are a recent area of investigation connecting medicine to biology.

In this work, it was presented a review of the information concerning cancer and mathematical models.

After understanding the cell biology, the cell cycle and the cell death, the candidate used the “RPIM software for cellular growth and division”, and performed several validation tests, like time scale, convergence test, influence domain study and integration scheme. All tests are important because a new methodology was used in this work and the results of model validation showed a robust and convergence methodology. Besides that, the creation of a gradient mesh in domain of interest showed that is possible decrease the computational costs but maintain good results and lastly, a new growth law was achieved simulated what really happen in *in vitro* experiments.

The results showed that the “RPIM software for cellular growth and division” is a numerical tool that can be adapted to biological sciences and can help and complement biological and healthy problems. In the future, it will be necessary to create a relationship between the mathematical model and *in vitro* experiments, in order to decrease the time and costs experiences, as well as justify and understand why some event occur *in vitro*.

So, it is very important to continue improving “RPIM software for cellular growth and division” by creating a cancer nodule and understand what happens to cells at low or no concentrations of oxygen and nutrients like glucose. It is also important to test these cells with drugs and understand how they react. All this tasks are possible to be done applying mathematical models as this work shows.

References

- [1] A. Jemal, F. Bray, and J. Ferlay, "Global Cancer Statistics," vol. 61, no. 2, pp. 69-90, 2011.
- [2] American Cancer Society, "Ovarian Cancer," p. 63, 2014.
- [3] E. Süli, "Finite Element Methods for Partial Differential Equations," no. December, p. 106, 2012.
- [4] S. Matsunaga, N. Takano, Y. Tamatsu, S. Abe, and Y. Ide, "Biomechanics of Jaw Bone Considering Structural Properties of Trabecular Bone," *J. Oral Biosci.*, vol. 53, no. 2, pp. 143-147, 2011.
- [5] N. J. Reddy, "An introduction to the finite element method," *McGraw-Hill Education*, 2005. [Online]. Available: <http://pt.slideshare.net/JohnnyBravo9/an-introduction-to-the-finite-element-method-3rd-ed-j-n-reddy>. [Accessed: 02-Jun-2016].
- [6] T. Belytschko, Y. Krongauz, D. Organ, M. Fleming, and P. Krysl, "Meshless methods: An overview and recent developments," *Comput. Methods Appl. Mech. Eng.*, vol. 139, no. 1-4, pp. 3-47, Dec. 1996.
- [7] W. Liu, S. Jun, and Y. Zhang, "Reproducing kernel particle methods," *Int. J. Numer. methods fluids*, vol. 20, no. 8-9, pp. 1081-1106, 1995.
- [8] T. Belytschko, Y. Y. Lu, and L. Gu, "Element-free Galerkin methods," *Int. J. Numer. Methods Eng.*, vol. 37, no. 2, pp. 229-256, Jan. 1994.
- [9] S. N. Atluri and T. Zhu, "A new Meshless Local Petrov-Galerkin (MLPG) approach in computational mechanics," *Comput. Mech.*, vol. 22, no. 2, pp. 117-127, Aug. 1998.
- [10] S. De and K. J. Bathe, "The method of finite spheres," *Comput. Fluid Solid Mech.*, vol. 25, pp. 1546-1549, 2001.
- [11] E. Oñate and S. R. Idelsohn, "A mesh-free finite point method for advective-diffusive transport and fluid flow problems," *Comput. Mech.*, vol. 21, no. 4-5, pp. 283-292, 1998.
- [12] E. J. Kansa, "Multiquadrics-A scattered data approximation scheme with applications to computational fluid-dynamics-I surface approximations and partial derivative estimates," *Comput. Math. with Appl.*, vol. 19, no. 8-9, pp. 127-145, 1990.
- [13] L. M. J. S. Dinis, R. M. Natal Jorge, and J. Belinha, "Analysis of 3D solids using the natural neighbour radial point interpolation method," *Comput. Methods Appl. Mech. Eng.*, vol. 196, no. 13-16, pp. 2009-2028, Mar. 2007.
- [14] G. R. Liu and Y. T. Gu, "A point interpolation method for two-dimensional solids," *Int. J. Numer. Methods Eng.*, vol. 50, no. 4, pp. 937-951, Feb. 2001.
- [15] G. R. Liu, "A point assembly method for stress analysis for two-dimensional solids," *Int. J. Solids Struct.*, vol. 39, no. 1, pp. 261-276, 2001.
- [16] S. R. Idelsohn, E. Onate, N. Calvo, and F. Del Pin, "The meshless finite element method," *Int. J. Numer. Methods Eng.*, vol. 58, no. 6, pp. 893-912, 2003.
- [17] N. Sukumar, B. Moran, A. Y. Semenov, and V. V. Belikov, "Natural neighbour Galerkin methods," *Int. J. Numer. Methods Eng.*, vol. 50, no. 1, pp. 1-27, 2000.
- [18] J. Braun and M. Sambridge, "A numerical method for solving partial differential equations on highly irregular evolving grids," *Nature*, vol. 376, no. 6542, pp. 655-660, 1995.
- [19] N. Sukumar and T. Belytschko, "The natural element method in solid mechanics," *Int. J. Numer. Methods Eng.*, vol. 43, no. 5, pp. 839-887, 1998.
- [20] E. Cueto, M. Doblaré, and L. Gracia, "Imposing essential boundary conditions in the natural element method by means of density-scaled α -shapes," *Int. J. Numer. Methods Eng.*, vol. 49, no. 4, pp. 519-546, 2000.

- [21] J. G. Wang and G. R. Liu, "A point interpolation meshless method based on radial basis functions," *Int. J. Numer. Methods Eng.*, vol. 54, no. 11, pp. 1623-1648, Aug. 2002.
- [22] J. G. Wang and G. R. Liu, "On the optimal shape parameters of radial basis functions used for 2-D meshless methods," *Comput. Methods Appl. Mech. Eng.*, vol. 191, no. 23-24, pp. 2611-2630, Mar. 2002.
- [23] P. M. Georges, "Nouvelles applications des parametres continus à la th  orie des formes quadratiques . Domaines de formes quadratiques correspondant aux diff  rents types de paraboloides primitifs ."
- [24] R. Wasserman, R. Acharya, C. Sibata, and K. H. Shin, "A patient-specific in vivo tumor model," *Math. Biosci.*, vol. 136, no. 2, pp. 111-140, 1996.
- [25] H. H. Chen, "Cell-Level Finite Element Studies of Viscous Cells in Planar Aggregates," *J. Biomech. Eng.*, vol. 122, no. 4, p. 394, 2000.
- [26] J. Zeng, J. J. Bauer, and S. K. Mun, "Modeling and mapping of prostate cancer," *Comput. Graph.*, vol. 24, no. 5, pp. 683-694, 2000.
- [27] S. Sun, M. F. Wheeler, M. Obeyesekere, and C. Patrick Jr., "Multiscale angiogenesis modeling using mixed finite element methods," *Multiscale Model. Simul.*, vol. 4, no. 4, pp. 1137-1167, 2005.
- [28] X. Zheng, S. M. Wise, and V. Cristini, "Nonlinear simulation of tumor necrosis, neo-vascularization and tissue invasion via an adaptive finite-element/level-set method," *Bull. Math. Biol.*, vol. 67, no. 2, pp. 211-259, 2005.
- [29] O. Clatz *et al.*, "Realistic Simulation of the 3D Growth of Brain Tumors in MR Images Coupling Diffusion with Biomechanical Deformation," *IEEE Trans Med Imaging*, vol. 24, no. 10, pp. 1334-1346, 2005.
- [30] J. W. Peterson, G. F. Carey, D. J. Knezevic, and B. T. Murray, "Adaptive finite element methodology for tumour angiogenesis modelling," *Int. J. Numer. Methods Eng.*, no. July 2006, pp. 1212-1238, 2006.
- [31] S. Nema and V. P. Saxena, "FEM Based Study of Concentration of Proliferating Cell in Brain Tumor," *Appl. Math.*, vol. 3, no. August, pp. 935-942, 2012.
- [32] A. Madzvamuse and U. Zenas George, "The moving grid finite element method applied to cell movement and deformation," *Finite Elem. Anal. Des.*, vol. 74, pp. 76-82, 2013.
- [33] J. Zhao, H. Naveed, S. Kachalo, Y. Cao, W. Tian, and J. Liang, "Dynamic mechanical finite element model of biological cells for studying cellular pattern formation," *Conf. Proc. ... Annu. Int. Conf. IEEE Eng. Med. Biol. Soc. IEEE Eng. Med. Biol. Soc. Annu. Conf.*, vol. 2013, pp. 4517-4520, 2013.
- [34] S. DONG, Z. LONG, L. TANG, Y. I. JIANG, and Y. YAN, "Simulation of Growth and Division of 3D Cells Based on Finite Element Method," *Int. J. Appl. Mech.*, vol. 6, no. 4, p. 1450041, 2014.
- [35] E. Nutu, H. A. Petrescu, D. Vlasceanu, L. Gruionu, and S. D. Pastrama, "Development of a Finite Element Model for Lung Tumor Displacements During Breathing," *Mater. Today Proc.*, vol. 3, no. 4, pp. 1091-1096, 2016.
- [36] I. Mellal, E. Kengne, K. El Guemhioui, and A. Lakhssassi, "3D Modeling Using the Finite Element Method for Directional Removal of a Cancerous Tumor," *J. Biomed. Sci.*, vol. 5, no. 4, pp. 1-8, 2016.
- [37] S. Ganesan and S. Lingeshwaran, "Galerkin finite element method for cancer invasion mathematical model," *Comput. Math. with Appl.*, vol. 73, no. 12, pp. 2603-2617, 2017.
- [38] M. Dehghan and V. Mohammadi, "Comparison between two meshless methods based on collocation technique for the numerical solution of four-species tumor growth model," *Commun. Nonlinear Sci. Numer. Simul.*, vol. 44, pp. 204-219, 2017.
- [39] P. Pisani, F. Bray, and D. M. Parkin, "Estimates of the world-wide prevalence of cancer for 25 sites in the adult population," *Int. J. cancer*, vol. 97, no. 1, pp. 72-81, Jan. 2002.
- [40] M. Mistry, D. M. Parkin, A. S. Ahmad, and P. Sasieni, "Cancer incidence in the United Kingdom: projections to the year 2030," *Br. J. Cancer*, vol. 105, no. 11, pp. 1795-1803, Nov. 2011.
- [41] A. S. Ahmad, N. Ormiston-Smith, and P. D. Sasieni, "Trends in the lifetime risk of developing cancer in Great Britain: comparison of risk for those born from 1930 to 1960.," *Br. J. Cancer*, vol. 112, no. 5, pp. 943-7, 2015.
- [42] H. Creighton, B. Beach, and S.-M. Bamford, *Rethinking cancer*, no. 6. 2015.
- [43] M. Cl  udia *et al.*, "IMPACTO S  CIO-ECON  MICO DO C  NCER NA VIDA DE PACIENTES, DO SEXO

- FEMININO, APÓS O DIAGNÓSTICO DA DOENÇA,” vol. 80, no. 1999, 2010.
- [44] American Cancer Society, “Cancer facts & Figures,” 2015.
 - [45] E. R. Simpson and K. A. Brown, “Minireview: Obesity and Breast Cancer: A Tale of Inflammation and Dysregulated Metabolism,” *Mol. Endocrinol.*, vol. 27, no. 5, pp. 715-725, May 2013.
 - [46] N. Hou, S. Hong, W. Wang, O. I. Olopade, J. J. Dignam, and D. Huo, “Hormone replacement therapy and breast cancer: heterogeneous risks by race, weight, and breast density,” *J. Natl. Cancer Inst.*, vol. 105, no. 18, pp. 1365-72, Sep. 2013.
 - [47] N. E. Allen *et al.*, “Moderate alcohol intake and cancer incidence in women,” *J. Natl. Cancer Inst.*, vol. 101, no. 5, pp. 296-305, Mar. 2009.
 - [48] S. ID and B. V., “Socioeconomic differences in reproductive behaviour,” *IARC Sci. Publ.*, no. 138, pp. 285-308, 1997.
 - [49] G. L. Albrecht, R. Fitzpatrick, and S. Scrimshaw, *Handbook of social studies in health and medicine*. Sage, 2000.
 - [50] A. Baum, T. A. Revenson, and J. E. Singer, *Handbook of health psychology*. Psychology Press, 2012.
 - [51] T. Kisić, N. Konstantinidis, J. Kolarović, and N. Kačanski, “[Importance of psychological support for families of children with cancer],” *Med. Pregl.*, vol. 65, no. 5-6, pp. 223-7.
 - [52] G. M. Cooper and R. Hausman, *The Cell: A molecular Approach*, 4th ed. U.S.A: Sinauer Associates, Inc., 2007.
 - [53] G. M. Cooper, *The Cell*. Sinauer Associates, 2000.
 - [54] J. P. Ward and J. R. King, “Mathematical modelling of avascular-tumour growth,” *IMA J. Math. Appl. Med. Biol.*, vol. 14, no. 1, pp. 39-69, Mar. 1997.
 - [55] B. Alberts, J. Wilson, and T. Hunt, *Molecular biology of the cell*. Garland Science, 2007.
 - [56] G. M. Cooper, “The Eukaryotic Cell Cycle,” Sinauer Associates, 2000.
 - [57] P. T. Seeley Rod R., Trent D. Stephens, *Anatomy & physiology*, 6th ed. McGraw-Hill Higher Education, 2003.
 - [58] E. L. Bearer *et al.*, “Multiparameter Computational Modeling of Tumor Invasion,” *Cancer Res.*, vol. 69, no. 10, pp. 4493-4501, May 2009.
 - [59] R. Kafri, J. Levy, M. B. Ginzberg, S. Oh, G. Lahav, and M. W. Kirschner, “Dynamics extracted from fixed cells reveal feedback linking cell growth to cell cycle,” *Nature*, vol. 494, no. 7438, pp. 480-483, 2013.
 - [60] M. Mir *et al.*, “Optical measurement of cycle-dependent cell growth,” *Proc. Natl. Acad. Sci.*, vol. 108, no. 32, pp. 13124-13129, 2011.
 - [61] A. Tzur, R. Kafri, V. Lebleu, G. Lahav, and M. Kirschner, “Cell Growth and Size Homeostasis in Proliferating Animal Cells,” vol. 167, no. 2009, 2011.
 - [62] P. Jorgensen and M. Tyers, “How cells coordinate growth and division,” *Curr. Biol.*, vol. 14, no. 23, pp. 1014-1027, 2004.
 - [63] J. M. Mitchison, “Growth during the cell cycle,” *Int. Rev. Cytol.*, vol. 226, pp. 165-258, 2003.
 - [64] J. F. Collins and M. H. Richmond, “Rate of growth of *Bacillus cereus* between divisions,” *J. Gen. Microbiol.*, vol. 28, no. May, pp. 15-33, 1962.
 - [65] D. Kipling, *The telomere*. Oxford University Press, 1995.
 - [66] G. B. Morin, “The implications of telomerase biochemistry for human disease,” *Eur. J. Cancer*, vol. 33, no. 5, pp. 750-760, Apr. 1997.
 - [67] S. F. Gilbert, “Aging: The Biology of Senescence,” 2000.
 - [68] D. Kanduc *et al.*, “Cell death: apoptosis versus necrosis,” *Int. J. Oncol.*, vol. 21, pp. 165-70, 2002.
 - [69] T. Vanden Berghe *et al.*, “Regulated necrosis: the expanding network of non-apoptotic cell death pathways,” *Nat. Rev. Mol. Cell Biol.*, vol. 15, no. 2, pp. 135-47, 2014.
 - [70] V. Nikolettou, M. Markaki, K. Palikaras, and N. Tavernarakis, “Crosstalk between apoptosis, necrosis and autophagy,” *Biochim. Biophys. Acta - Mol. Cell Res.*, vol. 1833, no. 12, pp. 3448-3459, 2013.
 - [71] J. R. McLaughlin *et al.*, “Reproductive risk factors for ovarian cancer in carriers of BRCA1 or BRCA2 mutations: a case-control study,” *Lancet. Oncol.*, vol. 8, no. 1, pp. 26-34, Jan. 2007.
 - [72] L.-M. Chen and J. Berek, “Overview of epithelial carcinoma of the ovary, fallopian tube, and peritoneum,” 2016. [Online]. Available: <http://www.uptodate.com/contents/overview-of-epithelial-carcinoma-of-the-ovary-fallopian-tube-and-peritoneum>. [Accessed: 01-Jun-2016].

- [73] D. J. Grant, P. G. Moorman, L. Akushevich, R. T. Palmieri, R. C. Bentley, and J. M. Schildkraut, "Primary peritoneal and ovarian cancers: an epidemiological comparative analysis.," *Cancer Causes Control*, vol. 21, no. 7, pp. 991-8, Jul. 2010.
- [74] E. Hiyama and K. Hiyama, "Clinical utility of telomerase in cancer," *Oncogene*, vol. 21, no. 4, pp. 643-649, Jan. 2002.
- [75] E. Samper, J. M. Flores, and M. A. Blasco, "Restoration of telomerase activity rescues chromosomal instability and premature aging in *Terc*^{-/-} mice with short telomeres.," *EMBO Rep.*, vol. 2, no. 9, pp. 800-7, Sep. 2001.
- [76] M. T. Hemann, M. A. Strong, L. Y. Hao, and C. W. Greider, "The shortest telomere, not average telomere length, is critical for cell viability and chromosome stability.," *Cell*, vol. 107, no. 1, pp. 67-77, Oct. 2001.
- [77] S. Rudraraju, K. L. Mills, R. Kemkemer, and K. Garikipati, "Multiphysics Modeling of Reactions, Mass Transport and Mechanics of Tumor Growth," in *Computer Models in Biomechanics*, 2013, pp. 293-303.
- [78] R. A. Gatenby, E. T. Gawlinski, A. F. Gmitro, B. Kaylor, and R. J. Gillies, "Acid-Mediated Tumor Invasion : a Multidisciplinary Study," no. 10, pp. 5216-5224, 2006.
- [79] A. L. Harris, "Hypoxia — a Key Regulatory Factor in Tumour Growth," *Nat. Rev. Cancer*, vol. 2, no. 1, pp. 38-47, 2002.
- [80] M. Höckel and P. Vaupel, "Tumor hypoxia: definitions and current clinical, biologic, and molecular aspects.," *J. Natl. Cancer Inst.*, vol. 93, no. 4, pp. 266-276, 2001.
- [81] V. Vukovic, H. K. Haugland, T. Nicklee, A. J. Morrison, and D. W. Hedley, "Hypoxia-inducible Factor-1 α Is an Intrinsic Marker for Hypoxia in Cervical Cancer Xenografts," *Cancer Res.*, vol. 61, no. 20, 2001.
- [82] H. Hashizume *et al.*, "Openings between Defective Endothelial Cells Explain Tumor Vessel Leakiness," *Am. J. Pathol.*, vol. 156, no. 4, pp. 1363-1380, Apr. 2000.
- [83] R. K. Jain, "Delivery of molecular medicine to solid tumors: lessons from in vivo imaging of gene expression and function.," *J. Control. Release*, vol. 74, no. 1-3, pp. 7-25, Jul. 2001.
- [84] R. K. Jain, "Determinants of tumor blood flow: a review.," *Cancer Res.*, vol. 48, no. 10, pp. 2641-58, May 1988.
- [85] R. K. Jain, "Physiological barriers to delivery of monoclonal antibodies and other macromolecules in tumors.," *Cancer Res.*, vol. 50, no. 3 Suppl, p. 814s-819s, Feb. 1990.
- [86] D. M. Brizel *et al.*, "Tumor oxygenation predicts for the likelihood of distant metastases in human soft tissue sarcoma.," *Cancer Res.*, vol. 56, no. 5, pp. 941-3, Mar. 1996.
- [87] D. M. Brizel, G. S. Sibley, L. R. Prosnitz, R. L. Scher, and M. W. Dewhirst, "Tumor hypoxia adversely affects the prognosis of carcinoma of the head and neck," *Int. J. Radiat. Oncol. Biol. Phys.*, vol. 38, no. 2, pp. 285-289, 1997.
- [88] M. Hockel, K. Schlenger, B. Aral, M. Mitze, U. Schaffer, and P. Vaupel, "Association between tumor hypoxia and malignant progression in advanced cancer of the uterine cervix.," *Cancer Res.*, vol. 56, no. 19, pp. 4509-15, Oct. 1996.
- [89] M. Höckel, K. Schlenger, S. Höckel, and P. Vaupel, "Hypoxic cervical cancers with low apoptotic index are highly aggressive.," *Cancer Res.*, vol. 59, no. 18, pp. 4525-8, Sep. 1999.
- [90] K. Sundfør, H. Lyng, and E. K. Rofstad, "Tumour hypoxia and vascular density as predictors of metastasis in squamous cell carcinoma of the uterine cervix.," *Br. J. Cancer*, vol. 78, no. 6, pp. 822-7, Sep. 1998.
- [91] R. A. Cairns, T. Kalliomaki, and R. P. Hill, "Acute (cyclic) hypoxia enhances spontaneous metastasis of KHT murine tumors.," *Cancer Res.*, vol. 61, no. 24, pp. 8903-8, Dec. 2001.
- [92] K. De Jaeger, M.-C. Kavanagh, and R. P. Hill, "Relationship of hypoxia to metastatic ability in rodent tumours," *Br. J. Cancer*, vol. 84, no. 9, pp. 1280-1285, May 2001.
- [93] J. Rozhin, M. Sameni, G. Ziegler, and B. F. Sloane, "Pericellular pH affects distribution and secretion of cathepsin B in malignant cells.," *Cancer Res.*, vol. 54, no. 24, pp. 6517-25, Dec. 1994.
- [94] L. M. Postovit, M. A. Adams, G. E. Lash, J. P. Heaton, and C. H. Graham, "Oxygen-mediated regulation of tumor cell invasiveness: Involvement of a nitric oxide signaling pathway," *J. Biol. Chem.*, vol. 277, no. 38, pp. 35730-35737, 2002.
- [95] E. K. Rofstad and E. F. Halsør, "Hypoxia-associated spontaneous pulmonary metastasis in human melanoma xenografts: involvement of microvascular hot spots induced in hypoxic foci by interleukin 8.," *Br. J. Cancer*, vol. 86, no. 2, pp. 301-8, Jan. 2002.
- [96] E. K. Rofstad, H. Rasmussen, K. Galappathi, B. Mathiesen, K. Nilsen, and B. A. Graff,

- "Hypoxia promotes lymph node metastasis in human melanoma xenografts by up-regulating the urokinase-type plasminogen activator receptor.," *Cancer Res.*, vol. 62, no. 6, pp. 1847-53, Mar. 2002.
- [97] B. Capogrosso Sansone, M. Scalerandi, and C. A. Condat, "Emergence of Taxis and Synergy in Angiogenesis," *Phys. Rev. Lett.*, vol. 87, no. 12, p. 128102, Sep. 2001.
 - [98] S. D. Young, R. S. Marshall, and R. P. Hill, "Hypoxia induces DNA overreplication and enhances metastatic potential of murine tumor cells.," *Proc. Natl. Acad. Sci. U. S. A.*, vol. 85, no. 24, pp. 9533-7, Dec. 1988.
 - [99] H. J. J. A. Bernsen and A. J. van der Kogel, "Antiangiogenic Therapy in Brain Tumor Models," *J. Neurooncol.*, vol. 45, no. 3, pp. 247-255, 1999.
 - [100] Bloemendal, Logtenberg, and Voest, "New strategies in anti-vascular cancer therapy," *Eur. J. Clin. Invest.*, vol. 29, no. 9, pp. 802-809, Sep. 1999.
 - [101] R. A. J. KUIPER, J. H. M. SCHELLENS, G. H. BLIJHAM, J. H. BEIJNEN, and E. E. VOEST, "CLINICAL RESEARCH ON ANTIANGIOGENIC THERAPY," *Pharmacol. Res.*, vol. 37, no. 1, pp. 1-16, 1998.
 - [102] H. S. Rugo, "Bevacizumab in the treatment of breast cancer: rationale and current data.," *Oncologist*, vol. 9 Suppl 1, pp. 43-9, 2004.
 - [103] P. S. Steeg, "Angiogenesis inhibitors: motivators of metastasis?," *Nat. Med.*, vol. 9, no. 7, pp. 822-823, Jul. 2003.
 - [104] L. Bello, "Combinatorial Administration of Molecules That Simultaneously Inhibit Angiogenesis and Invasion Leads to Increased Therapeutic Efficacy in Mouse Models of Malignant Glioma," *Clin. Cancer Res.*, vol. 10, no. 13, pp. 4527-4537, Jul. 2004.
 - [105] P. Kunkel *et al.*, "Inhibition of glioma angiogenesis and growth in vivo by systemic treatment with a monoclonal antibody against vascular endothelial growth factor receptor-2.," *Cancer Res.*, vol. 61, no. 18, pp. 6624-8, Sep. 2001.
 - [106] K. Lamszus, P. Kunkel, and M. Westphal, "Invasion as limitation to anti-angiogenic glioma therapy.," *Acta Neurochir. Suppl.*, vol. 88, pp. 169-77, 2003.
 - [107] S. Pennacchietti, P. Michieli, M. Galluzzo, M. Mazzone, S. Giordano, and P. M. Comoglio, "Hypoxia promotes invasive growth by transcriptional activation of the met protooncogene.," *Cancer Cell*, vol. 3, no. 4, pp. 347-61, Apr. 2003.
 - [108] J. L. Rubenstein *et al.*, "Anti-VEGF antibody treatment of glioblastoma prolongs survival but results in increased vascular cooption.," *Neoplasia*, vol. 2, no. 4, pp. 306-14, 2000.
 - [109] E. A. Seftor *et al.*, "Molecular determinants of human uveal melanoma invasion and metastasis.," *Clin. Exp. Metastasis*, vol. 19, no. 3, pp. 233-46, 2002.
 - [110] H. Andersen *et al.*, "Immediate and delayed effects of E-cadherin inhibition on gene regulation and cell motility in human epidermoid carcinoma cells.," *Mol. Cell. Biol.*, vol. 25, no. 20, pp. 9138-50, Oct. 2005.
 - [111] T. W. Bauer *et al.*, "Targeting of urokinase plasminogen activator receptor in human pancreatic carcinoma cells inhibits c-Met- and insulin-like growth factor-I receptor-mediated migration and invasion and orthotopic tumor growth in mice.," *Cancer Res.*, vol. 65, no. 17, pp. 7775-81, Sep. 2005.
 - [112] L. Derycke, V. Van Marck, H. Depypere, and M. Bracke, "Molecular Targets of Growth, Differentiation, Tissue Integrity, and Ectopic Cell Death in Cancer Cells," *Cancer Biother. Radiopharm.*, vol. 20, no. 6, pp. 579-588, Dec. 2005.
 - [113] J. A. Eble and J. Haier, "Integrins in cancer treatment.," *Curr. Cancer Drug Targets*, vol. 6, no. 2, pp. 89-105, Mar. 2006.
 - [114] C. Hayot, O. Debeir, P. Van Ham, M. Van Damme, R. Kiss, and C. Decaestecker, "Characterization of the activities of actin-affecting drugs on tumor cell migration," *Toxicol. Appl. Pharmacol.*, vol. 211, no. 1, pp. 30-40, Feb. 2006.
 - [115] Q. Huang, H.-M. Shen, and C.-N. Ong, "Emodin inhibits tumor cell migration through suppression of the phosphatidylinositol 3-kinase-Cdc42/Rac1 pathway," *C. Cell. Mol. Life Sci.*, vol. 62, no. 10, pp. 1167-1175, May 2005.
 - [116] J. Lockett, S. Yin, X. Li, Y. Meng, and S. Sheng, "Tumor suppressive maspin and epithelial homeostasis," *J. Cell. Biochem.*, vol. 97, no. 4, pp. 651-660, Mar. 2006.
 - [117] G. W. McLean, N. O. Carragher, E. Avizienyte, J. Evans, V. G. Brunton, and M. C. Frame, "The role of focal-adhesion kinase in cancer – a new therapeutic opportunity," *Nat. Rev. Cancer*, vol. 5, no. 7, pp. 505-515, Jul. 2005.
 - [118] S. Yin *et al.*, "Maspin Retards Cell Detachment via a Novel Interaction with the Urokinase-

- Type Plasminogen Activator/Urokinase-Type Plasminogen Activator Receptor System," *Cancer Res.*, vol. 66, no. 8, pp. 4173-4181, Apr. 2006.
- [119] R. M. Sutherland, J. A. McCredie, and W. R. Inch, "Growth of multicell spheroids in tissue culture as a model of nodular carcinomas," *J. Natl. Cancer Inst.*, vol. 46, no. 1, pp. 113-20, Jan. 1971.
 - [120] W. R. Inch, J. A. McCredie, and R. M. Sutherland, "Growth of nodular carcinomas in rodents compared with multi-cell spheroids in tissue culture," *Growth*, vol. 34, no. 3, pp. 271-82, Sep. 1970.
 - [121] R. M. Sutherland and R. E. Durand, "Radiation response of multicell spheroids--an in vitro tumour model," *Curr. Top. Radiat. Res. Q.*, vol. 11, no. 1, pp. 87-139, Jan. 1976.
 - [122] J. P. Freyer and R. M. Sutherland, "Selective dissociation and characterization of cells from different regions of multicell tumor spheroids," *Cancer Res.*, vol. 40, no. 11, pp. 3956-65, Nov. 1980.
 - [123] J. Landry, J. P. Freyer, and R. M. Sutherland, "Shedding of mitotic cells from the surface of multicell spheroids during growth," *J. Cell. Physiol.*, vol. 106, no. 1, pp. 23-32, Jan. 1981.
 - [124] J. Carlsson, "A proliferation gradient in three-dimensional colonies of cultured human glioma cells," *Int. J. cancer*, vol. 20, no. 1, pp. 129-36, Jul. 1977.
 - [125] M. Haji-Karim and J. Carlsson, "Proliferation and viability in cellular spheroids of human origin," *Cancer Res.*, vol. 38, no. 5, pp. 1457-64, May 1978.
 - [126] J. M. Yuhas and A. P. Li, "Growth fraction as the major determinant of multicellular tumor spheroid growth rates," *Cancer Res.*, vol. 38, no. 6, pp. 1528-32, Jun. 1978.
 - [127] J. M. Yuhas, A. E. Tarleton, and K. B. Molzen, "Multicellular tumor spheroid formation by breast cancer cells isolated from different sites," *Cancer Res.*, vol. 38, no. 8, pp. 2486-91, Aug. 1978.
 - [128] J. Folkman and M. Hochberg, "Self-regulation of growth in three dimensions," *J. Exp. Med.*, vol. 138, no. 4, pp. 745-53, Oct. 1973.
 - [129] A. C. Burton, "Rate of growth of solid tumours as a problem of diffusion," *Growth*, vol. 30, no. 2, pp. 157-76, Jun. 1966.
 - [130] H. P. Greenspan, "Models for the Growth of a Solid Tumor by Diffusion," *Studies in Applied Mathematics*, vol. 51, no. 4, pp. 317-340, 1972.
 - [131] R. M. Shymko, "Cellular and geometric control of tissue growth and mitotic instability," *J. Theor. Biol.*, vol. 63, no. 2, pp. 355-74, Dec. 1976.
 - [132] M. A. J. Chaplain, "Avascular growth, angiogenesis and vascular growth in solid tumours: The mathematical modelling of the stages of tumour development," *Math. Comput. Model.*, vol. 23, no. 6, pp. 47-87, 1996.
 - [133] K. D. Bagshawe, *Recent Results in Cancer Research*, vol. 29, no. 4, 1975.
 - [134] R. Born, O. Hug, and K.-R. Trott, "The effect of prolonged hypoxia on growth and viability of Chinese hamster cells," *Int. J. Radiat. Oncol.*, vol. 1, no. 7, pp. 687-697, 1976.
 - [135] D. C. Shrieve, D. F. Deen, and J. W. Harris, "Effects of extreme hypoxia on the growth and viability of EMT6/SF mouse tumor cells in vitro," *Cancer Res.*, vol. 43, no. 8, pp. 3521-7, Aug. 1983.
 - [136] C. S. Heacock and R. M. Sutherland, "Induction characteristics of oxygen regulated proteins," *Int. J. Radiat. Oncol.*, vol. 12, no. 8, pp. 1287-1290, 1986.
 - [137] E. L. Alpen and M. S. Mendonca, "Nutritionally induced quiescence of 9L cells; correlations with increased survival after x-irradiation," *Radiat. Res. Soc.*, p. 129, 1986.
 - [138] C. Ceccarini and H. Eagle, "pH as a Determinant of Cellular Growth and Contact Inhibition," *Proc. Natl. Acad. Sci. U. S. A.*, vol. 68, no. 1, p. 229, 1971.
 - [139] R. Baserga, "Resting cells and the G1 phase of the cell cycle," *J. Cell. Physiol.*, vol. 95, no. 3, pp. 377-82, Jun. 1978.
 - [140] J. J. Sciandra and J. R. Subjeck, "The effects of glucose on protein synthesis and thermosensitivity in Chinese hamster ovary cells," *J. Biol. Chem.*, vol. 258, no. 20, pp. 12091-3, Oct. 1983.
 - [141] C. K. Li, "The glucose distribution in 9L rat brain multicell tumor spheroids and its effect on cell necrosis," *Cancer*, vol. 50, no. 10, pp. 2066-73, Nov. 1982.
 - [142] J. P. Freyer and R. M. Sutherland, "A reduction in the in situ rates of oxygen and glucose consumption of cells in EMT6/Ro spheroids during growth," *J. Cell. Physiol.*, vol. 124, no. 3, pp. 516-524, 1985.
 - [143] W. F. Mueller-Klieser and R. M. Sutherland, "Oxygen tensions in multicell spheroids of two

- cell lines.," *Br. J. Cancer*, vol. 45, no. 2, pp. 256-64, Feb. 1982.
- [144] W. Mueller-Klieser, J. P. Freyer, and R. M. Sutherland, "Influence of glucose and oxygen supply conditions on the oxygenation of multicellular spheroids.," *Br. J. Cancer*, vol. 53, no. 3, pp. 345-53, 1986.
 - [145] N. Kaufman, H. I. Bicher, F. W. Hetzel, and M. Brown, "A system for determining the pharmacology of indirect radiation sensitizer drugs on multicellular spheroids.," *Cancer Clin. Trials*, vol. 4, no. 2, pp. 199-204, 1981.
 - [146] J. J. Casciari, S. V. Sotirchos, and R. M. Sutherland, "Variations in tumor cell growth rates and metabolism with oxygen concentration, glucose concentration, and extracellular pH," *J. Cell. Physiol.*, vol. 151, no. 2, pp. 386-394, 1992.
 - [147] R. A. Gatenby and P. K. Maini, "Mathematical oncology: Cancer summed up," *Nature*, vol. 421, no. 6921, pp. 321-321, Jan. 2003.
 - [148] H. Byrne, "USING MATHEMATICS TO STUDY SOLID TUMOUR GROWTH."
 - [149] D. Hanahan and R. A. Weinberg, "The hallmarks of cancer.," *Cell*, vol. 100, no. 1, pp. 57-70, Jan. 2000.
 - [150] J. A. Adam, "General Aspects of Modeling Tumor Growth and Immune Response," in *A Survey of Models for Tumor-Immune System Dynamics*, Boston, MA: Birkhäuser Boston, 1997, pp. 15-87.
 - [151] A. Friedman, "A free boundary problem for a coupled system of elliptic, hyperbolic, and Stokes equations modeling tumor growth," *Interfaces Free Boundaries*, vol. 8, no. 2, pp. 247-261, 2006.
 - [152] J. MOREIRA and A. DEUTSCH, "CELLULAR AUTOMATON MODELS OF TUMOR DEVELOPMENT: A CRITICAL REVIEW," *Adv. Complex Syst.*, vol. 5, no. 02n03, pp. 247-267, Jun. 2002.
 - [153] N. Bellomo, E. De Angelis, and L. Preziosi, "Multiscale Modeling and Mathematical Problems Related to Tumor Evolution and Medical Therapy," *J. Theor. Med.*, vol. 5, no. 2, pp. 111-136, 2003.
 - [154] R. P. Araujo and D. L. S. McElwain, "A history of the study of solid tumour growth: The contribution of mathematical modelling," *Bull. Math. Biol.*, vol. 66, no. 5, pp. 1039-1091, 2004.
 - [155] A. R. A. Anderson and V. Quaranta, "Integrative mathematical oncology," *Nat. Rev. Cancer*, vol. 8, no. 3, pp. 227-234, Mar. 2008.
 - [156] N. BELLOMO, N. K. LI, and P. K. MAINI, "ON THE FOUNDATIONS OF CANCER MODELLING: SELECTED TOPICS, SPECULATIONS, AND PERSPECTIVES," *Math. Model. Methods Appl. Sci.*, vol. 18, no. 4, pp. 593-646, Apr. 2008.
 - [157] H. . Byrne, T. Alarcon, M. . Owen, S. . Webb, and P. . Maini, "Modelling aspects of cancer dynamics: a review," *Philos. Trans. R. Soc. A Math. Phys. Eng. Sci.*, vol. 364, no. 1843, pp. 1563-1578, Jun. 2006.
 - [158] A. Friedman, "A HIERARCHY OF CANCER MODELS AND THEIR MATHEMATICAL CHALLENGES," vol. 4, no. 1, pp. 147-159, 2004.
 - [159] V. Cristini *et al.*, "Nonlinear Modeling and Simulation of Tumor Growth."
 - [160] A. FRIEDMAN, "MATHEMATICAL ANALYSIS AND CHALLENGES ARISING FROM MODELS OF TUMOR GROWTH," *Math. Model. Methods Appl. Sci.*, vol. 17, no. supp01, pp. 1751-1772, Nov. 2007.
 - [161] L. Graziano and L. Preziosi, "Mechanics in Tumor Growth," in *Modeling of Biological Materials*, Boston, MA: Birkhäuser Boston, 2007, pp. 263-321.
 - [162] H. L. P. Harpold, E. C. Alvord, and K. R. Swanson, "The Evolution of Mathematical Modeling of Glioma Proliferation and Invasion," *J. Neuropathol. Exp. Neurol.*, vol. 66, no. 1, pp. 1-9, Jan. 2007.
 - [163] T. L. Jackson, R. Ashkenazi, S. Heusel, and H. V. Jain, "Cancer modeling: a perspective on what's new and what's next," 2006, pp. 153-171.
 - [164] M. L. Martins, S. C. Ferreira, and M. J. Vilela, "Multiscale models for the growth of avascular tumors," *Phys. Life Rev.*, vol. 4, no. 2, pp. 128-156, 2007.
 - [165] N. V. Mantzaris, S. Webb, and H. G. Othmer, "Mathematical modeling of tumor-induced angiogenesis," *J. Math. Biol.*, vol. 49, no. 2, pp. 111-87, Aug. 2004.
 - [166] V. Quaranta, A. M. Weaver, P. T. Cummings, and A. R. A. Anderson, "Mathematical modeling of cancer: The future of prognosis and treatment," *Clin. Chim. Acta*, vol. 357, no. 2, pp. 173-179, Jul. 2005.
 - [167] L. Preziosi and A. Tosin, "Multiphase and Multiscale Trends in Cancer Modelling," *Math. Model. Nat. Phenom.*, vol. 4, no. 3, pp. 1-11, 2009.

- [168] T. Roose, S. J. Chapman, and P. K. Maini, "Mathematical models of avascular tumor growth," *Siam Rev.*, vol. 49, no. 2, pp. 179-208, 2007.
- [169] S. Sanga, H. B. Frieboes, X. Zheng, R. Gatenby, E. L. Bearer, and V. Cristini, "Predictive oncology: A review of multidisciplinary, multiscale in silico modeling linking phenotype, morphology and growth," *Neuroimage*, vol. 37, pp. S120-S134, Jan. 2007.
- [170] K. R. Swanson, C. Bridge, J. D. Murray, and E. C. Alvord, "Virtual and real brain tumors: using mathematical modeling to quantify glioma growth and invasion.," *J. Neurol. Sci.*, vol. 216, no. 1, pp. 1-10, Dec. 2003.
- [171] I. M. M. van Leeuwen, C. M. Edwards, M. Ilyas, and H. M. Byrne, "Towards a multiscale model of colorectal cancer.," *World J. Gastroenterol.*, vol. 13, no. 9, pp. 1399-407, Mar. 2007.
- [172] A. C. Ventura, T. L. Jackson, and S. D. Merajver, "On the role of cell signaling models in cancer research.," *Cancer Res.*, vol. 69, no. 2, pp. 400-2, Jan. 2009.
- [173] Z. Wang and T. S. Deisboeck, "Computational modeling of brain tumors: discrete, continuum or hybrid?," *Sci. Model. Simul. SMNS*, vol. 15, no. 1-3, pp. 381-393, Apr. 2008.
- [174] Y. KIM, M. A. STOLARSKA, and H. G. OTHMER, "A HYBRID MODEL FOR TUMOR SPHEROID GROWTH IN VITRO: THEORETICAL DEVELOPMENT AND EARLY RESULTS," *Math. Model. Methods Appl. Sci.*, vol. 17, no. supp01, pp. 1773-1798, Nov. 2007.
- [175] J. S. Lowengrub *et al.*, "Nonlinear modelling of cancer: bridging the gap between cells and tumours.," *Nonlinearity*, vol. 23, no. 1, pp. R1-R9, 2010.
- [176] M. S. Alber, M. A. Kiskowski, J. A. Glazier, and Y. Jiang, "On Cellular Automaton Approaches to Modeling Biological Cells," Springer New York, 2003, pp. 1-39.
- [177] R. G. Abbott, S. Forrest, and K. J. Pienta, "Simulating the Hallmarks of Cancer," *Artif. Life*, vol. 12, no. 4, pp. 617-634, Oct. 2006.
- [178] A. R. A. Anderson, M. A. J. Chaplain, and K. A. Rejniak, *Single-cell-based models in biology and medicine*. Birkhäuser, 2007.
- [179] T. S. Deisboeck, L. Zhang, J. Yoon, and J. Costa, "In silico cancer modeling: is it ready for prime time?," *Nat. Clin. Pract. Oncol.*, vol. 6, no. 1, pp. 34-42, Jan. 2009.
- [180] J. Galle, G. Aust, G. Schaller, T. Beyer, and D. Drasdo, "Individual cell-based models of the spatial-temporal organization of multicellular systems—Achievements and limitations," *Cytom. Part A*, vol. 69A, no. 7, pp. 704-710, Jul. 2006.
- [181] V. Quaranta, K. A. Rejniak, P. Gerlee, and A. R. A. Anderson, "Invasion emerges from cancer cell adaptation to competitive microenvironments: Quantitative predictions from multiscale mathematical models," *Semin. Cancer Biol.*, vol. 18, no. 5, pp. 338-348, Oct. 2008.
- [182] B. C. Thorne, A. M. Bailey, and S. M. Peirce, "Combining experiments with multi-cell agent-based modeling to study biological tissue patterning," *Brief. Bioinform.*, vol. 8, no. 4, pp. 245-257, Mar. 2007.
- [183] L. Zhang, Z. Wang, J. A. Sagotsky, and T. S. Deisboeck, "Multiscale agent-based cancer modeling," *J. Math. Biol.*, vol. 58, no. 4-5, pp. 545-559, Apr. 2009.
- [184] H. P. Greenspan, "On the growth and stability of cell cultures and solid tumors," *J. Theor. Biol.*, vol. 56, no. 1, pp. 229-242, 1976.
- [185] P. K. Burgess, P. M. Kulesa, J. D. Murray, and E. C. Alvord, "The interaction of growth rates and diffusion coefficients in a three-dimensional mathematical model of gliomas.," *J. Neuropathol. Exp. Neurol.*, vol. 56, no. 6, pp. 704-13, Jun. 1997.
- [186] M. A. Chaplain, M. Ganesh, and I. G. Graham, "Spatio-temporal pattern formation on spherical surfaces: numerical simulation and application to solid tumour growth.," *J. Math. Biol.*, vol. 42, no. 5, pp. 387-423, May 2001.
- [187] G. C. CRUYWAGEN, D. E. WOODWARD, P. TRACQUI, G. T. BARTOO, J. D. MURRAY, and E. C. ALVORD, "THE MODELLING OF DIFFUSIVE TUMOURS," *J. Biol. Syst.*, vol. 3, no. 4, pp. 937-945, Dec. 1995.
- [188] S. Jbabdi *et al.*, "Simulation of anisotropic growth of low-grade gliomas using diffusion tensor imaging," *Magn. Reson. Med.*, vol. 54, no. 3, pp. 616-624, Sep. 2005.
- [189] J. A. Sherratt, "Traveling Wave Solutions of a Mathematical Model for Tumor Encapsulation," *SIAM J. Appl. Math.*, vol. 60, pp. 392-407, 1999.
- [190] J. A. Sherratt and M. A. Chaplain, "A new mathematical model for avascular tumour growth.," *J. Math. Biol.*, vol. 43, no. 4, pp. 291-312, Oct. 2001.
- [191] K. R. Swanson, E. C. Alvord, and J. D. Murray, "A quantitative model for differential motility of gliomas in grey and white matter.," *Cell Prolif.*, vol. 33, no. 5, pp. 317-29, Oct. 2000.

- [192] K. R. Swanson, R. C. Rostomily, E. C. Alvord, and Jr, "A mathematical modelling tool for predicting survival of individual patients following resection of glioblastoma: a proof of principle.," *Br. J. Cancer*, vol. 98, no. 1, pp. 113-9, Jan. 2008.
- [193] H. M. BYRNE and M. A. J. CHAPLAIN, "Free boundary value problems associated with the growth and development of multicellular spheroids," *Eur. J. Appl. Math.*, vol. 8, no. 6, pp. 639-658, 1997.
- [194] S. Cui and A. Friedman, "A FREE BOUNDARY PROBLEM FOR A SINGULAR SYSTEM OF DIFFERENTIAL EQUATIONS: AN APPLICATION TO A MODEL OF TUMOR GROWTH," vol. 355, no. 903, pp. 3537-3590, 2003.
- [195] G. Pettet, C. P. Please, M. J. Tindall, and D. L. McElwain, "The Migration of Cells in Multicell Tumor Spheroids," *Bull. Math. Biol.*, vol. 63, no. 2, pp. 231-257, Mar. 2001.
- [196] J. P. Ward and J. R. King, "Mathematical modelling of drug transport in tumour multicell spheroids and monolayer cultures.," *Math. Biosci.*, vol. 181, no. 2, pp. 177-207, Feb. 2003.
- [197] J. A. Adam, "A mathematical model of tumor growth. III. comparison with experiment," *Math. Biosci.*, vol. 86, no. 2, pp. 213-227, 1987.
- [198] D. Ambrosi and F. Mollica, "On the mechanics of a growing tumor," *Int. J. Eng. Sci.*, vol. 40, no. 12, pp. 1297-1316, 2002.
- [199] T. Roose, P. A. Netti, L. L. Munn, Y. Boucher, and R. K. Jain, "Solid stress generated by spheroid growth estimated using a linear poroelasticity model.," *Microvasc. Res.*, vol. 66, no. 3, pp. 204-12, Nov. 2003.
- [200] A. F. Jones, H. M. Byrne, J. S. Gibson, and J. W. Dold, "A mathematical model of the stress induced during avascular tumour growth," *J. Math. Biol.*, vol. 40, no. 6, pp. 473-499, Jun. 2000.
- [201] S. Cui and A. Friedman, "Analysis of a mathematical model of the effect of inhibitors on the growth of tumors.," *Math. Biosci.*, vol. 164, no. 2, pp. 103-37, Apr. 2000.
- [202] A. Chauviere, L. Preziosi, and H. Byrne, "A model of cell migration within the extracellular matrix based on a phenotypic switching mechanism," *Math. Med. Biol.*, vol. 27, no. 3, pp. 255-281, Sep. 2010.
- [203] P. Friedl and K. Wolf, "Tumour-cell invasion and migration: diversity and escape mechanisms," *Nat. Rev. Cancer*, vol. 3, no. 5, pp. 362-374, May 2003.
- [204] H. B. Frieboes, F. Jin, Y.-L. Chuang, S. M. Wise, J. S. Lowengrub, and V. Cristini, "Three-dimensional multispecies nonlinear tumor growth-II: Tumor invasion and angiogenesis.," *J. Theor. Biol.*, vol. 264, no. 4, pp. 1254-78, Jun. 2010.
- [205] J. Belinha, *Meshless Methods in Biomechanics: Bone Tissue Remodelling Analysis. Lecture Notes in Computational Vision and Biomechanics*. Springer International Publisher Switzerland, 2014.
- [206] J.-S. Chen, C.-T. Wu, S. Yoon, and Y. You, "A stabilized conforming nodal integration for Galerkin mesh-free methods," *Int. J. Numer. Methods Eng.*, vol. 50, no. 2, pp. 435-466, Jan. 2001.
- [207] W. Elmer, J. S. Chen, M. Puso, and E. Taciroglu, "A stable, meshfree, nodal integration method for nearly incompressible solids," *Finite Elem. Anal. Des.*, vol. 51, pp. 81-85, Apr. 2012.
- [208] K. Y. Sze, J. S. Chen, N. Sheng, and X. H. Liu, "Stabilized conforming nodal integration: exactness and variational justification," *Finite Elem. Anal. Des.*, vol. 41, no. 2, pp. 147-171, Nov. 2004.
- [209] P. Wriggers, "Computational Contact Mechanics," *Springer*, 2006. [Online]. Available: <http://www.springer.com/us/book/9783540326083>. [Accessed: 02-Jun-2016].
- [210] P. W. (Peter W. Atkins and J. De Paula, *Physical chemistry*, 8th ed. Oxford University Press, 2006.
- [211] L. D. Landau and E. M. Lifshitz, *Fluid mechanics*, 2nd ed. Elsevier, 1987.
- [212] A. Einstein, "Über die von der molekularkinetischen Theorie der Wärme geforderte Bewegung von in ruhenden Flüssigkeiten suspendierten Teilchen," *Ann. Phys.*, vol. 322, no. 8, pp. 549-560, 1905.
- [213] G. R. Liu and S. S. Quek, *The finite element method : a practical course*. Elsevier Science - Butterworth-Heinemann, 2003.
- [214] J. P. Freyer, R. M. Sutherland, and J. P. F. R. M. Sutherland, "Regulation of Growth Saturation and Development of Necrosis in EMT6 / Ro Multicellular Spheroids by the Glucose and Oxygen Supply Regulation of Growth Saturation and Development of Necrosis in EMT6 /

- Ro Multicellular Spheroids by the Glucose and Oxygen," *Cancer Res.*, no. 46, pp. 3504-3512, 1986.
- [215] J. Landry, J. Freyer, and R. Sutherland, "A model for the growth of multicellular spheroids," *Cell Prolif.*, pp. 585-594, 1982.